Expected tracking performance of the ATLAS Inner Tracker at the High-Luminosity LHC

Published by IOP Publishing for Sissa Medialab

Received: *December 20, 2024*
Accepted: *January 20, 2025*
Published: *February 18, 2025*

Expected tracking performance of the ATLAS Inner Tracker at the High-Luminosity LHC

The ATLAS collaboration

E-mail: atlas.publications@cern.ch

Abstract: The high-luminosity phase of LHC operations (HL-LHC), will feature a large increase in simultaneous proton-proton interactions per bunch crossing up to 200, compared with a typical leveling target of 64 in Run 3. Such an increase will create a very challenging environment in which to perform charged particle trajectory reconstruction, a task crucial for the success of the ATLAS physics program, and will exceed the capabilities of the current ATLAS Inner Detector (ID). A new all-silicon Inner Tracker (ITk) will replace the current ID in time for the start of the HL-LHC. To ensure successful use of the ITk capabilities in Run 4 and beyond, the ATLAS tracking software has been successfully adapted to achieve state-of-the-art track reconstruction in challenging high-luminosity conditions with the ITk detector. This paper presents the expected tracking performance of the ATLAS ITk based on the latest available developments since the ITk technical design reports.

Keywords: Gaseous imaging and tracking detectors; Particle tracking detectors (Solid-state detectors); Pattern recognition, cluster finding, calibration and fitting methods; Vertexing algorithms

ArXiv ePrint: 2412.15090

https://doi.org/10.1088/1748-0221/20/02/P02018

Contents

1 Introduction

The Large Hadron Collider (LHC) [1] has enabled detailed exploration of the energy frontier since 2009 with a successful program of proton-proton and heavy-ion collisions. It is slated to be upgraded in time for its fourth period of operation (Run 4) to deliver a nominal luminosity of 5.0×10^{34} cm^{-2}s^{-1} to the general-purpose detectors ATLAS [2] and CMS [3], in a configuration known as high-luminosity LHC (HL-LHC) [4]. Such an increase in instantaneous luminosity creates a very challenging environment for particle detectors since it is achieved at the cost of a drastic increase in the average number of proton-proton interactions in the same bunch crossing ($\langle\mu\rangle$, also known as "pile-up"), expected to rise up to as much as 140 in the ATLAS detector during Run 4, as compared with a typical leveling target of 64 during Run 3. For subsequent runs, further luminosity increases up to 7.5×10^{34} cm^{-2}s^{-1} are under discussion, which would bring the pile-up up to 200, extreme conditions under which the reconstruction will have to maintain robust performances. Moreover, the performance of the ATLAS Inner Detector subsystem [5, 6] is already affected by radiation damage [7, 8], which degrades its operational capabilities. Furthermore, the subsystem will face challenges in addressing the increased fluence and

2025 JINST 20 P02018

occupancy resulting from HL-LHC collisions, with bandwidth limitations and the need to minimize the material budget likely exacerbating these issues. Therefore, the ATLAS Collaboration will install a new all-silicon tracking detector, the Inner Tracker (ITk) [9, 10], as a part of its Phase-II detector upgrade program [11, 12] in preparation for HL-LHC data-taking. Following the publication of the technical design reports, further refinements were made to the detector design, which are detailed in this document.

The reconstructed trajectories (tracks) of charged particles produced in collisions are a key input to many other reconstruction algorithms [13–18], and they are also used directly by a number of physics analyses (for example refs. [19–21]). To achieve high tracking efficiency, the ATLAS tracking chain [22, 23] is designed around a combinatorial variant of the well-known Kalman filter algorithm [24], augmented by an ambiguity solving stage designed to keep the low-quality and duplicate track creation rates at a minimum. This paper presents the expected performance of a version of this track reconstruction chain tuned specifically for the challenging environment of HL-LHC collisions and using the ITk detector.

The ATLAS Collaboration has produced notes detailing the expected performance of flavor-tagging [25, 26] as well as the integrated performance of the whole Run 4 detector [27, 28]. Reports about the concomitant upgrade to the CMS detector can be found in refs. [29, 30]. Extensive information about the physics prospects at the HL-LHC for both the ATLAS and CMS collaborations can be found in refs. [31, 32].

The rest of this paper is structured as follows: the ITk detector layout is detailed in section 2; the simulation framework and samples, and the track reconstruction strategy are described in section 3 and 4, respectively; the expected ITk tracking and vertexing performance is reported in section 5; and concluding remarks can be found in section 6.

2 The ATLAS Inner Tracker

2.1 Overview

The ITk is designed to be a silicon-based detector that comprises a pixel [10] and a strip subsystem [9]. The pixel subsystem covers a pseudorapidity[1] range of $|\eta| < 4.0$ and consists of five flat barrel layers and five layers of inclined or vertical rings for forward region coverage. The strip subsystem spans $|\eta| < 2.7$ and includes four strip layers in the barrel region and six disks in the endcaps, all using double-sided modules. The active area of the detector will be shielded from the neutron flux coming from the calorimeters by a neutron moderator surrounding the strip detector.

The ITk will operate within a solenoidal magnetic field of 2 T, which is aligned with the beam axis. This magnetic field plays a crucial role by bending the trajectories of charged particles, allowing to estimate their transverse momentum, p_{T}. The overall ITk configuration aims to achieve a minimum of nine measurements per track across the entire expected beam spot size, assuming a Gaussian distribution with a longitudinal width of 50 mm, and aims to reconstruct tracks left by charged particles with $p_{\mathrm{T}} > 1$ GeV passing through the detector in the $|\eta| < 4.0$ range.

[1] ATLAS uses a right-handed coordinate system with its origin at the nominal interaction point (IP) in the center of the detector and the z-axis along the beam pipe. The x-axis points from the IP to the center of the LHC ring, and the y-axis points upwards. Polar coordinates (r, ϕ) are used in the transverse plane, ϕ being the azimuthal angle around the z-axis. The pseudorapidity is defined in terms of the polar angle θ as $\eta = -\ln\tan(\theta/2)$ and is equal to the rapidity $y = \frac{1}{2}\ln\left(\frac{E+p_z}{E-p_z}\right)$ in the relativistic limit. Angular distance is measured in units of $\Delta R \equiv \sqrt{(\Delta y)^2 + (\Delta\phi)^2}$.

2025 JINST 20 P02018

2.2 ITk layout

After the release of the technical design reports [9, 10], the detector design underwent additional refinement, as outlined in the following description. The resulting ITk layout is labeled as 03-00-00 and is presented in figure 1.

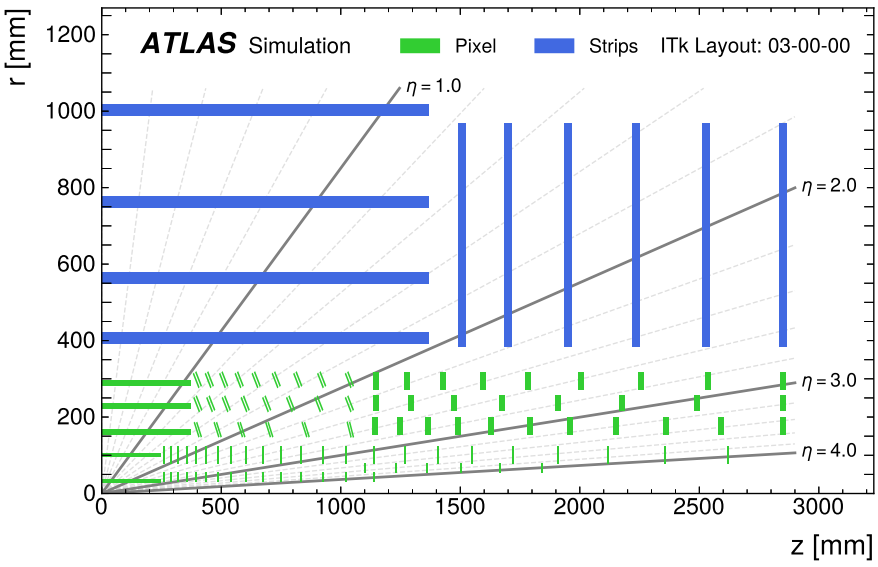

(a)

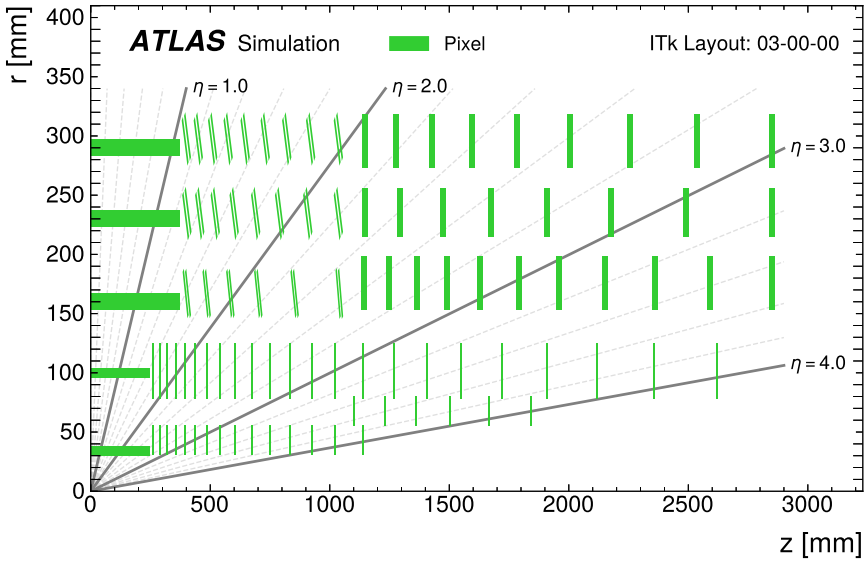

(b)

Figure 1. (a) A schematic depiction of the ITk Layout 03-00-00 as presented in this document. (b) A zoomed-in view of the pixel detector. In each case, only one quadrant and only active detector elements are shown. The horizontal axis is along the beam line with zero being the nominal interaction point. The vertical axis is the radius measured from the interaction point. Thicker lines in the flat barrel sections are due to their tilt in the ϕ-direction, while thicker lines in the endcap disks are due to their staggering along the z-direction, where z-positions vary between distinct values as a function of ϕ location.

Updates were made to the tilt angles in the azimuthal direction of the barrel strip modules in the first two layers, and the radius of the first layer was modified. These changes were implemented to ensure sufficient space during installation, while still maintaining ample overlap between the modules of adjacent staves for alignment purposes and hermeticity,[2] as detailed in table 1. Following the decision to incorporate the high-granularity timing detector (HGTD) [33] into the Phase-II upgrade of ATLAS, necessary adjustments were also made to the overall spatial dimensions of the ITk to accommodate the HGTD. Table 2 provides a summary of the resulting disk locations. The innermost pixel layer uses smaller modules based on 3D pixel sensor technology. These modules consist of a single active element with front-end (FE) read-out chips bump-bonded to the sensors and grouped in triplets. In contrast, all other layers use planar "quad" modules, where four FE chips are bump-bonded to the silicon sensor.

Table 1. Radius, extent in the z direction, tilt angle and strip length for the strip barrel in the ITk Layout 03-00-00. The number of staves reported are for the full barrel.

Barrel layer	Number of staves	Radius [mm]	|z| [mm]	Tilt angle [degrees]	Strip length [cm]
0	56	399	0–1372	13	2.5
1	80	562	0–1372	12	2.5
2	112	762	0–1372	12	5
3	144	1000	0–1372	11	5

Table 2. Position of disks of the strip endcap in the ITk Layout 03-00-00.

Disk	Radius [mm]	Position [mm]
0	385	1512
1	385	1702
2	385	1952
3	385	2237
4	385	2532
5	385	2850

A redesign of the pixel endcap ring system took into consideration the altered envelope along the z-axis and the need to provide space for service routing in the radial direction. To meet the latter requirement, adjustments were made to the radial extent of the support tube in the inner pixel barrel. The redesign of the inner two layers of the pixel system involved incorporating staves for the traditional barrel region, featuring "flat" modules parallel to the beam line, and replacing the former inclined section with coupled rings sharing the same support structure for the two layers. This change has the advantage of allowing the services to be routed to modules in the innermost pixel layer outward in the radial direction, thereby minimizing the material in the innermost part of the detector. The transition to coupled rings required a re-optimization of the ring locations in the previously inclined section to ensure hermeticity and an adequate number of predicted hits within the constraints of the new support structure.

[2]Hermeticity is the ability of the detector to provide complete coverage of the particle trajectories in all directions, without any gaps or regions where particles could potentially escape detection.

2025 JINST 20 P02018

A substantial redesign was also implemented in the three outermost layers of the barrel pixel system to help the incorporation of quad modules, each consisting of 2×2 readout chips, within the inclined section. These modules in the inclined sections are mounted on rings supported by a shell structure. The transition from the initially planned dual chip (2×1) to quad chip modules results in a 50% reduction in the total number of rings. This adjustment allows the entire ITk to be equipped with both single- and quad-chip modules, eliminating the necessity for dual-chip modules. Additionally, it contributes to a reduction in the length of the inclined outer barrel. The inclination angles of the modules in the $r - z$ plane were re-optimized in accordance with the new layout. Furthermore, the length of the flat section in the three outermost pixel barrel layers was shortened to accommodate nine quad modules.

One of the most recent and significant modifications pertains to the innermost pixel layer. Following an extensive technical review, the ATLAS Collaboration decided in early 2020 to adjust the ITk layout, bringing this layer closer to the beam line to enhance the tracking performance. Consequently, the radius of the barrel section for this pixel layer was reduced from 39 to 34 mm, and the innermost point of the endcap rings was shifted inward from 36 to 33.2 mm. The reduction in the radius of the barrel section allowed a decrease in the number of staves from 16 to 12, and a re-optimization of the number and position of endcap rings in the innermost pixel layers, maintaining hit coverage equivalent to the previous layout. Additionally, the pixel sensor dimensions for the innermost pixel layer in the barrel were adjusted to 25 µm in the transverse plane and 100 µm in the longitudinal plane, while the rest of the pixel detector uses the original $50 \times 50\,\mu m^2$ pixels. While the innermost layer will suffer higher radiation damage with this smaller radius, the two innermost pixel layers are designed to be replaceable before the end of the HL-LHC data-taking.

The updated layout of the pixel barrel and endcaps is summarized in tables 3 and 4. A display of the full ITk layout presented in this document is shown in figures 2 and 3.

Table 3. Parameters for the pixel flat barrel and inclined rings in the ITk Layout 03-00-00. The number of sensors per row refers to a complete stave in the central, flat part of the barrel where sensors are placed parallel to the beam line. The number of inclined rings refers to both sides of the detector. "Triplets" consist of three connected read-out chips, each associated with a $2 \times 2\,cm^2$ sensor, while "quad" modules are made of four connected read-out chips associated with a single $4 \times 4\,cm^2$ sensor.

Barrel layer	Radius [mm]	Rows of sensors	Flat barrel $\lvert z \rvert$ [mm]	Flat sensors per row	Incl. rings $\lvert z \rvert$ [mm]	Incl. rings	Module type	Sensor dim. [μm^2]
0	34	12	0–245	24	–	–	triplets	25×100
1	99	20	0–245	12	–	–	quads	50×50
2	160	32	0–372	18	380–1035	2×6	quads	50×50
3	228	44	0–372	18	380–1035	2×8	quads	50×50
4	291	56	0–372	18	380–1035	2×9	quads	50×50

Figure 4 depicts the overall count of expected pixel and strip measurements along a track depending on its pseudorapidity. The data are derived from simulated single-muon events with a transverse momentum of 1 GeV . Across the entire detector acceptance, a minimum of nine measurements is maintained, with rare exceptions occurring only in cases where tracks pass through the gaps between pixel or strip barrel modules, in particular for particles produced at $z = 0$ cm and $\eta \sim 0$. This feature is enhanced in figure 4 given the generation of particles at $z = 0$ cm.

2025 JINST 20 P02018

Table 4. Parameters for the pixel endcaps in the ITk Layout 03-00-00. The radii refer to the innermost point of the sensors on a ring. The number of rings refers to both sides of the detector. "Triplets" consist of three connected read-out chips, each associated with a $2 \times 2\,\mathrm{cm}^2$ sensor, while "quad" modules are made of four connected read-out chips associated with a single $4 \times 4\,\mathrm{cm}^2$ sensor.

Ring layer	Radius [mm]	$\lvert z \rvert$ [mm]	Rings	Sensors per ring	Module type	Sensor dim. [$\mu\mathrm{m}^2$]
0	33.20	263–1142	2×15	18	triplets	50×50
0.5	58.70	1103–1846	2×6	30	triplets	50×50
1	80.00	263–2621	2×23	20	quads	50×50
2	154.50	1145.5–2850	2×11	32	quads	50×50
3	214.55	1145.5–2850	2×8	44	quads	50×50
4	274.60	1145.5–2850	2×9	52	quads	50×50

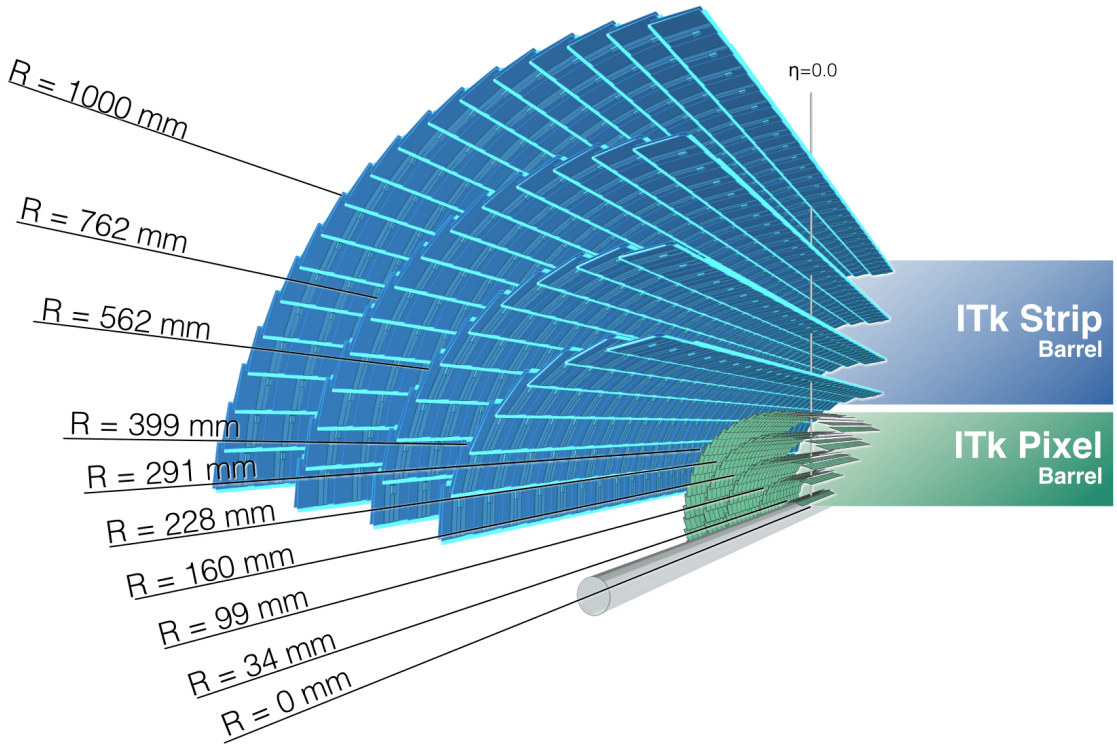

Figure 2. Transverse view of the Inner Tracker Layout 03-00-00 presented in this document.

3 Simulation

3.1 Geometry description and material

A major effort has been put over the last years in a new implementation of the simulation of the ITk Pixel and Strip detectors using the ATLAS software suite [34]. This new implementation makes use of the GeoModel tool suite [35] and relies on atomic XML configuration files assembled to create the full detector. It benefits from a significantly improved clarity and long-term maintainability, the latter guaranteed by the commitment of the ATLAS Collaboration to use the GeoModel library as the basis for its detector simulation for Run 4 and beyond [36].

2025 JINST 20 P02018

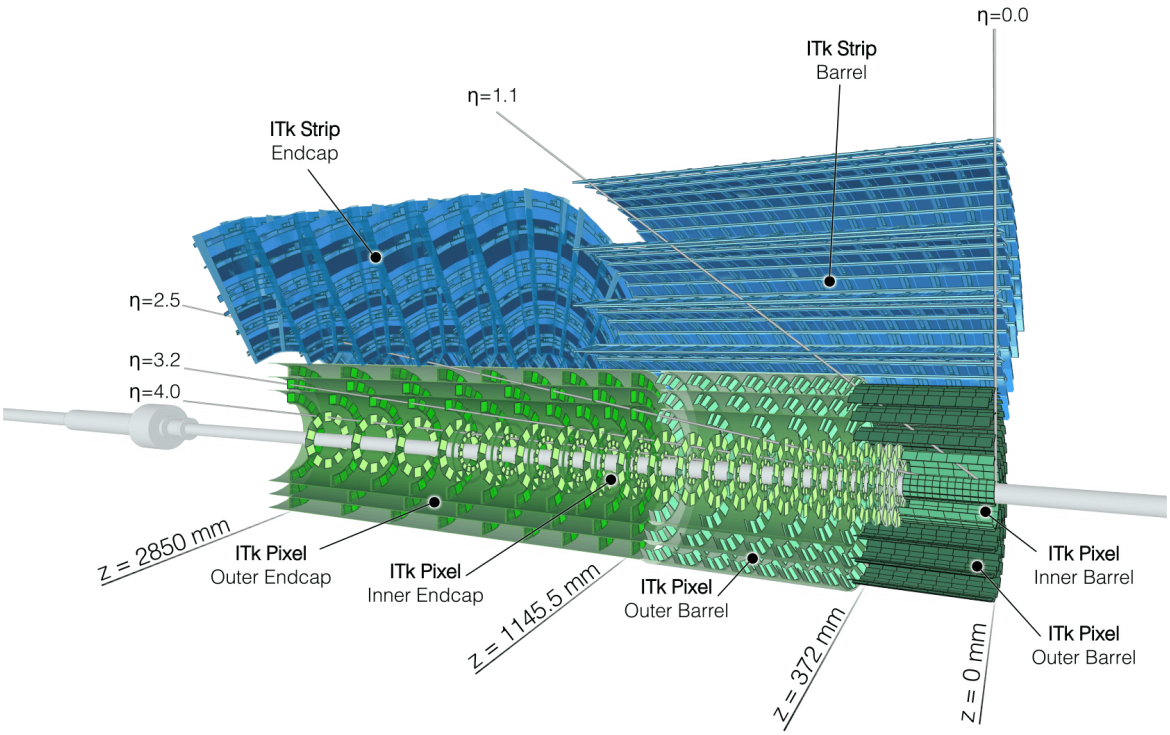

Figure 3. Longitudinal view of the Inner Tracker Layout 03-00-00 presented in this document.

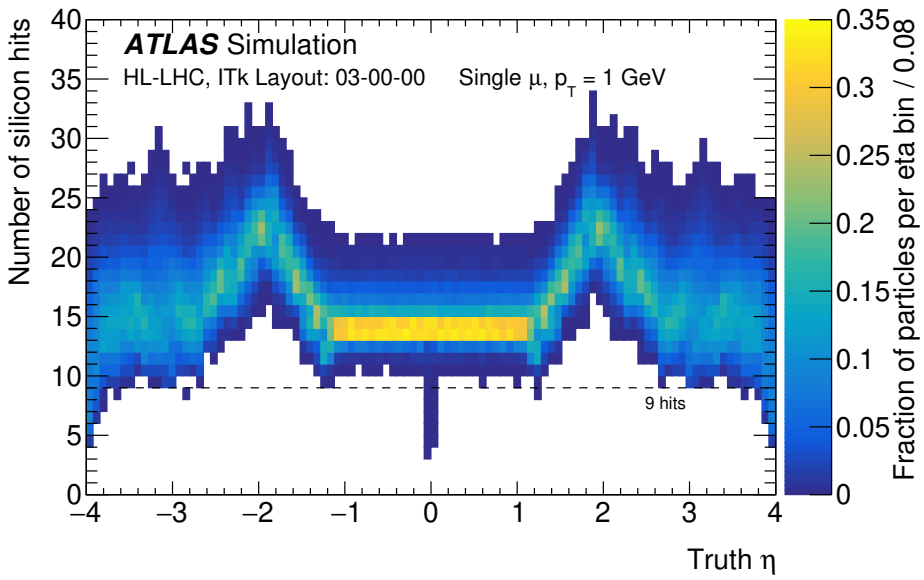

Figure 4. Number of combined potential strip and pixel measurements along a particle trajectory as a function of the truth particle pseudorapidity for the ITk Layout 03-00-00. A sample of single-muon events with $p_{\mathrm{T}} = 1$ GeV is used. The muons are produced with a uniform distribution between 0 to 2 mm in transverse distance to the beam line and at fixed values of $z = -15$ cm, 0 cm, and 15 cm, in equal amounts.

2025 JINST 20 P02018

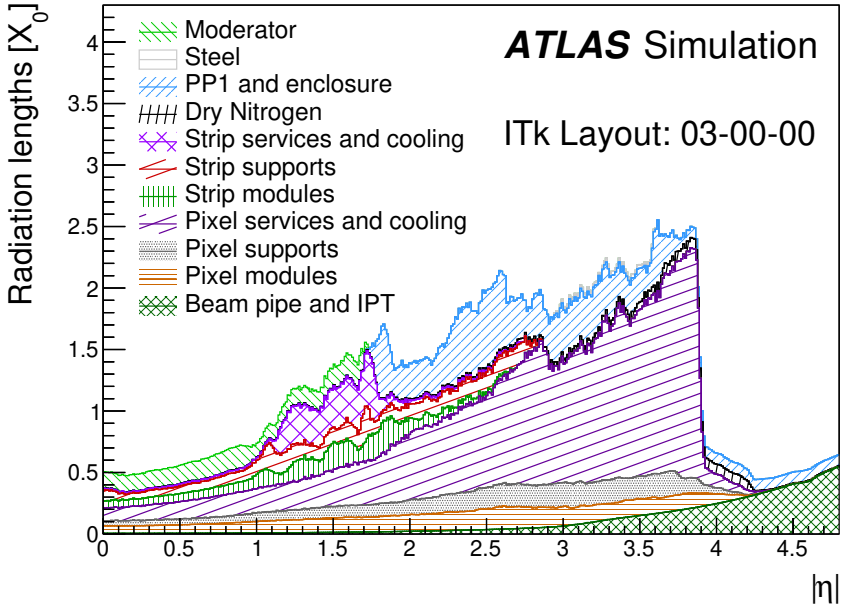

Figure 5. Integrated radiation length (X_0) traversed by a straight track as a function of the absolute pseudorapidity $|\eta|$ at the exit of the ITk volume for the ITk Layout 03-00-00, broken down by sub-system and material category. The Inner Positioning Tube (IPT) is a support carbon-fibre cylinder just outside the beam pipe. The Patch Panel 1 (PP1) is an interface located in the endcaps that facilitates power distribution, signal transmission, and optical conversion between the detector modules and external systems. The moderator is located beyond the active detector area.

Figures 5 and 6 present the integrated radiation length (X_0) and nuclear interaction length (Λ_0)[3] traversed by a straight track as a function of the absolute pseudorapidity at the exit of the ITk volume. The position of the origin of those tracks follows the expected HL-LHC beam spot distribution. The mean radiation and interaction lengths traversed by particles before reaching the minimum number of hits required for track reconstruction (see section 4.1) is shown in figure 7. The material budget in the central region $|\eta| < 1.5$ demonstrates an increase of up to 50% relative to the Run 3 Inner Detector, while significant reductions in the material are present in the more forward region. The material location in the r-z frame simulated for the studies presented here is illustrated in figure 8.

3.2 Simulation samples

To evaluate the performance of the generic track reconstruction, single-particle (muon, electron and charged pion) samples are simulated with a uniform η distribution for $|\eta| < 4.0$ and a fixed transverse momentum of 2, 10, or 100 GeV . To replicate the expected HL-LHC beam spot dimensions and positions, the particle origin positions are generated based on a Gaussian distribution with a width of 50 mm centered at $z = 0$ in the longitudinal direction, while a width of 12 µm centered at $r = 0$ is used for the transverse direction.

[3]The radiation length is defined as the average distance after which an electron's energy is decreased to 1/e of its initial value by material interactions, while the nuclear interaction length is defined as the mean distance between nuclear interactions sustained by a hadron.

2025 JINST 20 P02018

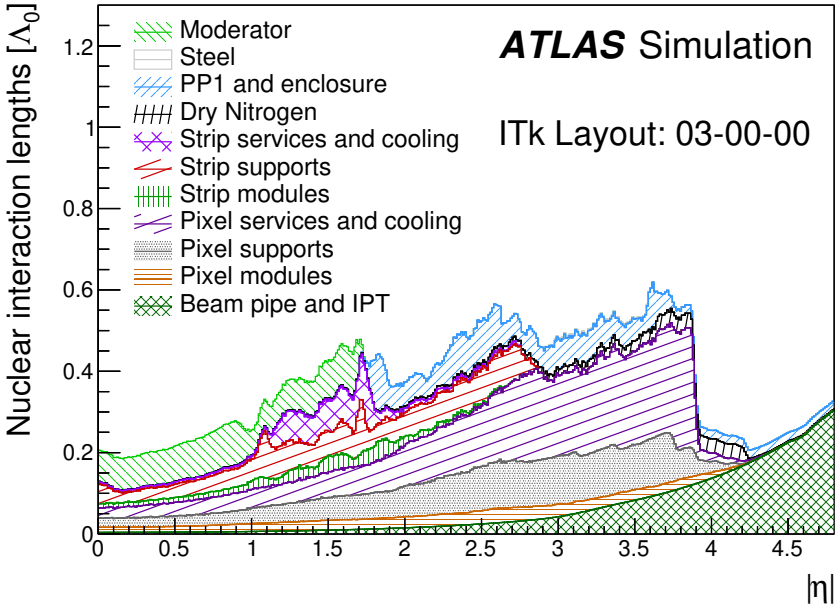

Figure 6. Integrated nuclear interaction length (Λ_0) traversed by a straight track as a function of the absolute pseudorapidity $|\eta|$ at the exit of the ITk volume for the ITk Layout 03-00-00, broken down by sub-system and material category. The Inner Positioning Tube (IPT) is a support carbon-fibre cylinder just outside the beam pipe. The Patch Panel 1 (PP1) is an interface located in the endcaps that facilitates power distribution, signal transmission, and optical conversion between the detector modules and external systems. The moderator is located beyond the active detector area.

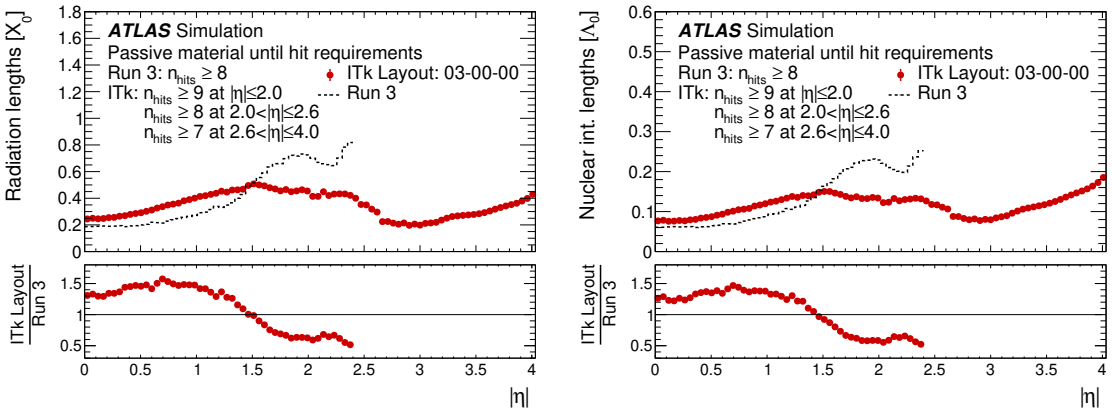

(a) (b)

Figure 7. Material thickness in (a) radiation lengths (X_0) and (b) nuclear interaction lengths (Λ_0) seen by particles until reaching the minimum number of hits required for track reconstruction. The ITk detector is compared with the Run 3 detector.

In addition, a $t\bar{t}$ sample at $\sqrt{s} = 14$ TeV is simulated to assess the performance of the track and vertex reconstruction, with different average pile-up ranges from 50 to 70, 130 to 150, and 190 to 210, labeled respectively as $\langle\mu\rangle = 60$, 140 and 200. For every simulated event, the number of pile-up

2025 JINST 20 P02018

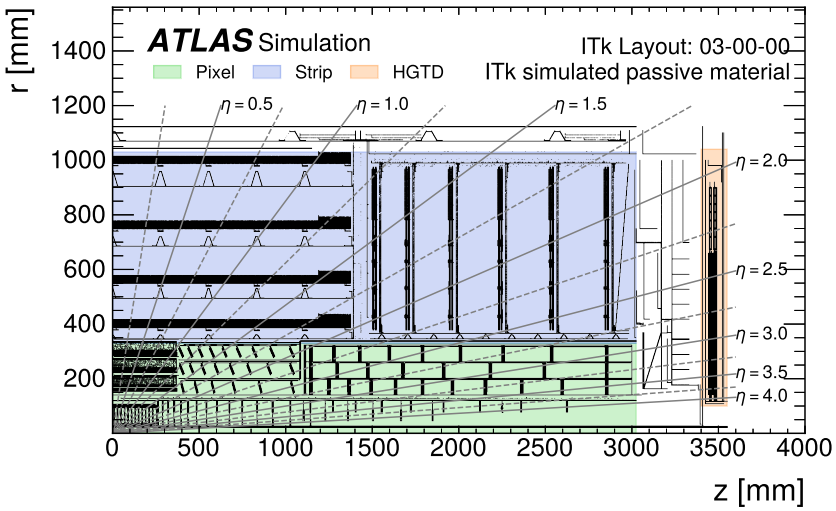

Figure 8. Location of the material for one quadrant of the ITk Layout 03-00-00.

interactions is randomly sampled from a Poisson distribution with a mean corresponding to the average pile-up. For comparison with the Run 3 detector performance, a $t\bar{t}$ sample at $\sqrt{s}$ = 13.6 TeV produced with the Run 3 detector geometry and a uniform pile-up profile between 0 and 80 is used. The production of $t\bar{t}$ events is modeled using the Powheg Box v2 [37–40] generator at next-to-leading-order in QCD with the NNPDF3.0nlo [41] parton distribution functions (PDF) and the h_{damp} parameter[4] fixed to 1.5 m_{top} [42], with m_{top} = 172.5 GeV used for the top-quark mass. The events are interfaced to Pythia 8.230 [43] to model the parton shower, hadronization, and underlying event, with the A14 set of tuned parameters [44] and using the NNPDF2.3lo set of PDFs [45]. The decays of bottom and charm hadrons are performed by EvtGen 1.6.0 [46]. Only $t\bar{t}$ events with a single leptonic W boson decay are considered. Minimum bias simulation samples are used in addition for specific studies, in which the average pile-up ranges are extended to cover the ranges 0 to 105, 95 to 175 and 165 to 210.

Finally, a sample of hypothetical Z' particles with a mass of $m_{Z'}$ = 4 TeV decaying with roughly equal probabilities into b-, c-, and light-quark jets is used to study the tracking performance in the core of high-p_{T} jets. The sample is constructed so that the resulting jet p_{T} spectrum is roughly uniform up to 5 TeV . The Z' events are produced with the Pythia 8.307 [47] Monte Carlo generator, using the A14 set of tuned parameters and the NNPDF2.3lo PDF set. The decay of heavy-flavor hadrons is handled by the EvtGen 2.1.1 [46] package. No additional proton-proton interactions are included in this sample.

The simulated events are processed through the full ATLAS detector simulation [48] based on the Geant4 toolkit [49].

3.3 Simulation of digitized readout signals

The energy depositions created by Geant4 undergo a digitization process to mimic the behavior of detector electronics and produce the readout signals [7]. This involves utilizing the energy deposited during each Geant4 step within the active silicon volume to calculate both the free charge and the

[4]The h_{damp} parameter is a resummation damping factor and one of the parameters that controls the matching of Powheg matrix elements to the parton shower and thus effectively regulates the high-p_{T} radiation against which the $t\bar{t}$ system recoils.

drift time to the readout surface. These calculations take into account various parameters such as sensor thickness, carrier mobility, depletion and bias voltages, and effects due to the magnetic field such as the directional drift of electrons, known as the Lorentz shift. Additionally, the simulation accounts for contributions from noise and capacitive coupling to neighboring channels. The algorithm then assesses the amount of charge collected in each channel, and if it surpasses a predetermined threshold, the corresponding channel is labeled as having fired.

The Bichsel straggling function [50] is used to simulate realistic charge depositions for thin pixel sensors. Modules in the innermost layer of the barrel, equipped with pixels with a pitch of $25 \times 100\ \mu m^2$, use a discriminator threshold of $900\,e$, while all other modules use a threshold of $600\,e$. Those thresholds are motivated by the expected behavior of the ITkPixV2 front-end chip to be used for the ITk Pixel detector [51]. When a pixel registers a charge exceeding the discriminator threshold, a 4-bit measurement of time-over-threshold (ToT) is emulated through a calibration function. This emulation results in an average ToT of seven bunch crossings for a charge of $10000\,e$. All hits with a charge surpassing the threshold are attributed to the specific bunch crossing associated with the particle that contributed the most to the charge. Noise is added to the charge from ionizing particles with a standard deviation of $75\,e$ ($100\,e$ for the innermost barrel layer); however, random/thermal noise is not yet included in the modeling. The resolution of the charge measurement is in any case expected to be primarily influenced by the limited number of bits in the ToT measurement rather than the noise. In the innermost layer, 3D pixel sensors are approximated as planar sensors, with Lorentz effects disabled to mimic the 3D sensor designs.

4 Reconstruction

4.1 Track reconstruction and selection

The track reconstruction process[5] begins by creating clusters from the individual channels within the strip and pixel subdetectors. In the case of the pixel detector, ToT information from each channel is accessible and is transformed into a representative charge measurement. The ToT-based calibration exploits the charge distribution within the cluster, enhancing the precision of the cluster position determination and its estimated uncertainty [52]. Additionally, the position estimate incorporates an assessment of the local incident angle of the track to further refine the cluster measurements. The distribution of pixel and strip clusters can be seen in figure 9, showing a total occupancy of approximately 5×10^5 clusters per event at $\langle\mu\rangle = 200$.

Pixel and strip clusters are transformed into three-dimensional representations, referred to as space-points. Strip space-points are constructed combining clusters on opposite module sides, incorporating the relative stereo angle between the strips on the two sides and assuming that the track trajectory points to the interaction region.

Track finding starts with the track seeding stage [53], during which seeds are built from triplets of pixel or strip space-points compatible with a helical track model. These seeds define a search path, and a combinatorial Kalman filter (CKF) [24, 54] identifies track candidates compatible with the initial seed

[5]This section describes the main tracking reconstruction pass, aiming to reconstruct prompt particles originating from the interaction point. In addition, there exist some specialized passes, for instance aiming to reconstruct tracks produced away from the interaction point (i.e., large-radius tracking), or a calorimeter-seeded back-tracking pass aiming to recover tracks from photon conversions. Describing such passes is outside the scope of this work.

2025 JINST 20 P02018

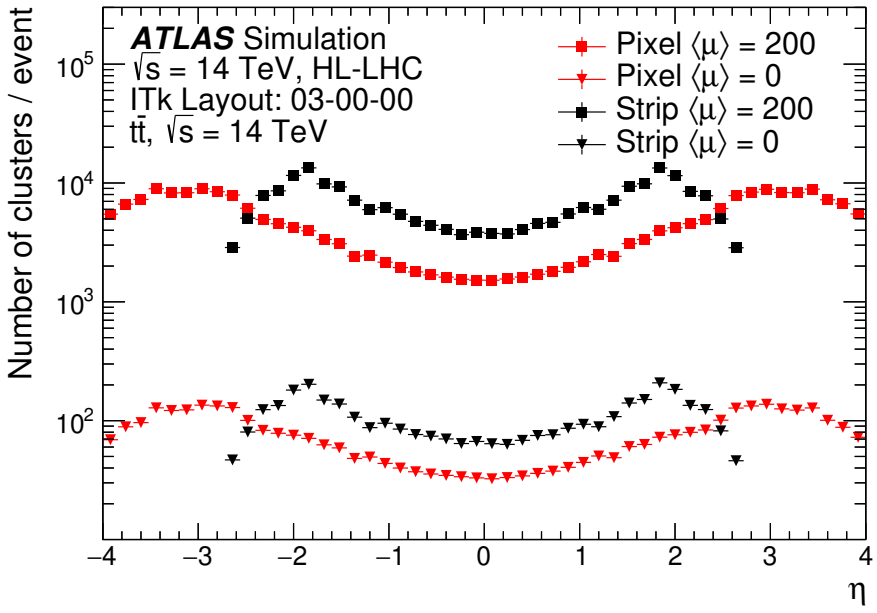

Figure 9. Distribution of the mean number of pixel and strip clusters vs η, at $\langle\mu\rangle = 0$ and $\langle\mu\rangle = 200$.

parameters, extending the seeds with additional space-points. In the CKF, the material interactions and noise contributions are approximated based on the number of detector layers crossed, rather than relying on detailed material and magnetic field description, which are used only in the final track fit. Seeds are skipped if they are constructed from clusters already associated with a track candidate. Two iterations of track finding are carried out sequentially, starting with strip seeds followed by pixel seeds, to enhance the overall track reconstruction efficiency. Strip seeding is performed first, as cluster density is lower in the outermost regions of the detector. This approach allows pixel clusters associated with a strip seed to be removed, reducing the number of possible pixel cluster combinations in the subsequent pixel seeding, which is computationally advantageous. Initially, a pion hypothesis is adopted to model the energy loss resulting from particle interactions with the detector material. If a track seed cannot be extended to form a complete track but aligns with an electromagnetic cluster detected in the calorimeter, the track finding algorithm is applied under an electron hypothesis. This electron hypothesis accommodates energy losses of up to 30% due to bremsstrahlung during each interaction with a detector material layer.

In the final stage of track reconstruction, an ambiguity-solving algorithm is executed to determine the definitive assignment of clusters to competing tracks. During this stage, a precision fit is performed using a global χ^2-minimization technique [55], incorporating precise data regarding the material model and magnetic field. Holes, defined as missing measurements on a track where active sensors should have registered hits, are assessed based on the track trajectory and information about the detector geometry and status. The tracks are ranked according to their hit count and the quality of their fit. Ambiguities between multiple track candidates are resolved by comparing their respective scores, and the track with the highest score is retained [23, 56].

In a high track density environment, such as the core of high-p_{T} jets, the separation between different charged particles is close to the detector granularity. In such cases, charge depositions from different particles can overlap and be reconstructed as single merged clusters. Tracks that share clusters

2025 JINST 20 P02018

Table 5. Set of requirements applied during the track reconstruction in different pseudorapidity intervals. A hole is an intersection of the predicted trajectory of the particle with an active sensor element from which no measurement is assigned to the track (inactive sensors are not taken into account). The hole counting does not consider layers before the first and after the last hit. The longitudinal and transverse impact parameters, z_0 and d_0, are defined relative to the mean position of the beam spot.

Requirements	Pseudorapidity interval		
	$\lvert\eta\rvert \leq 2.0$	$2.0 < \lvert\eta\rvert \leq 2.6$	$2.6 < \lvert\eta\rvert \leq 4.0$
Pixel + strip hits	≥ 9	≥ 8	≥ 7
Pixel hits	≥ 1	≥ 1	≥ 1
Holes	≤ 2	≤ 2	≤ 2
p_T [MeV]	> 900	> 400	> 400
$\lvert d_0\rvert$ [mm]	< 2.0	< 2.0	< 10.0
$\lvert z_0\rvert$ [cm]	< 20.0	< 20.0	< 20.0

are penalized in the ambiguity solver stage and they may consequently fail to satisfy the quality criteria and be rejected. The identification and special treatment of merged clusters is thus crucial for ensuring a high track reconstruction performance in dense environments, as it has a strong impact on the track reconstruction efficiency and the precision of the reconstructed track parameters. To optimize the tracking performance in this regime in Run 1, 2 and 3, ATLAS uses machine-learning-based algorithms dedicated to distinguishing clusters compatible with deposits from a single or multiple charged particles [57, 58]. This identification is performed only when a cluster is used by multiple tracks. The implementation and optimization of such algorithms for the ITk geometry is ongoing as of this writing, and an emulation of those algorithms based on particle-level information that reproduces the performance of the Run 3 machine-learning based algorithms is conservatively used in the meantime.

The accepted tracks must satisfy the η-dependent criteria outlined in table 5. The criteria are made η-dependent to accommodate for the non-trivial detector layout, both in terms of number of sensitive elements and of distribution of the material as a function of η. They give in particular the possibility to maintain a uniform track reconstruction efficiency through the detector.

4.2 Vertex reconstruction and selection

To distinguish the different proton-proton collisions in a single bunch crossing, the reconstructed tracks are used to identify the position of the interactions along the beam axis. These are referred to as primary vertices (PVs). Typically, only a single pp interaction per recorded bunch crossing generates physics of interest for analysis. The corresponding PV is known as the *hard-scatter* vertex and is selected among all the reconstructed PVs. The position of the hard-scatter vertex is used for example as a reference for pile-up rejection, or in flavor-tagging algorithms.

Primary vertex reconstruction, both with the Run 3 Inner Detector and ITk, relies on the adaptive multi-vertex finder (AMVF) algorithm [59], which simultaneously reconstructs multiple vertices, allowing tracks to be associated with several vertices at the same time. The primary vertex finding process incorporates only a subset of the entire set of reconstructed tracks. In addition to the track selection criteria applied during reconstruction, the selections outlined in table 6 are imposed to ensure reliable impact parameter estimates.

2025 JINST 20 P02018

Table 6. Set of requirements applied to tracks during the AMVF vertex reconstruction, for the ID Run 3 and ITk Run 4 configurations. The uncertainties associated with d_0 and $z_0 \sin\theta$, $\sigma(d_0)$ and $\sigma(z_0 \sin\theta)$, are estimated from the global χ^2 fit used in the track reconstruction, taking into account individual hit position uncertainties.

Requirements	ID Run 3	ITk Run 4
Pixel hits	≥ 1	≥ 3
Pixel holes	≤ 1	≤ 1
SCT / Strip hits	≥ 4	≥ 0
Silicon hits	≥ 6	≥ 7
p_T [MeV]	> 500	> 900
$\lvert d_0 \rvert$ [mm]	< 4.0	< 1.0
$\sigma(d_0)$ [mm]	< 5	< 0.35
$\sigma(z_0 \sin\theta)$ [mm]	< 10	< 2.5

The AMVF uses a vertex seed finder to identify potential vertex candidates along the beamline in the z-direction:

- Each track is represented by a Gaussian probability distribution $P(r, z)$ centered at its point of closest approach (d_0, z_0). The track densities are summed to identify global maxima in track density, representing the initial seeds used to reconstruct vertices.
- Through an iterative process, a new vertex candidate, along with all tracks with z_0 agreeing with the vertex candidate within a 0.5 mm window, is added to the pool of vertex candidates managed by the adaptive Kalman filter multi-vertex fit.
- All vertices undergo a refitting process using the adaptive Kalman filter multi-vertex fit, where each track may contribute to multiple vertices. Tracks with a low adaptive weight in the fit, computed based on a χ^2 compatibility criterion with the vertex position described in ref. [59], are eliminated from the fit of a specific vertex.
- The new vertex candidate is preserved if the vertex is identified with more than two tracks, the cumulative adaptive weights are not excessively low, and the new vertex is more than three standard deviations away from any other candidate.
- This procedure is reiterated until there are no more vertex candidates or the maximum number of iterations is reached.

Among all of the reconstructed vertices in each event, the one with the largest Σp_{T}^2 of its associated tracks, referred to as the hard-scatter vertex, is selected as the one of interest. This choice is motivated by the fact that pile-up events are dominated by soft QCD interactions.

5 Expected tracking and vertexing performance

5.1 Seeding performance

The performance of the seeding algorithm is assessed using different figures of merit that rely on associating seeds with stable charged particles produced by Monte Carlo simulation. A seed is

considered matched with a particle if more than half of its measurements originate from this particle, and the fraction of particles matched to at least one seed is defined as the *physics* seeding efficiency.

The *technical* seeding efficiency represents the efficiency to find seeds for reconstructable particles, and is defined as the fraction of seed matches among particles providing at least three measurements in the detector. By construction, this efficiency does not depend on the detector material or on the layout hermeticity, allowing the isolation of the algorithmic seeding efficiency.

Figure 10 displays the physics seeding efficiency as a function of the particle η and p_{T} (labeled as "Truth η" and "Truth p_{T}") in $t\bar{t}$ events with an average pile-up of 200, for particles from the hard-scatter event with p_{T} larger than 1 GeV . The technical and physics seeding efficiencies combining pixel and strip seeding are both displayed in figure 11. The η-dependence of the seeding efficiency directly reflects the number of available measurements in the detectors, which can be inferred from the detector layout visible in figure 1. An inclusive physics seeding efficiency larger than 85% is achieved over the whole phase space and reaches 95% or more for particles with p_{T} larger than 10 GeV . The lower efficiency at low p_{T} is related to material interactions, more likely to affect low-p_{T} particles. This affects strip seeds more significantly, as they are reconstructed after the particles have crossed a larger amount of material. The very high technical efficiency confirms that most of the physics inefficiency is indeed associated with material interactions.

While the pixel physics seeding efficiency is very close to the combined physics seeding efficiency, the strip seeds provide some useful redundancy in case of potential pixel detector defects. Figure 12 presents the number of seeds per particle as a function of η and p_{T}. On average, more than six seeds are found for all particles, as a particle typically leaves many hits in the detector, allowing for the construction of multiple triplets (seeds) from these hits. This abundance of seeds ensures the robustness of the seeding process against potential detector defects or misalignment.

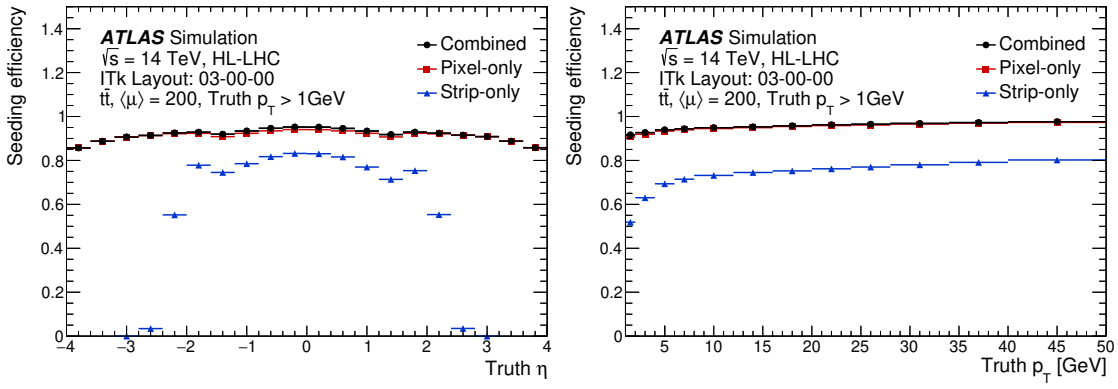

(a) (b)

Figure 10. Expected physics seeding efficiency as a function of (a) η and (b) p_{T} for $t\bar{t}$ events at $\langle\mu\rangle = 200$ for hard-scatter particles with $p_{\mathrm{T}} > 1$ GeV. The seeding efficiency is shown separately for pixel-only, strip-only and both combined.

5.2 Efficiency

Similarly to seeds, two different definitions of the tracking efficiency are used to distinguish between pattern recognition effects and detector effects. The physics tracking efficiency is defined as the

2025 JINST 20 P02018

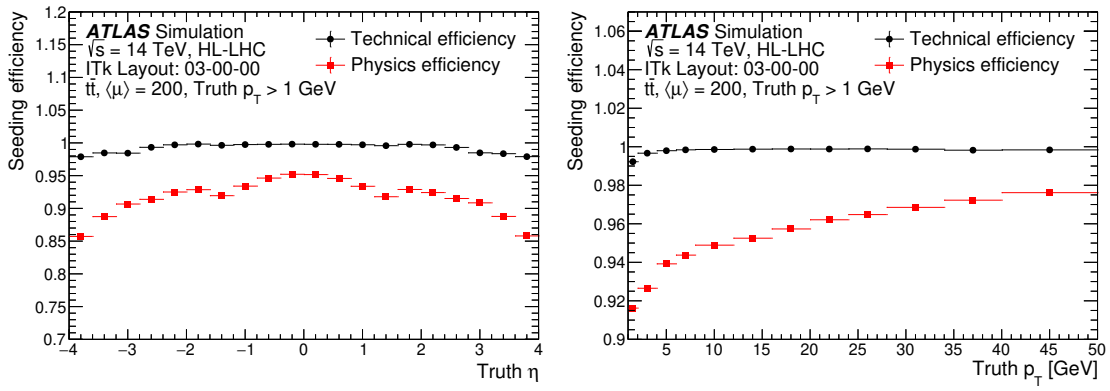

(a) (b)

Figure 11. Expected technical and physics seeding efficiencies as a function of (a) η and (b) p_{T} for $t\bar{t}$ events at $\langle\mu\rangle = 200$ for hard-scatter particles with $p_{\mathrm{T}} > 1\,\mathrm{GeV}$. The efficiency is shown for the combined pixel and strip seeding.

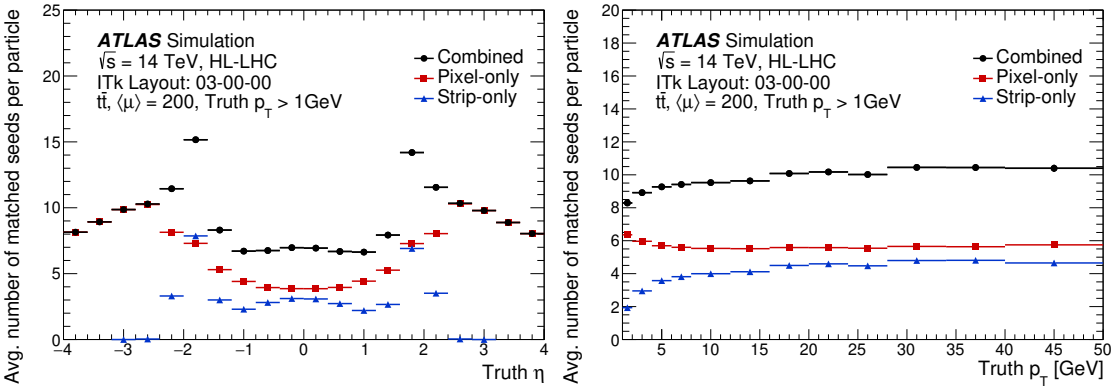

(a) (b)

Figure 12. Expected number of seeds per particle as a function of (a) η and (b) p_{T} for $t\bar{t}$ events at $\langle\mu\rangle = 200$ for hard-scatter particles with $p_{\mathrm{T}} > 1\,\mathrm{GeV}$, shown separately for pixel-only, strip-only and both combined.

fraction of charged particles associated with a reconstructed track. To do the particle-to-track matching, information about individual particle contributions to a given simulated silicon hit is used. The matching criterion is based on the weighted fraction of measurements used to reconstruct a track common with the charged particle of interest, defined as

$$R_{\mathrm{match}} = \frac{2 \times N_{\mathrm{common}}^{\mathrm{pix}} + N_{\mathrm{common}}^{\mathrm{strip}}}{2 \times N_{\mathrm{reco}}^{\mathrm{pix}} + N_{\mathrm{reco}}^{\mathrm{strip}}}, \tag{5.1}$$

with $N_{\mathrm{reco}}^{\mathrm{pix/strip}}$ ($N_{\mathrm{common}}^{\mathrm{pix/strip}}$) representing the number of clusters from the different subdetectors used in the reconstruction of a given track (associated both to the particle and the reconstructed track). Since strip sensors are installed in back-to-back stereo pairs, a particle crossing a strip module will usually acquire two silicon hits, as opposed to a single hit per pixel module; the different weights therefore give equal importance to the two measurement types. A charged particle is considered to be reconstructed if it is matched to a track with $R_{\mathrm{match}} > 0.5$.

2025 JINST 20 P02018

The *technical* tracking efficiency represents the fraction of track matches among the charged particles providing enough measurements in the detector to satisfy the reconstruction cuts. It is used to assess the algorithmic efficiency of the tracking reconstruction and decouple it from the detector material or the layout hermeticity.

The physics tracking efficiency for muons with $p_{\mathrm{T}} = 2$, 10 and 100 GeV without pile-up is presented in figure 13. The expected efficiency is compatible with the one obtained with the ATLAS Run 3 detector. The efficiency is above 99.5% for 2 GeV muons and compatible with 100% for larger p_{T} up to $|\eta| = 3.6$. A small drop of efficiency down to 99% is present in the very forward region of the ITk detector, due to the smaller number of available measurements in that region. The physics tracking efficiency for 10 GeV muons, electrons and pions is shown in figure 14. Although the tracking efficiency for electrons and pions is lower due to their higher interaction rate with the detector material, it is expected to remain above 85% for all types of prompt and stable charged particles. In the forward region ($|\eta| > 3.0$), figure 7 illustrates a steeper increase in nuclear interaction lengths compared with radiation lengths. Consistent with these material distributions, the tracking efficiency for pions in this region is more significantly reduced than that for electrons.

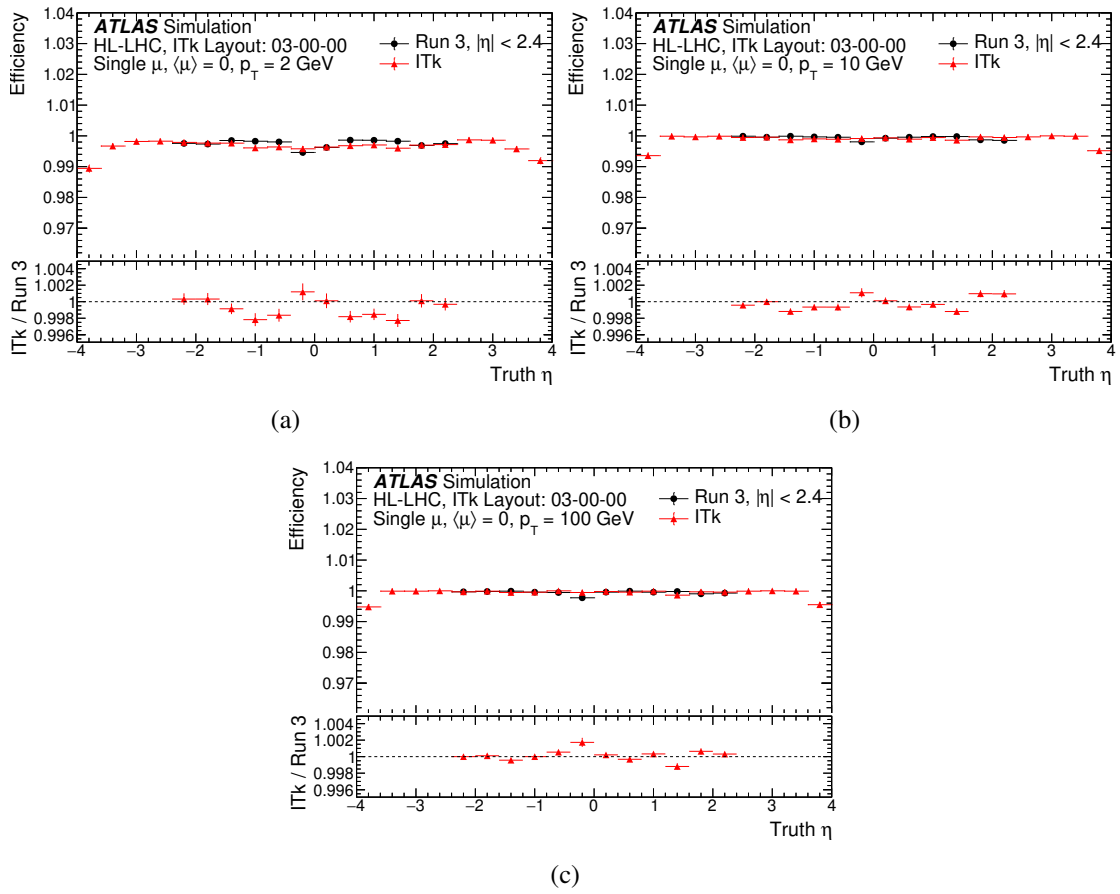

Figure 13. Expected physics tracking efficiency for single muons with (a) $p_{\mathrm{T}} = 2$, (b) 10 and (c) 100 GeV without pile-up. The results are compared for muons between the ITk and the Run 3 detector.

Figure 15 emphasizes the expected tracking performance at $\langle\mu\rangle = 200$, showcasing the physics efficiency in $t\bar{t}$ events for particles with $p_{\mathrm{T}} > 1$ GeV within the detector acceptance, stemming from

2025 JINST 20 P02018

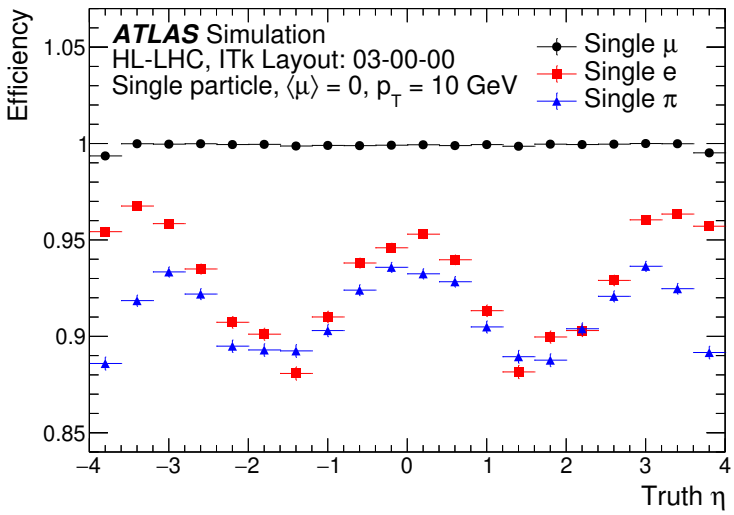

Figure 14. Expected physics tracking efficiency for single muons, electrons and pions with $p_{\mathrm{T}} = 10\,\mathrm{GeV}$ without pile-up.

the hard-scatter interaction. A comparison is made between this efficiency and that obtained with the Run 3 detector, in conditions with a uniform $\langle\mu\rangle$ distribution between 0 and 80. The physics efficiency in the central region of the ITk detector is expected to be maintained within 5% of that of the Run 3 detector, despite the larger material budget of ITk discussed in section 3.1. The efficiency achieved in the newly accessible forward region with $2.5| < |\eta| < 4.0$ is similar to the one achieved in the central region of ITk.

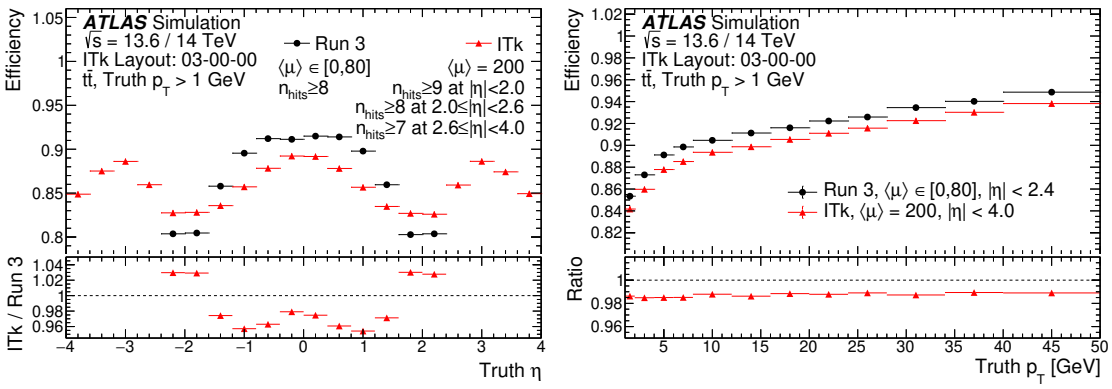

(a) (b)

Figure 15. Expected physics tracking efficiency as a function of (a) η and (b) p_{T} in $t\bar{t}$ events at $\langle\mu\rangle = 200$ for hard-scatter particles with $p_{\mathrm{T}} > 1\,\mathrm{GeV}$ with the ITk detector compared with the Run 3 detector, in conditions with a uniform $\langle\mu\rangle$ distribution between 0 and 80.

Figure 16 shows the technical tracking efficiency and the physics tracking efficiency for tracks from the hard-scatter interaction in $t\bar{t}$ events at $\langle\mu\rangle = 200$. The difference between the two quantities originates mainly from interactions of charged particles with detector material before reaching the required number of measurements.

2025 JINST 20 P02018

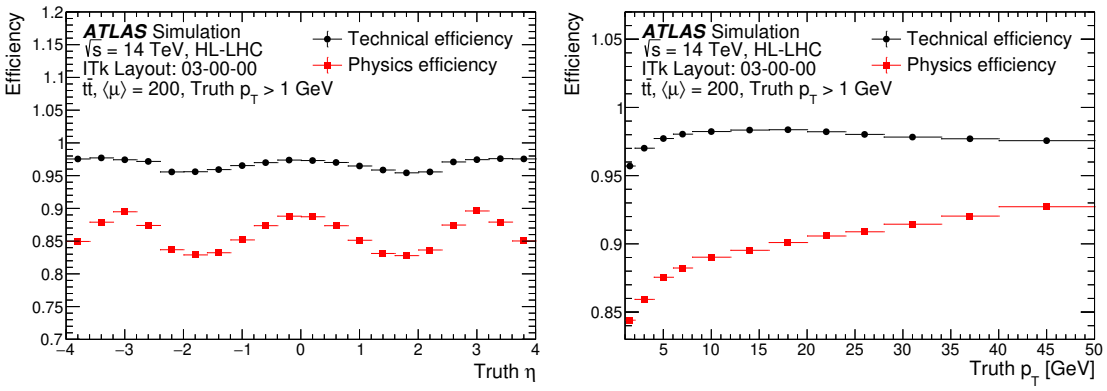

(a) (b)

Figure 16. Comparison between the expected technical and physics tracking efficiencies as a function of (a) η and (b) p_{T} in $t\bar{t}$ events at $\langle\mu\rangle = 200$ for hard-scatter particles with $p_{\mathrm{T}} > 1$ GeV with the ITk detector.

The stability of the physics tracking efficiency at different pile-up conditions and in different $|\eta|$ ranges is shown in figures 17 and 18. The efficiency at $\langle\mu\rangle = 200$ is within 0.5% of the efficiency achieved at $\langle\mu\rangle = 0$. A similar pile-up robustness is observed in the different $|\eta|$ ranges considered.

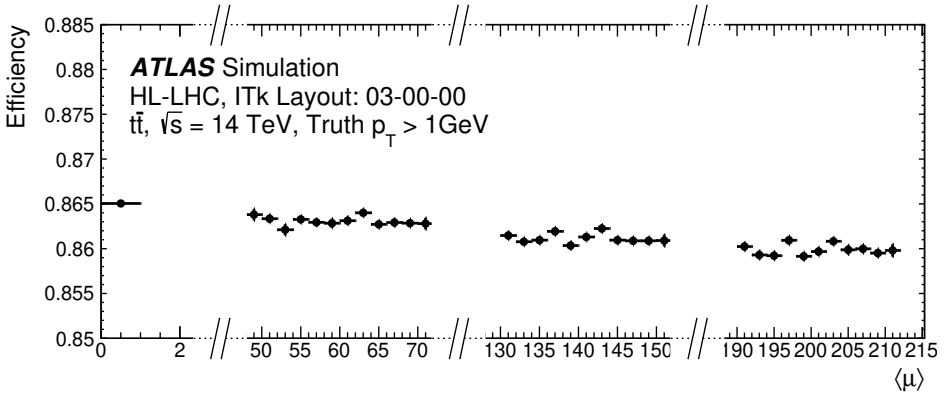

Figure 17. Expected physics tracking efficiency as a function of pile-up in $t\bar{t}$ events for hard-scatter particles with $p_{\mathrm{T}} > 1$ GeV with the ITk detector.

In the following, the performance of track reconstruction within jets is shown for a $Z'(m = 4\,\mathrm{TeV})$ Monte Carlo sample, where the rate of cluster merging is much higher than in $t\bar{t}$ events due to the larger fraction of high-p_{T} jets. For the studies presented here, jets are reconstructed by clustering energy deposits in the calorimeter with the anti-k_t algorithm [60] with a radius parameter $R = 0.4$, implemented in FastJet [61]. Tracks are matched to jets based on their angular separation ΔR(track, jet) from the jet axis, required to be lower than 0.4. To isolate the effects correlated with dense hadronic environments from those due to interactions with the detector material, the efficiency is presented for jets with $|\eta| < 1.2$, in the central region where the material budget is the lowest, and for particles with $p_{\mathrm{T}} > 10\,\mathrm{GeV}$, less impacted by material effects.

Figure 19(a) highlights the physics tracking efficiency expected for charged particles within high-p_{T} jets when no dedicated merged cluster identification is used. Tracks located in the core

2025 JINST 20 P02018

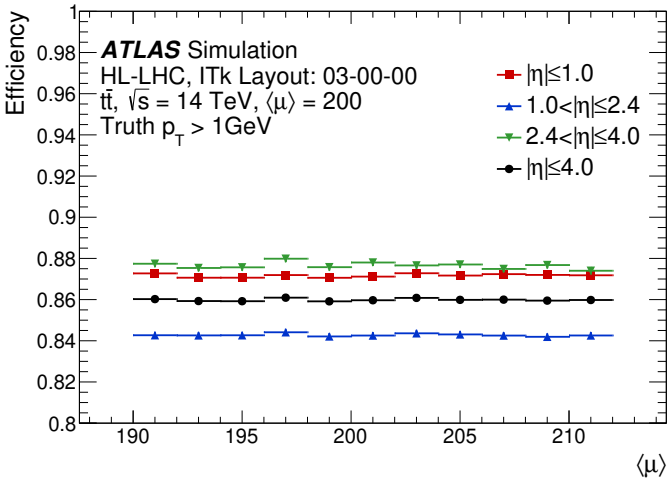

Figure 18. Expected physics tracking efficiency as a function of pile-up in $t\bar{t}$ events at $\langle\mu\rangle = 200$ for hard-scatter particles with $p_{\mathrm{T}} > 1$ GeV with the ITk detector in different $|\eta|$ ranges.

of the jets have on average a larger p_{T}, which explains why the efficiency is higher in the core of jets for a jet p_{T} up to 700 GeV . On the other hand, the particle density increases with the jet p_{T}, inducing a decrease in the physics tracking efficiency. This effect is more pronounced in the core of the jets where the particle density is highest. The potential benefit from a dedicated algorithm used for identifying merged clusters is shown in figure 19(b), which compares the performance obtained when no merged pixel cluster identification or when a perfect truth-based identification is used. To optimize the tracking performance in high track-density environments, ATLAS uses a machine-learning-based merged pixel cluster identification algorithm [57, 58] that has not yet been adapted for use in Run 4. The commissioning of dedicated algorithms for the ITk pixel detector will be one of the main focuses of upcoming developments.

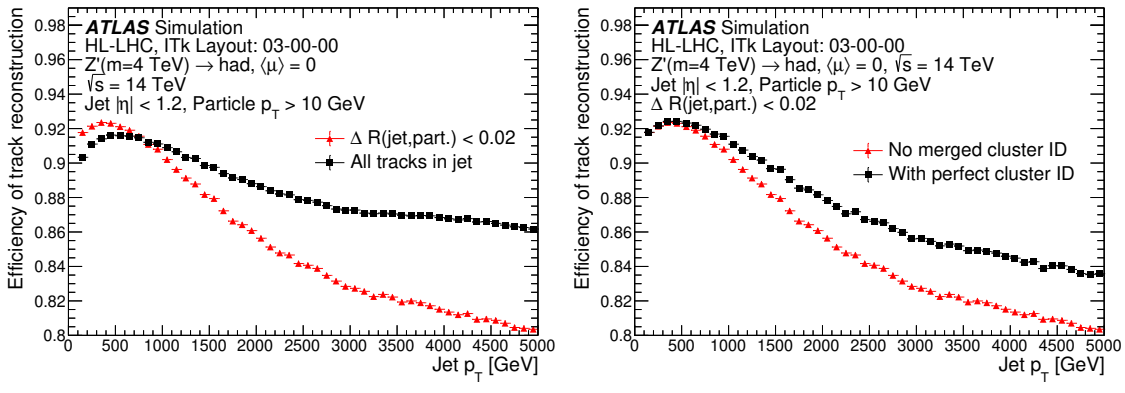

(a) (b)

Figure 19. Physics tracking efficiency for tracks in jets as a function of the jet p_T in Z' events in which the Z' decays hadronically, comparing (a) the inclusive efficiency for all tracks matched to the jet ($\Delta R < 0.4$) or within the jet core ($\Delta R < 0.02$) and (b) reconstruction scenarios with perfect, or no, classification of merged clusters in the jet core.

2025 JINST 20 P02018

5.3 Number of tracks, mis-reconstructed and fake track rates

Figure 20 illustrates the count of reconstructed tracks with $p_{\mathrm{T}} > 1\,\mathrm{GeV}$ at $\langle\mu\rangle = 200$ in $t\bar{t}$ events. In the ideal case where all tracks are well-reconstructed and the tracking efficiency is not reduced with pile-up, a linear increase in the number of tracks as a function of the number of interactions[6] is expected. In reality, a small quadratic component is observed in the number of reconstructed tracks as a function of the number of interactions, caused for instance by a certain fraction of particles that would not be reconstructed due to the minimum number of hits requirement (cf. table 5) but which are assigned to tracks also containing mis-attributed hits from pile-up particles, allowing them to satisfy the reconstruction criteria. There also exist a small fraction of tracks arising from combinations of hits not closely corresponding to any charged particle, known as fake tracks. Tracks from either source are collectively referred to as mis-reconstructed tracks, and their number is expected to scale super-linearly with the number of interactions. The number of well-reconstructed tracks as a function of the number of interactions can be estimated by fitting a linear function to the number of tracks distribution in the low pile-up regime, where the number of fake and mis-reconstructed tracks is expected to be negligible. The slope of this linear fit is then reduced linearly as a function of μ, to take into account the relative efficiency reduction of up to 0.7% at $\langle\mu\rangle = 200$. On the other hand, the total number of reconstructed tracks as a function of the number of interactions follows a quadratic function; therefore the fraction of mis-reconstructed tracks can be estimated from the difference between a quadratic fit to the number of tracks distribution and this linear fit, extrapolated to the full pile-up range. This fraction, shown in figure 21 for a minimum bias sample, reaches at most 2% at $\langle\mu\rangle = 200$. As a comparison, in Run 3 the mis-reconstructed track rate at the typical Run 3 leveling target of $\langle\mu\rangle = 64$ is approximately 6.5%. This reduction in the rate of mis-reconstructed tracks is primarily due to the optimized layout of the ITk detector, which provides in particular a greater number of silicon hits. These additional hits enhance the track reconstruction precision by enabling tighter selection criteria. The expected fake track creation rate can be estimated from Monte Carlo simulation, using the same matching probability distribution used to calculate the tracking efficiency. Figure 22 shows the expected fraction of tracks with a matching probability lower than 50% and features an expected fake track creation rate of approximately 3×10^{-4} at $\mu = 200$, showcasing the excellent fake track suppression capabilities of the ITk. Moreover, a comparison with figure 21 shows that fake tracks are not expected to be a dominant source of mis-reconstructed tracks.

5.4 Track parameter resolution

The resolution on track parameters is estimated from reconstructed tracks associated with charged particles. The distribution of the difference between the reconstructed track parameter and the corresponding quantity for the simulated particle is iteratively truncated from its outliers, which lie more than three standard deviations away from the mean of the distributions, until the distribution is left invariant. Up to 5% (1%) of the tracks associated with muons with $p_{\mathrm{T}} = 2\,\mathrm{GeV}$ (100 GeV) are found to be outliers in the process. The standard deviation of the core distribution is defined as the intrinsic measurement resolution of the track parameters.

Figures 23 to 25 display the expected resolution on the transverse (d_0) and longitudinal (z_0) impact parameters and the transverse momentum for simulated muons with $p_{\mathrm{T}} = 2$ and 100 GeV,

[6]The number of interactions follows a Poisson distribution with mean $\langle\mu\rangle$.

2025 JINST 20 P02018

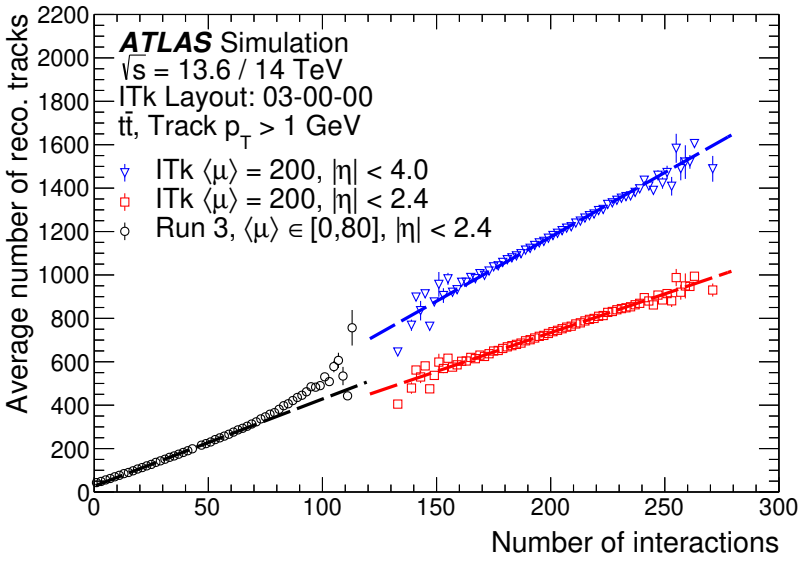

Figure 20. Number of reconstructed tracks per event with $p_{\mathrm{T}} > 1$ GeV as a function of the number of interactions for $t\bar{t}$ events at $\langle\mu\rangle = 200$ with the ITk detector compared with the Run 3 detector, in conditions with a uniform $\langle\mu\rangle$ distribution between 0 and 80. The dashed lines illustrate the results of linear fits performed over the limited range corresponding to $\langle\mu\rangle$ between 120 and 280 for the ITk and between 20 and 60 (extrapolated to 0–120) for the Run 3 detector to illustrate the pile-up dependence of this quantity.

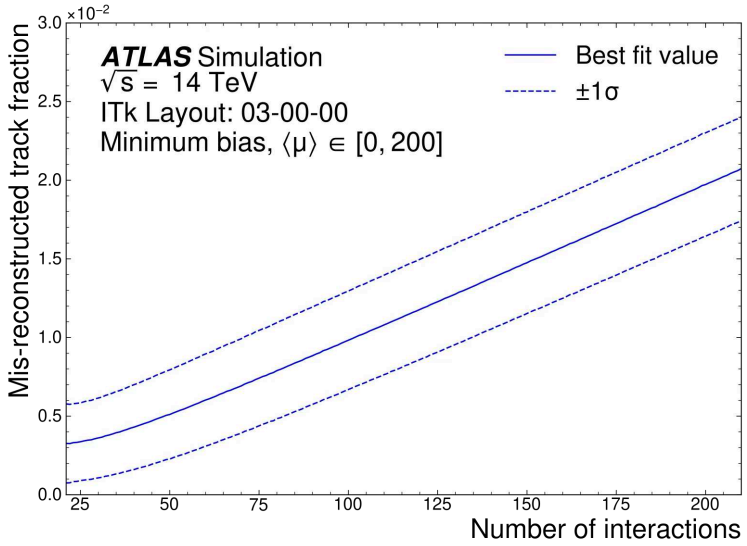

Figure 21. Fraction of mis-reconstructed tracks, defined as the difference between a quadratic fit in the full μ range and a linear fit extrapolated from the $\mu < 20$ region. The number of tracks corresponding to real particles and containing enough hits to satisfy the reconstruction criteria is expected to scale linearly with pile-up. The mis-reconstructed track population is composed of fake tracks not corresponding to any particle and tracks corresponding to actual particles but that include mis-attributed hits from pile-up particles, and is expected to increase faster than linearly with pile-up.

2025 JINST 20 P02018

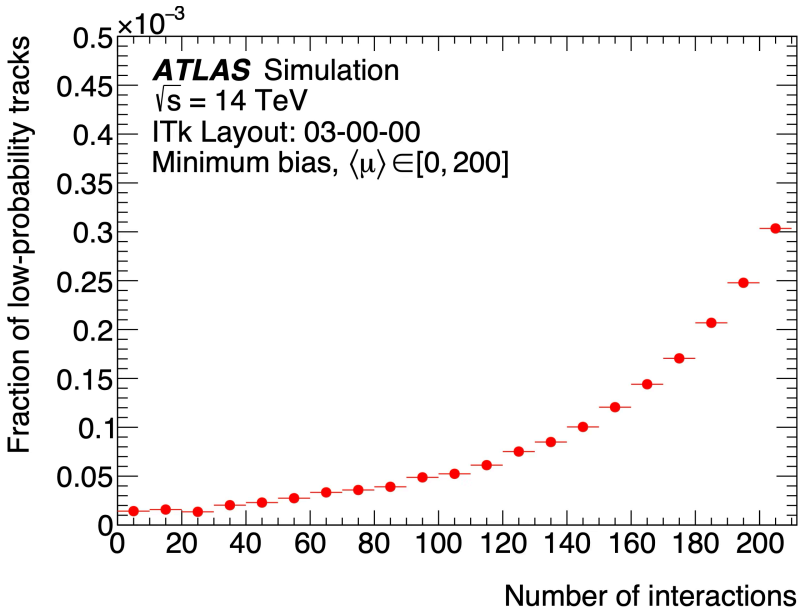

Figure 22. Fraction of all tracks with matching probability less than 50% as computed in Monte Carlo simulation, which estimates the fraction of tracks not closely corresponding to a charged particle, also known as the fake track creation rate.

compared between the ITk and the Run 3 ATLAS detector. The slight worsening of the z_0 resolution observed near $\eta = 0$ in figure 24 is associated with the fact that position measurements from the pixel detector are calibrated taking into account the charge distribution within the cluster and the angle of incidence of the track. As particles with $\eta \sim 0$ typically create one-pixel-wide clusters with normal incident angles, there is therefore no information to be exploited to improve the position resolution in such cases. Due to the comparable radius of the innermost pixel layers and thanks to the smaller pixel pitch (25×100 or $50 \times 50\,\mu m^2$ for ITk, $50 \times 250\,\mu m^2$ for the Run 3 detector [62, 63]), the d_0 resolution is improved by up to 20% and the z_0 resolution by up to a factor of two with ITk for 2 GeV muons, mainly in the central part of the detector where the material budget is minimal. This advantage is even more pronounced for 100 GeV muons, which are less affected by multiple scatterings from material. In this case, the d_0 and z_0 resolutions are significantly improved, by a factor of up to two and four respectively. The transverse momentum resolution with ITk is expected to surpass the Run 3 resolution due to the superior resolution in the bending plane provided by the silicon microstrip sensors in ITk compared with the straw tubes in the Run 3 detector. While the transverse momentum resolution in the forward region appears relatively poor for 100 GeV muons, the rate of such muons in that region of the detector is expected to be extremely low, since they correspond to forward muons with an energy of around 3 TeV.

5.5 Primary vertex reconstruction and identification

The local pile-up density is defined as the number of proton-proton interactions within a 4 mm window around the true hard-scatter vertex, normalized by this distance. In figure 26(a), the local pile-up density under HL-LHC conditions with $\langle\mu\rangle$ of 200 is shown, in comparison to the one used in the Run 3 sample. Figure 26(b) exhibits the efficiency of the hard-scatter vertex reconstruc-

2025 JINST 20 P02018

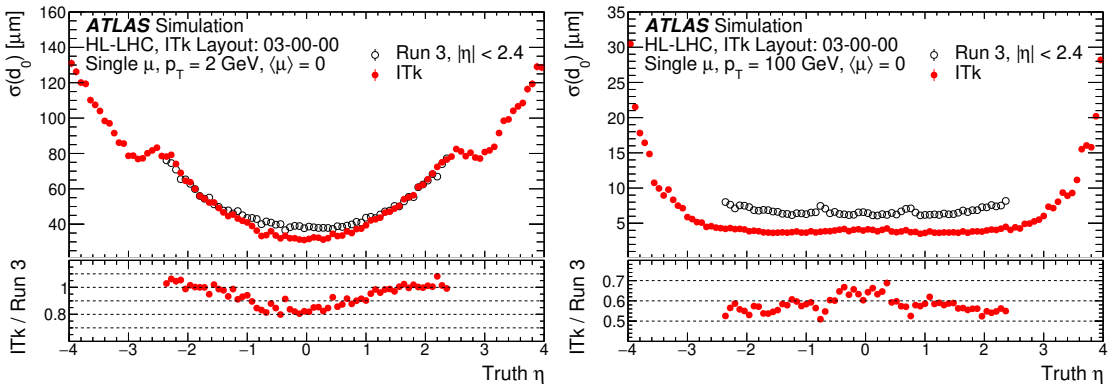

(a) (b)

Figure 23. Transverse impact parameter (d_0) resolution as a function of η for (a) 2 GeV and (b) 100 GeV muons without pile-up, compared between the ITk and the Run 3 detector.

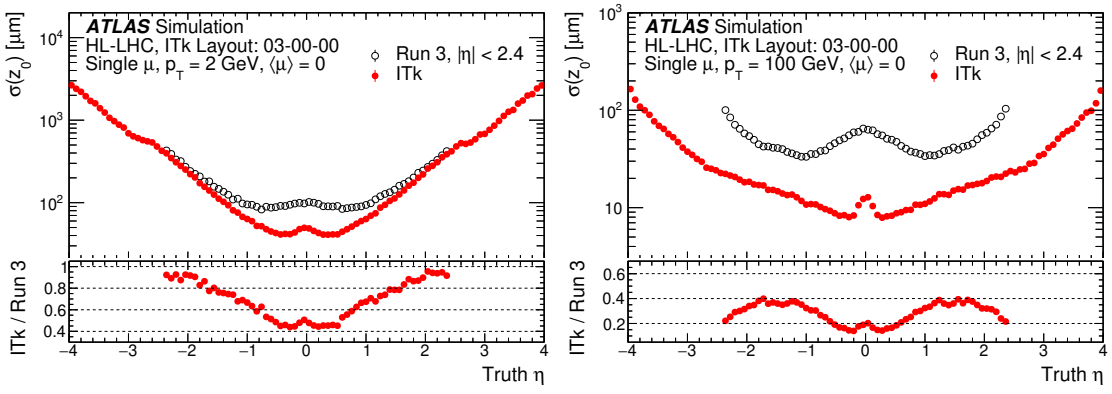

(a) (b)

Figure 24. Longitudinal impact parameter (z_0) resolution as a function of η for (a) 2 GeV and (b) 100 GeV muons without pile-up, compared between the ITk and the Run 3 detector.

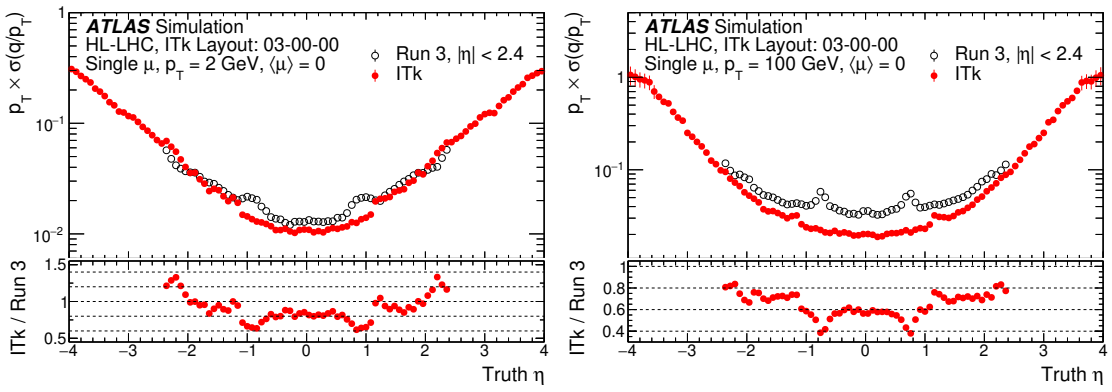

(a) (b)

Figure 25. Relative transverse momentum resolution as a function of η for (a) 2 GeV and (b) 100 GeV muons without pile-up, compared between the ITk and the Run 3 detector.

2025 JINST 20 P02018

tion, described in section 4.2, denoting the fraction of events in which a vertex is reconstructed within 0.1 mm of the true hard-scatter position along the longitudinal direction. The figure underscores the resilient performance achieved even under the highest expected pile-up density in HL-LHC conditions.

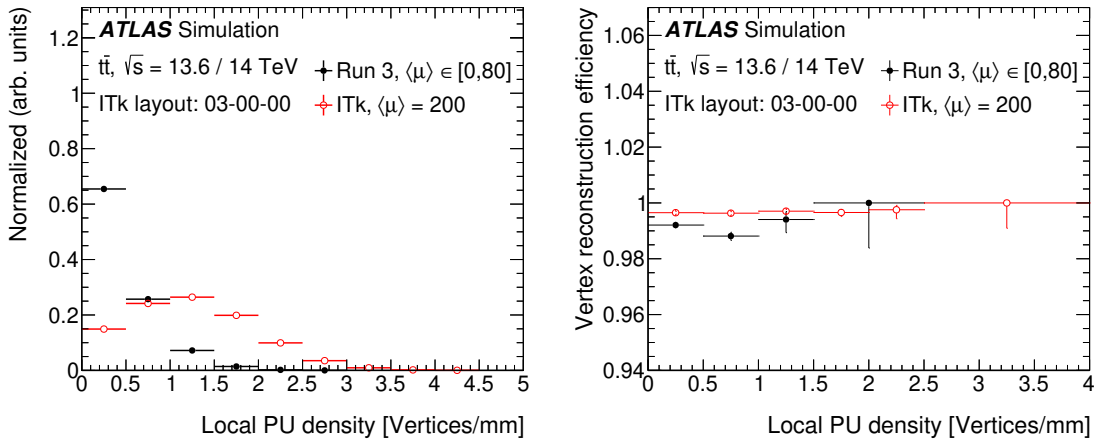

Figure 26. (a) Distribution of the number of local pile-up density around the hard-scatter vertex, evaluated in $t\bar{t}$ events with $\langle\mu\rangle = 200$ in the ITk sample and with a uniform pile-up profile between 0 and 80 in the Run 3 sample. (b) Primary vertex reconstruction efficiency evaluated in $t\bar{t}$ events with $\langle\mu\rangle = 200$ as a function of the local pile-up density around the hard-scatter vertex. For comparison, the performance obtained with the Run 3 ATLAS detector with a uniform pile-up profile between 0 and 80 is also shown.

Another relevant metric is the selection efficiency of the signal hard-scatter vertex, defined as the reconstructed primary vertex that has the largest number of tracks matched to true particles originating from the simulated hard-scatter interaction. The combined reconstruction and selection efficiency, i.e., the fraction of events in which the hard-scatter vertex is reconstructed and selected as the highest Σp_{T}^2 primary vertex, is expected to be influenced by various factors. The highest-Σp_{T}^2 vertex is chosen as the vertex of interest, but this choice may be compromised if the hard-scatter vertex is split into multiple reconstructed vertices due to nearby pile-up vertices. This effect is expected to be primarily correlated with the local pile-up density, and the efficiency is demonstrated to be highly robust against this variable in figure 27(a).

True pile-up vertices may also be merged into a single reconstructed vertex, increasing its associated Σp_{T}^2. Finally, there is a small probability for a pile-up interaction to genuinely yield a larger Σp_{T}^2 than the simulated hard-scatter process, even with a perfect vertex reconstruction algorithm. These effects are expected to be largely correlated with the number of interactions. Figure 27(b) displays the combined reconstruction and selection efficiency as a function of this variable. The efficiency is expected to be reduced down to 92% on average at a pile-up of 200.

The longitudinal position resolution obtained with the ITk detector is presented in figure 28 and exhibits a strong robustness against pile-up, being maintained at about 10 µm up to high pile-up density, improving by more than a factor of two the performance of the Run 3 detector. Strongly correlated with the improved track parameter resolution, this feature is thus expected to greatly benefit pile-up rejection in jets, hadronic τ reconstruction, lepton isolation, and flavor-tagging algorithms.

2025 JINST 20 P02018

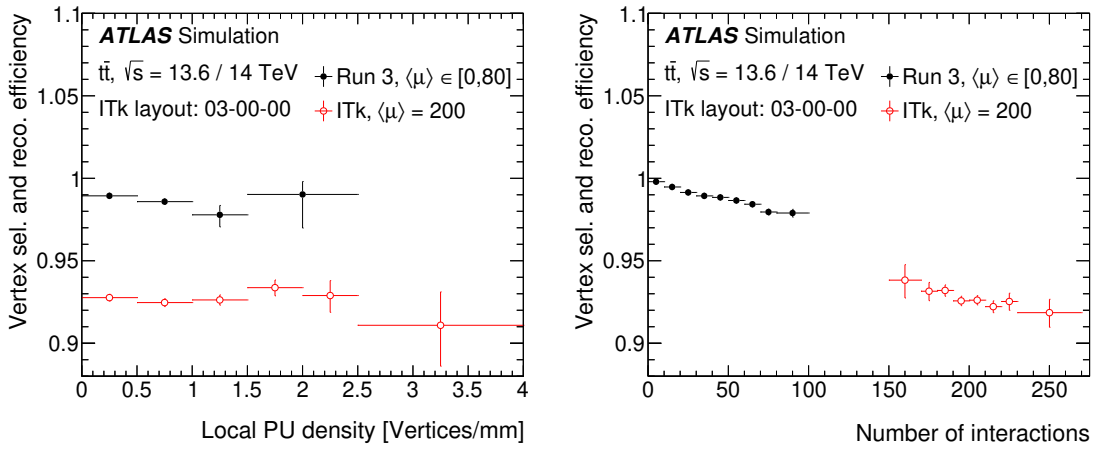

(a) (b)

Figure 27. Primary vertex combined reconstruction and selection efficiency evaluated in $t\bar{t}$ events with $\langle\mu\rangle = 200$. The efficiency is presented as a function of (a) the local pile-up density around the hard-scatter vertex and (b) the number of interactions. For comparison, the performance obtained with the Run 3 ATLAS detector with a uniform pile-up profile between 0 and 80 is also shown.

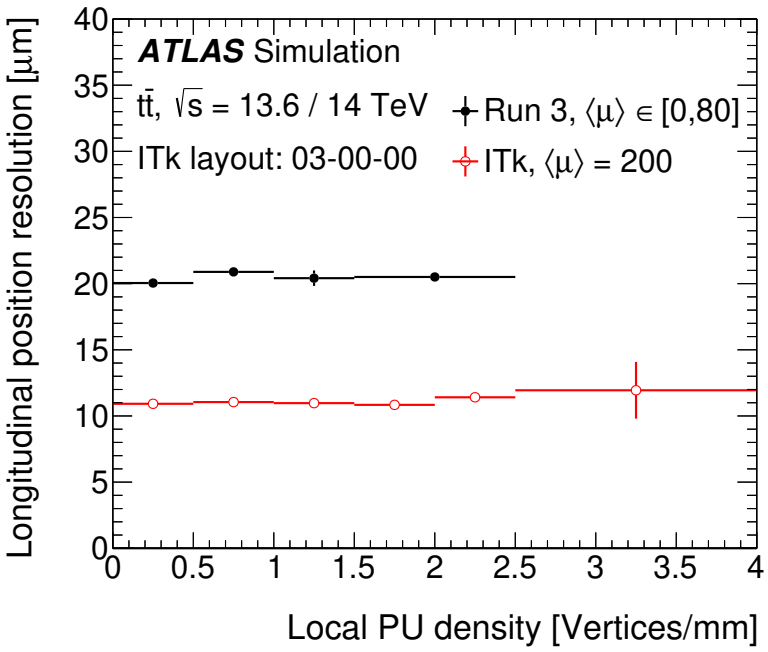

Figure 28. Longitudinal position resolution of the reconstructed primary vertex, evaluated in $t\bar{t}$ events with $\langle\mu\rangle = 200$. For comparison, the performance obtained with the Run 3 ATLAS detector with a uniform pile-up profile between 0 and 80 is also shown.

6 Conclusion

This paper presents the state-of-the-art tracking performance expected with the ITk detector during the high-luminosity LHC operation phase. The combination between the ITk design and the ATLAS

2025 JINST 20 P02018

tracking software is expected to perform to a high standard in very challenging high pile-up conditions. The track seeding performance exploits in particular the large multiplicity of high-precision silicon measurements to guarantee a high efficiency and redundancy, offering a strong robustness against detector misalignment or sensor defects. The full tracking efficiency is found to reach levels similar to Run 3, while the multiple high-precision silicon measurements on each track enables a quasi-linear scaling of the track multiplicity with pile-up, indicating much lower numbers of fake tracks expected than in Run 3 despite the increased pile-up expected at high luminosity. The resolution on track parameters, critical for the flavor-tagging and pile-up rejection performances, are significantly improved relative to the Run 3 detector thanks to the smaller pixel pitch used in the ITk. The tracking performance in the forward region with $2.4 < |\eta| < 4.0$, which will be newly covered by the ITk, is also shown to reach very high standards, compatible with the requirements expected from high-level object reconstruction and identification algorithms. The vertex position resolution is also improved relative to the Run 3 performance, while the vertex reconstruction and selection efficiency shows a very strong robustness against pile-up. Finally, the tracking performance is found to be degraded in the core of high-p_{T} jets due to the presence of merged charge clusters, and mitigation techniques inspired by the ones used with the Run 3 detector will have to be put in place for the ITk track reconstruction to guarantee high tracking performance in this challenging environment, which is crucial for many beyond-the-Standard-Model searches. The results presented in this paper represent a solid baseline for future developments expected to happen in the coming years, and will be used in particular as a reference for the expected evolution of the ATLAS tracking software before the start of the Run 4 data-taking.

Acknowledgments

We thank CERN for the very successful operation of the LHC and its injectors, as well as the support staff at CERN and at our institutions worldwide without whom ATLAS could not be operated efficiently.

The crucial computing support from all WLCG partners is acknowledged gratefully, in particular from CERN, the ATLAS Tier-1 facilities at TRIUMF/SFU (Canada), NDGF (Denmark, Norway, Sweden), CC-IN2P3 (France), KIT/GridKA (Germany), INFN-CNAF (Italy), NL-T1 (Netherlands), PIC (Spain), RAL (U.K.) and BNL (U.S.A.), the Tier-2 facilities worldwide and large non-WLCG resource providers. Major contributors of computing resources are listed in ref. [64].

We gratefully acknowledge the support of ANPCyT, Argentina; YerPhI, Armenia; ARC, Australia; BMWFW and FWF, Austria; ANAS, Azerbaijan; CNPq and FAPESP, Brazil; NSERC, NRC and CFI, Canada; CERN; ANID, Chile; CAS, MOST and NSFC, China; Minciencias, Colombia; MEYS CR, Czech Republic; DNRF and DNSRC, Denmark; IN2P3-CNRS and CEA-DRF/IRFU, France; SRNSFG, Georgia; BMBF, HGF and MPG, Germany; GSRI, Greece; RGC and Hong Kong SAR, China; ICHEP and Academy of Sciences and Humanities, Israel; INFN, Italy; MEXT and JSPS, Japan; CNRST, Morocco; NWO, Netherlands; RCN, Norway; MNiSW, Poland; FCT, Portugal; MNE/IFA, Romania; MSTDI, Serbia; MSSR, Slovakia; ARIS and MVZI, Slovenia; DSI/NRF, South Africa; MICIU/AEI, Spain; SRC and Wallenberg Foundation, Sweden; SERI, SNSF and Cantons of Bern and Geneva, Switzerland; NSTC, Taipei; TENMAK, Türkiye; STFC/UKRI, United Kingdom; DOE and NSF, United States of America.

Individual groups and members have received support from BCKDF, CANARIE, CRC and DRAC, Canada; CERN-CZ, FORTE and PRIMUS, Czech Republic; COST, ERC, ERDF, Horizon 2020, ICSC-NextGenerationEU and Marie Skłodowska-Curie Actions, European Union; Investissements

2025 JINST 20 P02018

d'Avenir Labex, Investissements d'Avenir Idex and ANR, France; DFG and AvH Foundation, Germany; Herakleitos, Thales and Aristeia programmes co-financed by EU-ESF and the Greek NSRF, Greece; BSF-NSF and MINERVA, Israel; NCN and NAWA, Poland; La Caixa Banking Foundation, CERCA Programme Generalitat de Catalunya and PROMETEO and GenT Programmes Generalitat Valenciana, Spain; Göran Gustafssons Stiftelse, Sweden; The Royal Society and Leverhulme Trust, United Kingdom.

In addition, individual members wish to acknowledge support from Armenia: Yerevan Physics Institute (FAPERJ); CERN: European Organization for Nuclear Research (CERN DOCT); Chile: Agencia Nacional de Investigación y Desarrollo (FONDECYT 1230812, FONDECYT 1230987, FONDECYT 1240864); China: Chinese Ministry of Science and Technology (MOST-2023YFA1605700, MOST-2023YFA1609300), National Natural Science Foundation of China (NSFC - 12175119, NSFC 12275265, NSFC-12075060); Czech Republic: Czech Science Foundation (GACR - 24-11373S), Ministry of Education Youth and Sports (FORTE CZ.02.01.01/00/22_008/0004632), PRIMUS Research Programme (PRIMUS/21/SCI/017); EU: H2020 European Research Council (ERC - 101002463); European Union: European Research Council (ERC - 948254, ERC 101089007, ERC, BARD, 101116429), European Union, Future Artificial Intelligence Research (FAIR-NextGenerationEU PE00000013), Italian Center for High Performance Computing, Big Data and Quantum Computing (ICSC, NextGenerationEU); France: Agence Nationale de la Recherche (ANR-20-CE31-0013, ANR-21-CE31-0013, ANR-21-CE31-0022, ANR-22-EDIR-0002); Germany: Baden-Württemberg Stiftung (BW Stiftung-Postdoc Eliteprogramme), Deutsche Forschungsgemeinschaft (DFG - 469666862, DFG - CR 312/5-2); Italy: Istituto Nazionale di Fisica Nucleare (ICSC, NextGenerationEU), Ministero dell'Università e della Ricerca (PRIN - 20223N7F8K - PNRR M4.C2.1.1); Japan: Japan Society for the Promotion of Science (JSPS KAKENHI JP22H01227, JSPS KAKENHI JP22H04944, JSPS KAKENHI JP22KK0227, JSPS KAKENHI JP23KK0245); Norway: Research Council of Norway (RCN-314472); Poland: Ministry of Science and Higher Education (IDUB AGH, POB8, D4 no 9722), Polish National Agency for Academic Exchange (PPN/PPO/2020/1/00002/U/00001), Polish National Science Centre (NCN 2021/42/E/ST2/00350, NCN OPUS 2023/51/B/ST2/02507, NCN OPUS nr 2022/47/B/ST2/03059, NCN UMO-2019/34/E/ST2/00393, UMO-2020/37/B/ST2/01043, UMO-2021/40/C/ST2/00187, UMO-2022/47/O/ST2/00148, UMO-2023/49/B/ST2/04085, UMO-2023/51/B/ST2/00920); Spain: Generalitat Valenciana (Artemisa, FEDER, IDIFEDER/2018/048), Ministry of Science and Innovation (MCIN & NextGenEU PCI2022-135018-2, MICIN & FEDER PID2021-125273NB, RYC2019-028510-I, RYC2020-030254-I, RYC2021-031273-I, RYC2022-038164-I); Sweden: Carl Trygger Foundation (Carl Trygger Foundation CTS 22:2312), Swedish Research Council (Swedish Research Council 2023-04654, VR 2018-00482, VR 2022-03845, VR 2022-04683, VR 2023-03403, VR grant 2021-03651), Knut and Alice Wallenberg Foundation (KAW 2018.0458, KAW 2019.0447, KAW 2022.0358); Switzerland: Swiss National Science Foundation (SNSF - PCEFP2_194658); United Kingdom: Leverhulme Trust (Leverhulme Trust RPG-2020-004), Royal Society (NIF-R1-231091); United States of America: U.S. Department of Energy (ECA DE-AC02-76SF00515), Neubauer Family Foundation.

References

[1] L. Evans and P. Bryant, *LHC Machine*, 2008 *JINST* **3** S08001.

[2] ATLAS collaboration, *The ATLAS Experiment at the CERN Large Hadron Collider*, 2008 *JINST* **3** S08003.

[3] CMS collaboration, *The CMS Experiment at the CERN LHC*, 2008 *JINST* **3** S08004.

2025 JINST 20 P02018

[4] O. Aberle et al., *High-Luminosity Large Hadron Collider (HL-LHC): Technical design report*, CERN-2020-010, CERN, Geneva (2020) [DOI:10.23731/CYRM-2020-0010].

[5] ATLAS collaboration, *ATLAS inner detector: Technical design report. Vol. 1*, CERN-LHCC-97-16 (1997).

[6] ATLAS collaboration, *ATLAS inner detector: Technical design report. Vol. 2*, CERN-LHCC-97-17 (1997).

[7] ATLAS collaboration, *Modelling radiation damage to pixel sensors in the ATLAS detector*, 2019 *JINST* **14** P06012 [arXiv:1905.03739].

[8] ATLAS collaboration, *Measurements of sensor radiation damage in the ATLAS inner detector using leakage currents*, 2021 *JINST* **16** P08025 [arXiv:2106.09287].

[9] ATLAS collaboration, *Technical Design Report for the ATLAS Inner Tracker Strip Detector*, CERN-LHCC-2017-005, CERN, Geneva (2017).

[10] ATLAS collaboration, *Technical Design Report for the ATLAS Inner Tracker Pixel Detector*, CERN-LHCC-2017-021, CERN, Geneva (2017) [DOI:10.17181/CERN.FOZZ.ZP3Q].

[11] ATLAS collaboration, *Letter of Intent for the Phase-II Upgrade of the ATLAS Experiment*, CERN-LHCC-2012-022, CERN, Geneva (2012).

[12] ATLAS collaboration, *ATLAS Phase-II Upgrade Scoping Document*, CERN-LHCC-2015-020, CERN, Geneva (2015) [DOI:10.17181/CERN.7CRX.AJHP].

[13] ATLAS collaboration, *Jet reconstruction and performance using particle flow with the ATLAS Detector*, *Eur. Phys. J. C* **77** (2017) 466 [arXiv:1703.10485].

[14] ATLAS collaboration, *ATLAS flavour-tagging algorithms for the LHC Run 2 pp collision dataset*, *Eur. Phys. J. C* **83** (2023) 681 [arXiv:2211.16345].

[15] ATLAS collaboration, *Graph Neural Network Jet Flavour Tagging with the ATLAS Detector*, ATL-PHYS-PUB-2022-027, CERN, Geneva (2022).

[16] ATLAS collaboration, *Electron and photon efficiencies in LHC Run 2 with the ATLAS experiment*, *JHEP* **05** (2024) 162 [arXiv:2308.13362].

[17] ATLAS collaboration, *Reconstruction, Identification, and Calibration of hadronically decaying tau leptons with the ATLAS detector for the LHC Run 3 and reprocessed Run 2 data*, ATL-PHYS-PUB-2022-044, CERN, Geneva (2022).

[18] ATLAS collaboration, *Muon reconstruction and identification efficiency in ATLAS using the full Run 2 pp collision data set at* $\sqrt{s} = 13$ *TeV*, *Eur. Phys. J. C* **81** (2021) 578 [arXiv:2012.00578].

[19] ATLAS collaboration, *Measurement of angular and momentum distributions of charged particles within and around jets in Pb+Pb and pp collisions at* $\sqrt{s_{\mathrm{NN}}} = 5.02$ *TeV with the ATLAS detector*, *Phys. Rev. C* **100** (2019) 064901 [*Erratum ibid.* **101** (2020) 059903] [arXiv:1908.05264].

[20] ATLAS collaboration, *Search for long-lived charginos based on a disappearing-track signature using* $136\,fb^{-1}$ *of pp collisions at* $\sqrt{s} = 13$ *TeV with the ATLAS detector*, *Eur. Phys. J. C* **82** (2022) 606 [arXiv:2201.02472].

[21] ATLAS collaboration, *Measurement of the production of a W boson in association with a charmed hadron in pp collisions at* $\sqrt{s} = 13$ TeV *with the ATLAS detector*, *Phys. Rev. D* **108** (2023) 032012 [arXiv:2302.00336].

[22] T. Cornelissen et al., *The new ATLAS track reconstruction (NEWT)*, *J. Phys. Conf. Ser.* **119** (2008) 032014.

2025 JINST 20 P02018

[23] ATLAS collaboration, *Software Performance of the ATLAS Track Reconstruction for LHC Run 3*, *Comput. Softw. Big Sci.* **8** (2024) 9 [arXiv:2308.09471].

[24] R. Fruhwirth, *Application of Kalman filtering to track and vertex fitting*, *Nucl. Instrum. Meth. A* **262** (1987) 444.

[25] ATLAS collaboration, *Expected b-tagging performance with the upgraded ATLAS Inner Tracker detector at the High-Luminosity LHC*, ATL-PHYS-PUB-2020-005, CERN, Geneva (2020).

[26] ATLAS collaboration, *Neural Network Jet Flavour Tagging with the Upgraded ATLAS Inner Tracker Detector at the High-Luminosity LHC*, ATL-PHYS-PUB-2022-047, CERN, Geneva (2022).

[27] ATLAS collaboration, *Expected performance of the ATLAS detector at the High-Luminosity LHC*, ATL-PHYS-PUB-2019-005, CERN, Geneva (2019).

[28] ATLAS collaboration, *Expected performance of the ATLAS detector under different High-Luminosity LHC conditions*, ATL-PHYS-PUB-2021-023, CERN, Geneva (2021).

[29] D. Contardo et al., *Technical Proposal for the Phase-II Upgrade of the CMS Detector*, CERN-LHCC-2015-010 (2015) [DOI:10.17181/CERN.VU8I.D59J].

[30] CMS collaboration, *The Phase-2 Upgrade of the CMS Tracker*, CERN-LHCC-2017-009, CERN, Geneva (2017) [DOI:10.17181/CERN.QZ28.FLHW].

[31] ATLAS and CMS collaborations, *Report on the Physics at the HL-LHC and Perspectives for the HE-LHC*, arXiv:1902.10229.

[32] ATLAS and CMS collaborations, *Snowmass White Paper Contribution: Physics with the Phase-2 ATLAS and CMS Detectors*, ATL-PHYS-PUB-2022-018, CERN, Geneva (2022).

[33] ATLAS collaboration, *A High-Granularity Timing Detector for the ATLAS Phase-II Upgrade: Technical Design Report*, CERN-LHCC-2020-007 (2091).

[34] ATLAS collaboration, *Software and computing for Run 3 of the ATLAS experiment at the LHC*, arXiv:2404.06335.

[35] M. Bandieramonte et al., *The GeoModel tool suite for detector description*, *EPJ Web Conf.* **251** (2021) 03007.

[36] ATLAS collaboration, *ATLAS HL-LHC Computing Conceptual Design Report*, CERN-LHCC-2020-015 (2020).

[37] S. Frixione, P. Nason and G. Ridolfi, *A positive-weight next-to-leading-order Monte Carlo for heavy flavour hadroproduction*, *JHEP* **09** (2007) 126 [arXiv:0707.3088].

[38] P. Nason, *A new method for combining NLO QCD with shower Monte Carlo algorithms*, *JHEP* **11** (2004) 040 [hep-ph/0409146].

[39] S. Frixione, P. Nason and C. Oleari, *Matching NLO QCD computations with Parton Shower simulations: the POWHEG method*, *JHEP* **11** (2007) 070 [arXiv:0709.2092].

[40] S. Alioli, P. Nason, C. Oleari and E. Re, *A general framework for implementing NLO calculations in shower Monte Carlo programs: the POWHEG BOX*, *JHEP* **06** (2010) 043 [arXiv:1002.2581].

[41] NNPDF collaboration, *Parton distributions for the LHC Run II*, *JHEP* **04** (2015) 040 [arXiv:1410.8849].

[42] ATLAS collaboration, *Studies on top-quark Monte Carlo modelling for Top2016*, ATL-PHYS-PUB-2016-020, CERN, Geneva (2016).

[43] T. Sjöstrand et al., *An introduction to PYTHIA 8.2*, *Comput. Phys. Commun.* **191** (2015) 159 [arXiv:1410.3012].

2025 JINST 20 P02018

[44] ATLAS collaboration, *ATLAS Pythia 8 tunes to 7 TeV data*, ATL-PHYS-PUB-2014-021, CERN, Geneva (2014).

[45] R.D. Ball et al., *Parton distributions with LHC data*, *Nucl. Phys. B* **867** (2013) 244 [arXiv:1207.1303].

[46] D.J. Lange, *The EvtGen particle decay simulation package*, *Nucl. Instrum. Meth. A* **462** (2001) 152.

[47] C. Bierlich et al., *A comprehensive guide to the physics and usage of PYTHIA 8.3*, *SciPost Phys. Codeb.* **2022** (2022) 8 [arXiv:2203.11601].

[48] ATLAS collaboration, *The ATLAS Simulation Infrastructure*, *Eur. Phys. J. C* **70** (2010) 823 [arXiv:1005.4568].

[49] GEANT4 collaboration, *GEANT4 — A Simulation Toolkit*, *Nucl. Instrum. Meth. A* **506** (2003) 250.

[50] H. Bichsel, *Straggling in Thin Silicon Detectors*, *Rev. Mod. Phys.* **60** (1988) 663.

[51] F. Loddo et al., *RD53 pixel chips for the ATLAS and CMS Phase-2 upgrades at HL-LHC*, *Nucl. Instrum. Meth. A* **1067** (2024) 169682.

[52] I. Gorelov et al., *A measurement of Lorentz angle and spatial resolution of radiation hard silicon pixel sensors*, *Nucl. Instrum. Meth. A* **481** (2002) 204.

[53] ATLAS collaboration, *ATLAS Run 3 charged particle track seed finding performance*, ATL-PHYS-PUB-2023-034, CERN, Geneva (2023).

[54] E. Lund, L. Bugge, I. Gavrilenko and A. Strandlie, *Track parameter propagation through the application of a new adaptive Runge-Kutta-Nystroem method in the ATLAS experiment*, 2009 *JINST* **4** P04001.

[55] T.G. Cornelissen et al., *The global chi**2 track fitter in ATLAS*, *J. Phys. Conf. Ser.* **119** (2008) 032013.

[56] T. Cornelissen et al., *Concepts, Design and Implementation of the ATLAS New Tracking (NEWT)*, ATL-SOFT-PUB-2007-007, CERN, Geneva (2007).

[57] ATLAS collaboration, *A neural network clustering algorithm for the ATLAS silicon pixel detector*, 2014 *JINST* **9** P09009 [arXiv:1406.7690].

[58] ATLAS collaboration, *Performance of the ATLAS Track Reconstruction Algorithms in Dense Environments in LHC Run 2*, *Eur. Phys. J. C* **77** (2017) 673 [arXiv:1704.07983].

[59] ATLAS collaboration, *Development of ATLAS Primary Vertex Reconstruction for LHC Run 3*, ATL-PHYS-PUB-2019-015, CERN, Geneva (2019).

[60] M. Cacciari, G.P. Salam and G. Soyez, *The anti-k_t jet clustering algorithm*, *JHEP* **04** (2008) 063 [arXiv:0802.1189].

[61] M. Cacciari, G.P. Salam and G. Soyez, *FastJet User Manual*, *Eur. Phys. J. C* **72** (2012) 1896 [arXiv:1111.6097].

[62] ATLAS collaboration, *ATLAS Insertable B-Layer Technical Design Report*, CERN-LHCC-2010-013 (2010) [addendum: CERN-LHCC-2012-009 (2012)].

[63] ATLAS IBL collaboration, *Production and Integration of the ATLAS Insertable B-Layer*, 2018 *JINST* **13** T05008 [arXiv:1803.00844].

[64] ATLAS collaboration, *ATLAS Computing Acknowledgements*, ATL-SOFT-PUB-2023-001, CERN, Geneva (2023).

2025 JINST 20 P02018

The ATLAS collaboration

G. Aad[105], E. Aakvaag[17], B. Abbott[124], S. Abdelhameed[120a], K. Abeling[56], N.J. Abicht[50], S.H. Abidi[30], M. Aboelela[46], A. Aboulhorma[36e], H. Abramowicz[158], Y. Abulaiti[121], B.S. Acharya[70a,70b,o], A. Ackermann[64a], C. Adam Bourdarios[4], L. Adamczyk[87a], S.V. Addepalli[150], M.J. Addison[104], J. Adelman[119], A. Adiguzel[22c], T. Adye[138], A.A. Affolder[140], Y. Afik[41], M.N. Agaras[13], A. Aggarwal[103], C. Agheorghiesei[28c], F. Ahmadov[40,ad], S. Ahuja[98], X. Ai[144b], G. Aielli[77a,77b], A. Aikot[170], M. Ait Tamlihat[36e], B. Aitbenchikh[36a], M. Akbiyik[103], T.P.A. Åkesson[101], A.V. Akimov[152], D. Akiyama[175], N.N. Akolkar[25], S. Aktas[22a], G.L. Alberghi[24b], J. Albert[172], P. Albicocco[54], G.L. Albouy[61], S. Alderweireldt[53], Z.L. Alegria[125], M. Aleksa[37], I.N. Aleksandrov[40], C. Alexa[28b], T. Alexopoulos[10], F. Alfonsi[24b], M. Algren[57], M. Alhroob[174], B. Ali[136], H.M.J. Ali[94,x], S. Ali[32], S.W. Alibocus[95], M. Aliev[34c], G. Alimonti[72a], W. Alkakhi[56], C. Allaire[67], B.M.M. Allbrooke[153], J.S. Allen[104], J.F. Allen[53], P.P. Allport[21], A. Aloisio[73a,73b], F. Alonso[93], C. Alpigiani[143], Z.M.K. Alsolami[94], A. Alvarez Fernandez[103], M. Alves Cardoso[57], M.G. Alviggi[73a,73b], M. Aly[104], Y. Amaral Coutinho[84b], A. Ambler[107], C. Amelung[37], M. Amerl[104], C.G. Ames[112], D. Amidei[109], B. Amini[55], K.J. Amirie[162], A. Amirkhanov[40], S.P. Amor Dos Santos[134a], K.R. Amos[170], D. Amperiadou[159], S. An[85], V. Ananiev[129], C. Anastopoulos[146], T. Andeen[11], J.K. Anders[95], A.C. Anderson[60], A. Andreazza[72a,72b], S. Angelidakis[9], A. Angerami[43], A.V. Anisenkov[40], A. Annovi[75a], C. Antel[57], E. Antipov[152], M. Antonelli[54], F. Anulli[76a], M. Aoki[85], T. Aoki[160], M.A. Aparo[153], L. Aperio Bella[49], C. Appelt[158], A. Apyan[27], S.J. Arbiol Val[88], C. Arcangeletti[54], A.T.H. Arce[52], J-F. Arguin[111], S. Argyropoulos[159], J.-H. Arling[49], O. Arnaez[4], H. Arnold[152], G. Artoni[76a,76b], H. Asada[114], K. Asai[122], S. Asai[160], N.A. Asbah[37], R.A. Ashby Pickering[174], A.M. Aslam[98], K. Assamagan[30], R. Astalos[29a], K.S.V. Astrand[101], S. Atashi[166], R.J. Atkin[34a], H. Atmani[36f], P.A. Atmasiddha[132], K. Augsten[136], A.D. Auriol[42], V.A. Austrup[104], G. Avolio[37], K. Axiotis[57], G. Azuelos[111,ah], A. Azzam[13], D. Babal[29b], H. Bachacou[139], K. Bachas[159,s], A. Bachiu[35], E. Bachmann[51], M.J. Backes[64a], A. Badea[41], T.M. Baer[109], P. Bagnaia[76a,76b], M. Bahmani[19], D. Bahner[55], K. Bai[127], J.T. Baines[138], L. Baines[97], O.K. Baker[179], E. Bakos[16], D. Bakshi Gupta[8], L.E. Balabram Filho[84b], V. Balakrishnan[124], R. Balasubramanian[4], E.M. Baldin[38], P. Balek[87a], E. Ballabene[24b,24a], F. Balli[139], L.M. Baltes[64a], W.K. Balunas[33], J. Balz[103], I. Bamwidhi[120b], E. Banas[88], M. Bandieramonte[133], A. Bandyopadhyay[25], S. Bansal[25], L. Barak[158], M. Barakat[49], E.L. Barberio[108], D. Barberis[18b], M. Barbero[105], M.Z. Barel[118], T. Barillari[113], M-S. Barisits[37], T. Barklow[150], P. Baron[126], D.A. Baron Moreno[104], A. Baroncelli[63], A.J. Barr[130], J.D. Barr[99], F. Barreiro[102], J. Barreiro Guimarães da Costa[14], M.G. Barros Teixeira[134a], S. Barsov[38], F. Bartels[64a], R. Bartoldus[150], A.E. Barton[94], P. Bartos[29a], A. Basan[103], M. Baselga[50], S. Bashiri[88], A. Bassalat[67,b], M.J. Basso[163a], S. Bataju[46], R. Bate[171], R.L. Bates[60], S. Batlamous[102], M. Battaglia[140], D. Battulga[19], M. Bauce[76a,76b], M. Bauer[80], P. Bauer[25], L.T. Bayer[49], L.T. Bazzano Hurrell[31], J.B. Beacham[113], T. Beau[131], J.Y. Beaucamp[93], P.H. Beauchemin[165], P. Bechtle[25], H.P. Beck[20,r], K. Becker[174], A.J. Beddall[83], V.A. Bednyakov[40], C.P. Bee[152], L.J. Beemster[16], M. Begalli[84d], M. Begel[30], J.K. Behr[49], J.F. Beirer[37], F. Beisiegel[25], M. Belfkir[120b], G. Bella[158], L. Bellagamba[24b], A. Bellerive[35], P. Bellos[21], K. Beloborodov[38], D. Benchekroun[36a], F. Bendebba[36a], Y. Benhammou[158], K.C. Benkendorfer[62], L. Beresford[49], M. Beretta[54], E. Bergeaas Kuutmann[168], N. Berger[4], B. Bergmann[136], J. Beringer[18a],

2025 JINST 20 P02018

G. Bernardi[5], C. Bernius[150], F.U. Bernlochner[25], F. Bernon[37], A. Berrocal Guardia[13], T. Berry[98], P. Berta[137], A. Berthold[51], S. Bethke[113], A. Betti[76a,76b], A.J. Bevan[97], L. Bezio[57], N.K. Bhalla[55], S. Bharthuar[113], S. Bhatta[152], D.S. Bhattacharya[173], P. Bhattarai[150], Z.M. Bhatti[121], K.D. Bhide[55], V.S. Bhopatkar[125], R.M. Bianchi[133], G. Bianco[24b,24a], O. Biebel[112], M. Biglietti[78a], C.S. Billingsley[46], Y. Bimgdi[36f], M. Bindi[56], A. Bingham[178], A. Bingul[22b], C. Bini[76a,76b], G.A. Bird[33], M. Birman[176], M. Biros[137], S. Biryukov[153], T. Bisanz[50], E. Bisceglie[24b,24a], J.P. Biswal[138], D. Biswas[148], I. Bloch[49], A. Blue[60], U. Blumenschein[97], J. Blumenthal[103], V.S. Bobrovnikov[40], M. Boehler[55], B. Boehm[173], D. Bogavac[37], A.G. Bogdanchikov[38], L.S. Boggia[131], V. Boisvert[98], P. Bokan[37], T. Bold[87a], M. Bomben[5], M. Bona[97], M. Boonekamp[139], A.G. Borbély[60], I.S. Bordulev[38], G. Borissov[94], D. Bortoletto[130], D. Boscherini[24b], M. Bosman[13], K. Bouaouda[36a], N. Bouchhar[170], L. Boudet[4], J. Boudreau[133], E.V. Bouhova-Thacker[94], D. Boumediene[42], R. Bouquet[58b,58a], A. Boveia[123], J. Boyd[37], D. Boye[30], I.R. Boyko[40], L. Bozianu[57], J. Bracinik[21], N. Brahimi[4], G. Brandt[178], O. Brandt[33], B. Brau[106], J.E. Brau[127], R. Brener[176], L. Brenner[118], R. Brenner[168], S. Bressler[176], G. Brianti[79a,79b], D. Britton[60], D. Britzger[113], I. Brock[25], R. Brock[110], G. Brooijmans[43], A.J. Brooks[69], E.M. Brooks[163b], E. Brost[30], L.M. Brown[172], L.E. Bruce[62], T.L. Bruckler[130], P.A. Bruckman de Renstrom[88], B. Brüers[49], A. Bruni[24b], G. Bruni[24b], D. Brunner[48a,48b], M. Bruschi[24b], N. Bruscino[76a,76b], T. Buanes[17], Q. Buat[143], D. Buchin[113], A.G. Buckley[60], O. Bulekov[38], B.A. Bullard[150], S. Burdin[95], C.D. Burgard[50], A.M. Burger[37], B. Burghgrave[8], O. Burlayenko[55], J. Burleson[169], J.T.P. Burr[33], J.C. Burzynski[149], E.L. Busch[43], V. Büscher[103], P.J. Bussey[60], J.M. Butler[26], C.M. Buttar[60], J.M. Butterworth[99], W. Buttinger[138], C.J. Buxo Vazquez[110], A.R. Buzykaev[40], S. Cabrera Urbán[170], L. Cadamuro[67], D. Caforio[59], H. Cai[133], Y. Cai[24b,115c,24a], Y. Cai[115a], V.M.M. Cairo[37], O. Cakir[3a], N. Calace[37], P. Calafiura[18a], G. Calderini[131], P. Calfayan[35], G. Callea[60], L.P. Caloba[84b], D. Calvet[42], S. Calvet[42], R. Camacho Toro[131], S. Camarda[37], D. Camarero Munoz[27], P. Camarri[77a,77b], M.T. Camerlingo[73a,73b], C. Camincher[172], M. Campanelli[99], A. Camplani[44], V. Canale[73a,73b], A.C. Canbay[3a], E. Canonero[98], J. Cantero[170], Y. Cao[169], F. Capocasa[27], M. Capua[45b,45a], A. Carbone[72a,72b], R. Cardarelli[77a], J.C.J. Cardenas[8], M.P. Cardiff[27], G. Carducci[45b,45a], T. Carli[37], G. Carlino[73a], J.I. Carlotto[13], B.T. Carlson[133,t], E.M. Carlson[172], J. Carmignani[95], L. Carminati[72a,72b], A. Carnelli[4], M. Carnesale[37], S. Caron[117], E. Carquin[141f], I.B. Carr[108], S. Carrá[72a], G. Carratta[24b,24a], A.M. Carroll[127], M.P. Casado[13,i], M. Caspar[49], F.L. Castillo[4], L. Castillo Garcia[13], V. Castillo Gimenez[170], N.F. Castro[134a,134e], A. Catinaccio[37], J.R. Catmore[129], T. Cavaliere[4], V. Cavaliere[30], L.J. Caviedes Betancourt[23b], Y.C. Cekmecelioglu[49], E. Celebi[83], S. Cella[37], V. Cepaitis[57], K. Cerny[126], A.S. Cerqueira[84a], A. Cerri[75a,75b], L. Cerrito[77a,77b], F. Cerutti[18a], B. Cervato[72a,72b], A. Cervelli[24b], G. Cesarini[54], S.A. Cetin[83], P.M. Chabrillat[131], J. Chan[18a], W.Y. Chan[160], J.D. Chapman[33], E. Chapon[139], B. Chargeishvili[156b], D.G. Charlton[21], C. Chauhan[137], Y. Che[115a], S. Chekanov[6], S.V. Chekulaev[163a], G.A. Chelkov[40,a], B. Chen[158], B. Chen[172], H. Chen[115a], H. Chen[30], J. Chen[145a], J. Chen[149], M. Chen[130], S. Chen[90], S.J. Chen[115a], X. Chen[145a], X. Chen[15,ag], Z. Chen[63], C.L. Cheng[177], H.C. Cheng[65a], S. Cheong[150], A. Cheplakov[40], E. Cheremushkina[49], E. Cherepanova[118], R. Cherkaoui El Moursli[36e], E. Cheu[7], K. Cheung[66], L. Chevalier[139], V. Chiarella[54], G. Chiarelli[75a], N. Chiedde[105], G. Chiodini[71a], A.S. Chisholm[21], A. Chitan[28b], M. Chitishvili[170], M.V. Chizhov[40,u], K. Choi[11], Y. Chou[143], E.Y.S. Chow[117], K.L. Chu[176], M.C. Chu[65a],

2025 JINST 20 P02018

X. Chu[14,115c], Z. Chubinidze[54], J. Chudoba[135], J.J. Chwastowski[88], D. Cieri[113], K.M. Ciesla[87a], V. Cindro[96], A. Ciocio[18a], F. Cirotto[73a,73b], Z.H. Citron[176], M. Citterio[72a], D.A. Ciubotaru[28b], A. Clark[57], P.J. Clark[53], N. Clarke Hall[99], C. Clarry[162], S.E. Clawson[49], C. Clement[48a,48b], Y. Coadou[105], M. Cobal[70a,70c], A. Coccaro[58b], R.F. Coelho Barrue[134a], R. Coelho Lopes De Sa[106], S. Coelli[72a], L.S. Colangeli[162], B. Cole[43], P. Collado Soto[102], J. Collot[61], P. Conde Muiño[134a,134g], M.P. Connell[34c], S.H. Connell[34c], E.I. Conroy[130], F. Conventi[73a,ai], H.G. Cooke[21], A.M. Cooper-Sarkar[130], F.A. Corchia[24b,24a], A. Cordeiro Oudot Choi[131], L.D. Corpe[42], M. Corradi[76a,76b], F. Corriveau[107,ac], A. Cortes-Gonzalez[19], M.J. Costa[170], F. Costanza[4], D. Costanzo[146], B.M. Cote[123], J. Couthures[4], G. Cowan[98], K. Cranmer[177], L. Cremer[50], D. Cremonini[24b,24a], S. Crépé-Renaudin[61], F. Crescioli[131], T. Cresta[74a,74b], M. Cristinziani[148], M. Cristoforetti[79a,79b], V. Croft[118], J.E. Crosby[125], G. Crosetti[45b,45a], A. Cueto[102], H. Cui[99], Z. Cui[7], W.R. Cunningham[60], F. Curcio[170], J.R. Curran[53], P. Czodrowski[37], M.J. Da Cunha Sargedas De Sousa[58b,58a], J.V. Da Fonseca Pinto[84b], C. Da Via[104], W. Dabrowski[87a], T. Dado[37], S. Dahbi[155], T. Dai[109], D. Dal Santo[20], C. Dallapiccola[106], M. Dam[44], G. D'amen[30], V. D'Amico[112], J. Damp[103], J.R. Dandoy[35], D. Dannheim[37], M. Danninger[149], V. Dao[152], G. Darbo[58b], S.J. Das[30], F. Dattola[49], S. D'Auria[72a,72b], A. D'Avanzo[73a,73b], T. Davidek[137], I. Dawson[97], H.A. Day-hall[136], K. De[8], C. De Almeida Rossi[162], R. De Asmundis[73a], N. De Biase[49], S. De Castro[24b,24a], N. De Groot[117], P. de Jong[118], H. De la Torre[119], A. De Maria[115a], A. De Salvo[76a], U. De Sanctis[77a,77b], F. De Santis[71a,71b], A. De Santo[153], J.B. De Vivie De Regie[61], J. Debevc[96], D.V. Dedovich[40], J. Degens[95], A.M. Deiana[46], J. Del Peso[102], L. Delagrange[131], F. Deliot[139], C.M. Delitzsch[50], M. Della Pietra[73a,73b], D. Della Volpe[57], A. Dell'Acqua[37], L. Dell'Asta[72a,72b], M. Delmastro[4], C.C. Delogu[103], P.A. Delsart[61], S. Demers[179], M. Demichev[40], S.P. Denisov[38], H. Denizli[22a,m], L. D'Eramo[42], D. Derendarz[88], F. Derue[131], P. Dervan[95], K. Desch[25], C. Deutsch[25], F.A. Di Bello[58b,58a], A. Di Ciaccio[77a,77b], L. Di Ciaccio[4], A. Di Domenico[76a,76b], C. Di Donato[73a,73b], A. Di Girolamo[37], G. Di Gregorio[37], A. Di Luca[79a,79b], B. Di Micco[78a,78b], R. Di Nardo[78a,78b], K.F. Di Petrillo[41], M. Diamantopoulou[35], F.A. Dias[118], T. Dias Do Vale[149], M.A. Diaz[141a,141b], A.R. Didenko[40], M. Didenko[170], E.B. Diehl[109], S. Díez Cornell[49], C. Diez Pardos[148], C. Dimitriadi[151], A. Dimitrievska[21], A. Dimri[152], J. Dingfelder[25], T. Dingley[130], I-M. Dinu[28b], S.J. Dittmeier[64b], F. Dittus[37], M. Divisek[137], B. Dixit[95], F. Djama[105], T. Djobava[156b], C. Doglioni[104,101], A. Dohnalova[29a], Z. Dolezal[137], K. Domijan[87a], K.M. Dona[41], M. Donadelli[84d], B. Dong[110], J. Donini[42], A. D'Onofrio[73a,73b], M. D'Onofrio[95], J. Dopke[138], A. Doria[73a], N. Dos Santos Fernandes[134a], P. Dougan[104], M.T. Dova[93], A.T. Doyle[60], M.A. Draguet[130], M.P. Drescher[56], E. Dreyer[176], I. Drivas-koulouris[10], M. Drnevich[121], M. Drozdova[57], D. Du[63], T.A. du Pree[118], F. Dubinin[40], M. Dubovsky[29a], E. Duchovni[176], G. Duckeck[112], P.K. Duckett[99], O.A. Ducu[28b], D. Duda[53], A. Dudarev[37], E.R. Duden[27], M. D'uffizi[104], L. Duflot[67], M. Dührssen[37], I. Duminica[28g], A.E. Dumitriu[28b], M. Dunford[64a], S. Dungs[50], K. Dunne[48a,48b], A. Duperrin[105], H. Duran Yildiz[3a], M. Düren[59], A. Durglishvili[156b], D. Duvnjak[35], B.L. Dwyer[119], G.I. Dyckes[18a], M. Dyndal[87a], B.S. Dziedzic[37], Z.O. Earnshaw[153], G.H. Eberwein[130], B. Eckerova[29a], S. Eggebrecht[56], E. Egidio Purcino De Souza[84e], G. Eigen[17], K. Einsweiler[18a], T. Ekelof[168], P.A. Ekman[101], S. El Farkh[36b], Y. El Ghazali[63], H. El Jarrari[37], A. El Moussaouy[36a], V. Ellajosyula[168], M. Ellert[168], F. Ellinghaus[178], N. Ellis[37], J. Elmsheuser[30], M. Elsawy[120a], M. Elsing[37],

2025 JINST 20 P02018

D. Emeliyanov[138], Y. Enari[85], I. Ene[18a], S. Epari[111], D. Ernani Martins Neto[88], M. Errenst[178], M. Escalier[67], C. Escobar[170], E. Etzion[158], G. Evans[134a,134b], H. Evans[69], L.S. Evans[98], A. Ezhilov[38], S. Ezzarqtouni[36a], F. Fabbri[24b,24a], L. Fabbri[24b,24a], G. Facini[99], V. Fadeyev[140], R.M. Fakhrutdinov[38], D. Fakoudis[103], S. Falciano[76a], L.F. Falda Ulhoa Coelho[134a], F. Fallavollita[113], G. Falsetti[45b,45a], J. Faltova[137], C. Fan[169], K.Y. Fan[65b], Y. Fan[14], Y. Fang[14,115c], M. Fanti[72a,72b], M. Faraj[70a,70b], Z. Farazpay[100], A. Farbin[8], A. Farilla[78a], T. Farooque[110], J.N. Farr[179], S.M. Farrington[138,53], F. Fassi[36e], D. Fassouliotis[9], L. Fayard[67], P. Federic[137], P. Federicova[135], O.L. Fedin[38,a], M. Feickert[177], L. Feligioni[105], D.E. Fellers[18a], C. Feng[144a], Z. Feng[118], M.J. Fenton[166], L. Ferencz[49], B. Fernandez Barbadillo[94], P. Fernandez Martinez[68], M.J.V. Fernoux[105], J. Ferrando[94], A. Ferrari[168], P. Ferrari[118,117], R. Ferrari[74a], D. Ferrere[57], C. Ferretti[109], M.P. Fewell[1], D. Fiacco[76a,76b], F. Fiedler[103], P. Fiedler[136], S. Filimonov[40], A. Filipčič[96], E.K. Filmer[163a], F. Filthaut[117], M.C.N. Fiolhais[134a,134c,c], L. Fiorini[170], W.C. Fisher[110], T. Fitschen[104], P.M. Fitzhugh[139], I. Fleck[148], P. Fleischmann[109], T. Flick[178], M. Flores[34d,ae], L.R. Flores Castillo[65a], L. Flores Sanz De Acedo[37], F.M. Follega[79a,79b], N. Fomin[33], J.H. Foo[162], A. Formica[139], A.C. Forti[104], E. Fortin[37], A.W. Fortman[18a], L. Fountas[9,j], D. Fournier[67], H. Fox[94], P. Francavilla[75a,75b], S. Francescato[62], S. Franchellucci[57], M. Franchini[24b,24a], S. Franchino[64a], D. Francis[37], L. Franco[117], V. Franco Lima[37], L. Franconi[49], M. Franklin[62], G. Frattari[27], Y.Y. Frid[158], J. Friend[60], N. Fritzsche[37], A. Froch[57], D. Froidevaux[37], J.A. Frost[130], Y. Fu[110], S. Fuenzalida Garrido[141f], M. Fujimoto[105], K.Y. Fung[65a], E. Furtado De Simas Filho[84e], M. Furukawa[160], J. Fuster[170], A. Gaa[56], A. Gabrielli[24b,24a], A. Gabrielli[162], P. Gadow[37], G. Gagliardi[58b,58a], L.G. Gagnon[18a], S. Gaid[89b], S. Galantzan[158], J. Gallagher[1], E.J. Gallas[130], A.L. Gallen[168], B.J. Gallop[138], K.K. Gan[123], S. Ganguly[160], Y. Gao[53], A. Garabaglu[143], F.M. Garay Walls[141a,141b], B. Garcia[30], C. García[170], A. Garcia Alonso[118], A.G. Garcia Caffaro[179], J.E. García Navarro[170], M. Garcia-Sciveres[18a], G.L. Gardner[132], R.W. Gardner[41], N. Garelli[165], R.B. Garg[150], J.M. Gargan[53], C.A. Garner[162], C.M. Garvey[34a], V.K. Gassmann[165], G. Gaudio[74a], V. Gautam[13], P. Gauzzi[76a,76b], J. Gavranovic[96], I.L. Gavrilenko[134a], A. Gavrilyuk[38], C. Gay[171], G. Gaycken[127], E.N. Gazis[10], A. Gekow[123], C. Gemme[58b], M.H. Genest[61], A.D. Gentry[116], S. George[98], W.F. George[21], T. Geralis[47], A.A. Gerwin[124], P. Gessinger-Befurt[37], M.E. Geyik[178], M. Ghani[174], K. Ghorbanian[97], A. Ghosal[148], A. Ghosh[166], A. Ghosh[7], B. Giacobbe[24b], S. Giagu[76a,76b], T. Giani[118], A. Giannini[63], S.M. Gibson[98], M. Gignac[140], D.T. Gil[87b], A.K. Gilbert[87a], B.J. Gilbert[43], D. Gillberg[35], G. Gilles[118], L. Ginabat[131], D.M. Gingrich[2,ah], M.P. Giordani[70a,70c], P.F. Giraud[139], G. Giugliarelli[70a,70c], D. Giugni[72a], F. Giuli[77a,77b], I. Gkialas[9,j], L.K. Gladilin[38], C. Glasman[102], G. Glemža[49], M. Glisic[127], I. Gnesi[45b], Y. Go[30], M. Goblirsch-Kolb[37], B. Gocke[50], D. Godin[111], B. Gokturk[22a], S. Goldfarb[108], T. Golling[57], M.G.D. Gololo[34c], D. Golubkov[38], J.P. Gombas[110], A. Gomes[134a,134b], G. Gomes Da Silva[148], A.J. Gomez Delegido[170], R. Gonçalo[134a], L. Gonella[21], A. Gongadze[156c], F. Gonnella[21], J.L. Gonski[150], R.Y. González Andana[53], S. González de la Hoz[170], C. Gonzalez Renteria[18a], M.V. Gonzalez Rodrigues[49], R. Gonzalez Suarez[168], S. Gonzalez-Sevilla[57], L. Goossens[37], B. Gorini[37], E. Gorini[71a,71b], A. Gorišek[96], T.C. Gosart[132], A.T. Goshaw[52], M.I. Gostkin[40], S. Goswami[125], C.A. Gottardo[37], S.A. Gotz[112], M. Gouighri[36b], A.G. Goussiou[143], N. Govender[34c], R.P. Grabarczyk[130], I. Grabowska-Bold[87a], K. Graham[35], E. Gramstad[129], S. Grancagnolo[71a,71b], C.M. Grant[1,139], P.M. Gravila[28f], F.G. Gravili[71a,71b], H.M. Gray[18a],

2025 JINST 20 P02018

M. Greco[113], M.J. Green[1], C. Grefe[25], A.S. Grefsrud[17], I.M. Gregor[49], K.T. Greif[166], P. Grenier[150], S.G. Grewe[113], A.A. Grillo[140], K. Grimm[32], S. Grinstein[13,y], J.-F. Grivaz[67], E. Gross[176], J. Grosse-Knetter[56], L. Guan[109], G. Guerrieri[37], R. Guevara[129], R. Gugel[103], J.A.M. Guhit[109], A. Guida[19], E. Guilloton[174], S. Guindon[37], F. Guo[14,115c], J. Guo[145a], L. Guo[49], L. Guo[115b,w], Y. Guo[109], A. Gupta[50], R. Gupta[133], S. Gurbuz[25], S.S. Gurdasani[49], G. Gustavino[76a,76b], P. Gutierrez[124], L.F. Gutierrez Zagazeta[132], M. Gutsche[51], C. Gutschow[99], C. Gwenlan[130], C.B. Gwilliam[95], E.S. Haaland[129], A. Haas[121], M. Habedank[60], C. Haber[18a], H.K. Hadavand[8], A. Haddad[42], A. Hadef[51], A.I. Hagan[94], J.J. Hahn[148], E.H. Haines[99], M. Haleem[173], J. Haley[125], G.D. Hallewell[105], L. Halser[20], K. Hamano[172], M. Hamer[25], S.E.D. Hammoud[67], E.J. Hampshire[98], J. Han[144a], L. Han[115a], L. Han[63], S. Han[18a], K. Hanagaki[85], M. Hance[140], D.A. Hangal[43], H. Hanif[149], M.D. Hank[132], J.B. Hansen[44], P.H. Hansen[44], D. Harada[57], T. Harenberg[178], S. Harkusha[180], M.L. Harris[106], Y.T. Harris[25], J. Harrison[13], N.M. Harrison[123], P.F. Harrison[174], N.M. Hartman[113], N.M. Hartmann[112], R.Z. Hasan[98,138], Y. Hasegawa[147], F. Haslbeck[130], S. Hassan[17], R. Hauser[110], M. Haviernik[137], C.M. Hawkes[21], R.J. Hawkings[37], Y. Hayashi[160], D. Hayden[110], C. Hayes[109], R.L. Hayes[118], C.P. Hays[130], J.M. Hays[97], H.S. Hayward[95], F. He[63], M. He[14,115c], Y. He[49], Y. He[99], N.B. Heatley[97], V. Hedberg[101], A.L. Heggelund[129], C. Heidegger[55], K.K. Heidegger[55], J. Heilman[35], S. Heim[49], T. Heim[18a], J.G. Heinlein[132], J.J. Heinrich[127], L. Heinrich[113,af], J. Hejbal[135], A. Held[177], S. Hellesund[17], C.M. Helling[171], S. Hellman[48a,48b], L. Henkelmann[33], A.M. Henriques Correia[37], H. Herde[101], Y. Hernández Jiménez[152], L.M. Herrmann[25], T. Herrmann[51], G. Herten[55], R. Hertenberger[112], L. Hervas[37], M.E. Hesping[103], N.P. Hessey[163a], J. Hessler[113], M. Hidaoui[36b], N. Hidic[137], E. Hill[162], S.J. Hillier[21], J.R. Hinds[110], F. Hinterkeuser[25], M. Hirose[128], S. Hirose[164], D. Hirschbuehl[178], T.G. Hitchings[104], B. Hiti[96], J. Hobbs[152], R. Hobincu[28e], N. Hod[176], M.C. Hodgkinson[146], B.H. Hodkinson[130], A. Hoecker[37], D.D. Hofer[109], J. Hofer[170], M. Holzbock[37], L.B.A.H. Hommels[33], V. Homsak[130], B.P. Honan[104], J.J. Hong[69], J. Hong[145a], T.M. Hong[133], B.H. Hooberman[169], W.H. Hopkins[6], M.C. Hoppesch[169], Y. Horii[114], M.E. Horstmann[113], S. Hou[155], M.R. Housenga[169], A.S. Howard[96], J. Howarth[60], J. Hoya[6], M. Hrabovsky[126], T. Hryn'ova[4], P.J. Hsu[66], S.-C. Hsu[143], T. Hsu[67], M. Hu[18a], Q. Hu[63], S. Huang[33], X. Huang[14,115c], Y. Huang[137], Y. Huang[115b], Y. Huang[103], Y. Huang[14], Z. Huang[104], Z. Hubacek[136], M. Huebner[25], F. Huegging[25], T.B. Huffman[130], M. Hufnagel Maranha De Faria[84a], C.A. Hugli[49], M. Huhtinen[37], S.K. Huiberts[17], R. Hulsken[107], C.E. Hultquist[18a], N. Huseynov[12,g], J. Huston[110], J. Huth[62], R. Hyneman[7], G. Iacobucci[57], G. Iakovidis[30], L. Iconomidou-Fayard[67], J.P. Iddon[37], P. Iengo[73a,73b], R. Iguchi[160], Y. Iiyama[160], T. Iizawa[130], Y. Ikegami[85], D. Iliadis[159], N. Ilic[162], H. Imam[84c], G. Inacio Goncalves[84d], S.A. Infante Cabanas[141c], T. Ingebretsen Carlson[48a,48b], J.M. Inglis[97], G. Introzzi[74a,74b], M. Iodice[78a], V. Ippolito[76a,76b], R.K. Irwin[95], M. Ishino[160], W. Islam[177], C. Issever[19], S. Istin[22a,am], K. Itabashi[85], H. Ito[175], R. Iuppa[79a,79b], A. Ivina[176], V. Izzo[73a], P. Jacka[135], P. Jackson[1], P. Jain[49], K. Jakobs[55], T. Jakoubek[176], J. Jamieson[60], W. Jang[160], S. Jankovych[137], M. Javurkova[106], P. Jawahar[104], L. Jeanty[127], J. Jejelava[156a], P. Jenni[55,f], C.E. Jessiman[35], C. Jia[144a], H. Jia[171], J. Jia[152], X. Jia[14,115c], Z. Jia[115a], C. Jiang[53], Q. Jiang[65b], S. Jiggins[49], J. Jimenez Pena[13], S. Jin[115a], A. Jinaru[28b], O. Jinnouchi[142], P. Johansson[146], K.A. Johns[7], J.W. Johnson[140], F.A. Jolly[49], D.M. Jones[153], E. Jones[49], K.S. Jones[8], P. Jones[33], R.W.L. Jones[94], T.J. Jones[95], H.L. Joos[56,37], R. Joshi[123],

2025 JINST 20 P02018

J. Jovicevic[16], X. Ju[18a], J.J. Junggeburth[37], T. Junkermann[64a], A. Juste Rozas[13,y], M.K. Juzek[88], S. Kabana[141e], A. Kaczmarska[88], M. Kado[113], H. Kagan[123], M. Kagan[150], A. Kahn[132], C. Kahra[103], T. Kaji[160], E. Kajomovitz[157], N. Kakati[176], N. Kakoty[13], I. Kalaitzidou[55], S. Kandel[8], N.J. Kang[140], D. Kar[34g], K. Karava[130], E. Karentzos[25], O. Karkout[118], S.N. Karpov[40], Z.M. Karpova[40], V. Kartvelishvili[94], A.N. Karyukhin[38], E. Kasimi[159], J. Katzy[49], S. Kaur[35], K. Kawade[147], M.P. Kawale[124], C. Kawamoto[90], T. Kawamoto[63], E.F. Kay[37], F.I. Kaya[165], S. Kazakos[110], V.F. Kazanin[38], Y. Ke[152], J.M. Keaveney[34a], R. Keeler[172], G.V. Kehris[62], J.S. Keller[35], J.J. Kempster[153], O. Kepka[135], J. Kerr[163b], B.P. Kerridge[138], B.P. Kerševan[96], L. Keszeghova[29a], R.A. Khan[133], A. Khanov[125], A.G. Kharlamov[38], T. Kharlamova[38], E.E. Khoda[143], M. Kholodenko[134a], T.J. Khoo[19], G. Khoriauli[173], J. Khubua[156b,*], Y.A.R. Khwaira[131], B. Kibirige[34g], D. Kim[6], D.W. Kim[48a,48b], Y.K. Kim[41], N. Kimura[99], M.K. Kingston[56], A. Kirchhoff[56], C. Kirfel[25], F. Kirfel[25], J. Kirk[138], A.E. Kiryunin[113], S. Kita[164], C. Kitsaki[10], O. Kivernyk[25], M. Klassen[165], C. Klein[35], L. Klein[173], M.H. Klein[46], S.B. Klein[57], U. Klein[95], A. Klimentov[30], T. Klioutchnikova[37], P. Kluit[118], S. Kluth[113], E. Kneringer[80], T.M. Knight[162], A. Knue[50], D. Kobylianskii[176], S.F. Koch[130], M. Kocian[150], P. Kodyš[137], D.M. Koeck[127], P.T. Koenig[25], T. Koffas[35], O. Kolay[51], I. Koletsou[4], T. Komarek[88], K. Köneke[56], A.X.Y. Kong[1], T. Kono[122], N. Konstantinidis[99], P. Kontaxakis[57], B. Konya[101], R. Kopeliansky[43], S. Koperny[87a], K. Korcyl[88], K. Kordas[159,e], A. Korn[99], S. Korn[56], I. Korolkov[13], N. Korotkova[38], B. Kortman[118], O. Kortner[113], S. Kortner[113], W.H. Kostecka[119], M. Kostov[29a], V.V. Kostyukhin[148], A. Kotsokechagia[37], A. Kotwal[52], A. Koulouris[37], A. Kourkoumeli-Charalampidi[74a,74b], C. Kourkoumelis[9], E. Kourlitis[113,af], O. Kovanda[127], R. Kowalewski[172], W. Kozanecki[127], A.S. Kozhin[38], V.A. Kramarenko[38], G. Kramberger[96], P. Kramer[25], M.W. Krasny[131], A. Krasznahorkay[106], A.C. Kraus[119], J.W. Kraus[178], J.A. Kremer[49], N.B. Krengel[148], T. Kresse[51], L. Kretschmann[178], J. Kretzschmar[95], K. Kreul[19], P. Krieger[162], K. Krizka[21], K. Kroeninger[50], H. Kroha[113], J. Kroll[135], J. Kroll[132], K.S. Krowpman[110], U. Kruchonak[40], H. Krüger[25], N. Krumnack[82], M.C. Kruse[52], O. Kuchinskaia[40], S. Kuday[3a], S. Kuehn[37], R. Kuesters[55], T. Kuhl[49], V. Kukhtin[40], Y. Kulchitsky[40], S. Kuleshov[141d,141b], M. Kumar[34g], N. Kumari[49], P. Kumari[163b], A. Kupco[135], T. Kupfer[50], A. Kupich[38], O. Kuprash[55], H. Kurashige[86], L.L. Kurchaninov[163a], O. Kurdysh[4], Y.A. Kurochkin[39], A. Kurova[38], M. Kuze[142], A.K. Kvam[106], J. Kvita[126], N.G. Kyriacou[109], L.A.O. Laatu[105], C. Lacasta[170], F. Lacava[76a,76b], H. Lacker[19], D. Lacour[131], N.N. Lad[99], E. Ladygin[40], A. Lafarge[42], B. Laforge[131], T. Lagouri[179], F.Z. Lahbabi[36a], S. Lai[56], J.E. Lambert[172], S. Lammers[69], W. Lampl[7], C. Lampoudis[159,e], G. Lamprinoudis[103], A.N. Lancaster[119], E. Lançon[30], U. Landgraf[55], M.P.J. Landon[97], V.S. Lang[55], O.K.B. Langrekken[129], A.J. Lankford[166], F. Lanni[37], K. Lantzsch[25], A. Lanza[74a], M. Lanzac Berrocal[170], J.F. Laporte[139], T. Lari[72a], D. Larsen[17], F. Lasagni Manghi[24b], M. Lassnig[37], V. Latonova[135], S.D. Lawlor[146], Z. Lawrence[104], R. Lazaridou[174], M. Lazzaroni[72a,72b], H.D.M. Le[110], E.M. Le Boulicaut[179], L.T. Le Pottier[18a], B. Leban[24b,24a], M. LeBlanc[104], F. Ledroit-Guillon[61], S.C. Lee[155], T.F. Lee[95], L.L. Leeuw[34c,ak], M. Lefebvre[172], C. Leggett[18a], G. Lehmann Miotto[37], M. Leigh[57], W.A. Leight[106], W. Leinonen[117], A. Leisos[159,v], M.A.L. Leite[84c], C.E. Leitgeb[19], R. Leitner[137], K.J.C. Leney[46], T. Lenz[25], S. Leone[75a], C. Leonidopoulos[53], A. Leopold[151], J.H. Lepage Bourbonnais[35], R. Les[110], C.G. Lester[33], M. Levchenko[38], J. Levêque[4], L.J. Levinson[176], G. Levrini[24b,24a], M.P. Lewicki[88],

2025 JINST 20 P02018

C. Lewis[143], D.J. Lewis[4], L. Lewitt[146], A. Li[30], B. Li[144a], C. Li[109], C-Q. Li[113], H. Li[63], H. Li[144a], H. Li[104], H. Li[15], H. Li[144a], J. Li[145a], K. Li[14], L. Li[145a], R. Li[179], S. Li[14,115c], S. Li[145b,145a,d], T. Li[5], X. Li[107], Z. Li[160], Z. Li[14,115c], Z. Li[63], S. Liang[14,115c], Z. Liang[14], M. Liberatore[139], B. Liberti[77a], K. Lie[65c], J. Lieber Marin[84e], H. Lien[69], H. Lin[109], L. Linden[112], R.E. Lindley[7], J.H. Lindon[2], J. Ling[62], E. Lipeles[132], A. Lipniacka[17], A. Lister[171], J.D. Little[69], B. Liu[14], B.X. Liu[115b], D. Liu[145b,145a], E.H.L. Liu[21], J.K.K. Liu[33], K. Liu[145b], K. Liu[145b,145a], M. Liu[63], M.Y. Liu[63], P. Liu[14], Q. Liu[145b,143,145a], X. Liu[63], X. Liu[144a], Y. Liu[115b,115c], Y.L. Liu[144a], Y.W. Liu[63], Z. Liu[67,l], S.L. Lloyd[97], E.M. Lobodzinska[49], P. Loch[7], E. Lodhi[162], T. Lohse[19], K. Lohwasser[146], E. Loiacono[49], J.D. Lomas[21], J.D. Long[43], I. Longarini[166], R. Longo[169], A. Lopez Solis[49], N.A. Lopez-canelas[7], N. Lorenzo Martinez[4], A.M. Lory[112], M. Losada[120a], G. Löschcke Centeno[153], O. Loseva[38], X. Lou[48a,48b], X. Lou[14,115c], A. Lounis[67], P.A. Love[94], G. Lu[14,115c], M. Lu[67], S. Lu[132], Y.J. Lu[155], H.J. Lubatti[143], C. Luci[76a,76b], F.L. Lucio Alves[115a], F. Luehring[69], B.S. Lunday[132], O. Lundberg[151], B. Lund-Jensen[151,*], N.A. Luongo[6], M.S. Lutz[37], A.B. Lux[26], D. Lynn[30], R. Lysak[135], V. Lysenko[136], E. Lytken[101], V. Lyubushkin[40], T. Lyubushkina[40], M.M. Lyukova[152], M.Firdaus M. Soberi[53], H. Ma[30], K. Ma[63], L.L. Ma[144a], W. Ma[63], Y. Ma[125], J.C. MacDonald[103], P.C. Machado De Abreu Farias[84e], R. Madar[42], T. Madula[99], J. Maeda[86], T. Maeno[30], P.T. Mafa[34c,k], H. Maguire[146], V. Maiboroda[67], A. Maio[134a,134b,134d], K. Maj[87a], O. Majersky[49], S. Majewski[127], R. Makhmanazarov[38], N. Makovec[67], V. Maksimovic[16], B. Malaescu[131], J. Malamant[129], Pa. Malecki[88], V.P. Maleev[38], F. Malek[61,q], M. Mali[96], D. Malito[98], U. Mallik[81,*], S. Maltezos[10], A. Malvezzi Lopes[84d], S. Malyukov[40], J. Mamuzic[13], G. Mancini[54], M.N. Mancini[27], G. Manco[74a,74b], J.P. Mandalia[97], S.S. Mandarry[153], I. Mandić[96], L. Manhaes de Andrade Filho[84a], I.M. Maniatis[176], J. Manjarres Ramos[92], D.C. Mankad[176], A. Mann[112], S. Manzoni[37], L. Mao[145a], X. Mapekula[34c], A. Marantis[159,v], R.R. Marcelo Gregorio[97], G. Marchiori[5], M. Marcisovsky[135], C. Marcon[72a], M. Marinescu[21], S. Marium[49], M. Marjanovic[124], A. Markhoos[55], M. Markovitch[67], M.K. Maroun[106], E.J. Marshall[94], Z. Marshall[18a], S. Marti-Garcia[170], J. Martin[99], T.A. Martin[138], V.J. Martin[53], B. Martin dit Latour[17], L. Martinelli[76a,76b], M. Martinez[13,y], P. Martinez Agullo[170], V.I. Martinez Outschoorn[106], P. Martinez Suarez[13], S. Martin-Haugh[138], G. Martinovicova[137], V.S. Martoiu[28b], A.C. Martyniuk[99], A. Marzin[37], D. Mascione[79a,79b], L. Masetti[103], J. Masik[104], A.L. Maslennikov[40], S.L. Mason[43], P. Massarotti[73a,73b], P. Mastrandrea[75a,75b], A. Mastroberardino[45b,45a], T. Masubuchi[128], T.T. Mathew[127], J. Matousek[137], D.M. Mattern[50], J. Maurer[28b], T. Maurin[60], A.J. Maury[67], B. Maček[96], D.A. Maximov[38], A.E. May[104], E. Mayer[42], R. Mazini[34g], I. Maznas[119], M. Mazza[110], S.M. Mazza[140], E. Mazzeo[72a,72b], J.P. Mc Gowan[172], S.P. Mc Kee[109], C.A. Mc Lean[6], C.C. McCracken[171], E.F. McDonald[108], A.E. McDougall[118], L.F. Mcelhinney[94], J.A. Mcfayden[153], R.P. McGovern[132], R.P. Mckenzie[34g], T.C. Mclachlan[49], D.J. Mclaughlin[99], S.J. McMahon[138], C.M. Mcpartland[95], R.A. McPherson[172,ac], S. Mehlhase[112], A. Mehta[95], D. Melini[170], B.R. Mellado Garcia[34g], A.H. Melo[56], F. Meloni[49], A.M. Mendes Jacques Da Costa[104], H.Y. Meng[162], L. Meng[94], S. Menke[113], M. Mentink[37], E. Meoni[45b,45a], G. Mercado[119], S. Merianos[159], C. Merlassino[70a,70c], C. Meroni[72a,72b], J. Metcalfe[6], A.S. Mete[6], E. Meuser[103], C. Meyer[69], J-P. Meyer[139], R.P. Middleton[138], L. Mijović[53], G. Mikenberg[176], M. Mikestikova[135], M. Mikuž[96], H. Mildner[103], A. Milic[37], D.W. Miller[41], E.H. Miller[150], L.S. Miller[35],

2025 JINST 20 P02018

A. Milov[176], D.A. Milstead[48a,48b], T. Min[115a], A.A. Minaenko[38], I.A. Minashvili[156b], A.I. Mincer[121], B. Mindur[87a], M. Mineev[40], Y. Mino[90], L.M. Mir[13], M. Miralles Lopez[60], M. Mironova[18a], M.C. Missio[117], A. Mitra[174], V.A. Mitsou[170], Y. Mitsumori[114], O. Miu[162], P.S. Miyagawa[97], T. Mkrtchyan[64a], M. Mlinarevic[99], T. Mlinarevic[99], M. Mlynarikova[37], S. Mobius[20], P. Mogg[112], M.H. Mohamed Farook[116], A.F. Mohammed[14,115c], S. Mohapatra[43], S. Mohiuddin[125], G. Mokgatitswane[34g], L. Moleri[176], B. Mondal[148], S. Mondal[136], K. Mönig[49], E. Monnier[105], L. Monsonis Romero[170], J. Montejo Berlingen[13], A. Montella[48a,48b], M. Montella[123], F. Montereali[78a,78b], F. Monticelli[93], S. Monzani[70a,70c], A. Morancho Tarda[44], N. Morange[67], A.L. Moreira De Carvalho[49], M. Moreno Llácer[170], C. Moreno Martinez[57], J.M. Moreno Perez[23b], P. Morettini[58b], S. Morgenstern[37], M. Morii[62], M. Morinaga[160], M. Moritsu[91], F. Morodei[76a,76b], P. Moschovakos[37], B. Moser[130], M. Mosidze[156b], T. Moskalets[46], P. Moskvitina[117], J. Moss[32,n], P. Moszkowicz[87a], A. Moussa[36d], Y. Moyal[176], E.J.W. Moyse[106], O. Mtintsilana[34g], S. Muanza[105], J. Mueller[133], R. Müller[37], G.A. Mullier[168], A.J. Mullin[33], J.J. Mullin[52], A.E. Mulski[62], D.P. Mungo[162], D. Munoz Perez[170], F.J. Munoz Sanchez[104], M. Murin[104], W.J. Murray[174,138], M. Muškinja[96], C. Mwewa[30], A.G. Myagkov[38,a], A.J. Myers[8], G. Myers[109], M. Myska[136], B.P. Nachman[18a], K. Nagai[130], K. Nagano[85], R. Nagasaka[160], J.L. Nagle[30,aj], E. Nagy[105], A.M. Nairz[37], Y. Nakahama[85], K. Nakamura[85], K. Nakkalil[5], H. Nanjo[128], E.A. Narayanan[46], Y. Narukawa[160], I. Naryshkin[38], L. Nasella[72a,72b], S. Nasri[120b], C. Nass[25], G. Navarro[23a], J. Navarro-Gonzalez[170], A. Nayaz[19], P.Y. Nechaeva[38], S. Nechaeva[24b,24a], F. Nechansky[135], L. Nedic[130], T.J. Neep[21], A. Negri[74a,74b], M. Negrini[24b], C. Nellist[118], C. Nelson[107], K. Nelson[109], S. Nemecek[135], M. Nessi[37,h], M.S. Neubauer[169], J. Newell[95], P.R. Newman[21], Y.W.Y. Ng[169], B. Ngair[120a], H.D.N. Nguyen[111], R.B. Nickerson[130], R. Nicolaidou[139], J. Nielsen[140], M. Niemeyer[56], J. Niermann[37], N. Nikiforou[37], V. Nikolaenko[38,a], I. Nikolic-Audit[131], P. Nilsson[30], I. Ninca[49], G. Ninio[158], A. Nisati[76a], N. Nishu[2], R. Nisius[113], N. Nitika[70a,70c], J-E. Nitschke[51], E.K. Nkadimeng[34g], T. Nobe[160], T. Nommensen[154], M.B. Norfolk[146], B.J. Norman[35], M. Noury[36a], J. Novak[96], T. Novak[96], R. Novotny[116], L. Nozka[126], K. Ntekas[166], N.M.J. Nunes De Moura Junior[84b], J. Ocariz[131], A. Ochi[86], I. Ochoa[134a], S. Oerdek[49,z], J.T. Offermann[41], A. Ogrodnik[137], A. Oh[104], C.C. Ohm[151], H. Oide[85], R. Oishi[160], M.L. Ojeda[37], Y. Okumura[160], L.F. Oleiro Seabra[134a], I. Oleksiyuk[57], S.A. Olivares Pino[141d], G. Oliveira Correa[13], D. Oliveira Damazio[30], J.L. Oliver[166], Ö.O. Öncel[55], A.P. O'Neill[20], A. Onofre[134a,134e], P.U.E. Onyisi[11], M.J. Oreglia[41], D. Orestano[78a,78b], R. Orlandini[78a,78b], R.S. Orr[162], L.M. Osojnak[132], Y. Osumi[114], G. Otero y Garzon[31], H. Otono[91], G.J. Ottino[18a], M. Ouchrif[36d], F. Ould-Saada[129], T. Ovsiannikova[143], M. Owen[60], R.E. Owen[138], V.E. Ozcan[22a], F. Ozturk[88], N. Ozturk[8], S. Ozturk[83], H.A. Pacey[130], K. Pachal[163a], A. Pacheco Pages[13], C. Padilla Aranda[13], G. Padovano[76a,76b], S. Pagan Griso[18a], G. Palacino[69], A. Palazzo[71a,71b], J. Pampel[25], J. Pan[179], T. Pan[65a], D.K. Panchal[11], C.E. Pandini[118], J.G. Panduro Vazquez[138], H.D. Pandya[1], H. Pang[139], P. Pani[49], G. Panizzo[70a,70c], L. Panwar[131], L. Paolozzi[57], S. Parajuli[169], A. Paramonov[6], C. Paraskevopoulos[54], D. Paredes Hernandez[65b], A. Pareti[74a,74b], K.R. Park[43], T.H. Park[113], F. Parodi[58b,58a], J.A. Parsons[43], U. Parzefall[55], B. Pascual Dias[42], L. Pascual Dominguez[102], E. Pasqualucci[76a], S. Passaggio[58b], F. Pastore[98], P. Patel[88], U.M. Patel[52], J.R. Pater[104], T. Pauly[37], F. Pauwels[137], C.I. Pazos[165], M. Pedersen[129], R. Pedro[134a], S.V. Peleganchuk[38], O. Penc[37], E.A. Pender[53], S. Peng[15], G.D. Penn[179], K.E. Penski[112], M. Penzin[38],

2025 JINST 20 P02018

B.S. Peralva[84d], A.P. Pereira Peixoto[143], L. Pereira Sanchez[150], D.V. Perepelitsa[30,aj], G. Perera[106], E. Perez Codina[163a], M. Perganti[10], H. Pernegger[37], S. Perrella[76a,76b], O. Perrin[42], K. Peters[49], R.F.Y. Peters[104], B.A. Petersen[37], T.C. Petersen[44], E. Petit[105], V. Petousis[136], A.R. Petri[72a,72b], C. Petridou[159,e], T. Petru[137], A. Petrukhin[148], M. Pettee[18a], A. Petukhov[83], K. Petukhova[37], R. Pezoa[141f], L. Pezzotti[24b,24a], G. Pezzullo[179], L. Pfaffenbichler[37], A.J. Pfleger[37], T.M. Pham[177], T. Pham[108], P.W. Phillips[138], G. Piacquadio[152], E. Pianori[18a], F. Piazza[127], R. Piegaia[31], D. Pietreanu[28b], A.D. Pilkington[104], M. Pinamonti[70a,70c], J.L. Pinfold[2], B.C. Pinheiro Pereira[134a], J. Pinol Bel[13], A.E. Pinto Pinoargote[131], L. Pintucci[70a,70c], K.M. Piper[153], A. Pirttikoski[57], D.A. Pizzi[35], L. Pizzimento[65b], A. Plebani[33], M.-A. Pleier[30], V. Pleskot[137], E. Plotnikova[40], G. Poddar[97], R. Poettgen[101], L. Poggioli[131], S. Polacek[137], G. Polesello[74a], A. Poley[149,163a], A. Polini[24b], C.S. Pollard[174], Z.B. Pollock[123], E. Pompa Pacchi[124], N.I. Pond[99], D. Ponomarenko[69], L. Pontecorvo[37], S. Popa[28a], G.A. Popeneciu[28d], A. Poreba[37], D.M. Portillo Quintero[163a], S. Pospisil[136], M.A. Postill[146], P. Postolache[28c], K. Potamianos[174], P.A. Potepa[87a], I.N. Potrap[40], C.J. Potter[33], H. Potti[154], J. Poveda[170], M.E. Pozo Astigarraga[37], A. Prades Ibanez[77a,77b], J. Pretel[172], D. Price[104], M. Primavera[71a], L. Primomo[70a,70c], M.A. Principe Martin[102], R. Privara[126], T. Procter[60], M.L. Proffitt[143], N. Proklova[132], K. Prokofiev[65c], G. Proto[113], J. Proudfoot[6], M. Przybycien[87a], W.W. Przygoda[87b], A. Psallidas[47], J.E. Puddefoot[146], D. Pudzha[55], D. Pyatiizbyantseva[117], J. Qian[109], R. Qian[110], D. Qichen[104], Y. Qin[13], T. Qiu[53], A. Quadt[56], M. Queitsch-Maitland[104], G. Quetant[57], R.P. Quinn[171], G. Rabanal Bolanos[62], D. Rafanoharana[55], F. Raffaeli[77a,77b], F. Ragusa[72a,72b], J.L. Rainbolt[41], J.A. Raine[57], S. Rajagopalan[30], E. Ramakoti[38], L. Rambelli[58b,58a], I.A. Ramirez-Berend[35], K. Ran[49,115c], D.S. Rankin[132], N.P. Rapheeha[34g], H. Rasheed[28b], V. Raskina[131], D.F. Rassloff[64a], A. Rastogi[18a], S. Rave[103], S. Ravera[58b,58a], B. Ravina[37], I. Ravinovich[176], M. Raymond[37], A.L. Read[129], N.P. Readioff[146], D.M. Rebuzzi[74a,74b], A.S. Reed[113], K. Reeves[27], J.A. Reidelsturz[178], D. Reikher[127], A. Rej[50], C. Rembser[37], H. Ren[63], M. Renda[28b], F. Renner[49], A.G. Rennie[166], A.L. Rescia[49], S. Resconi[72a], M. Ressegotti[58b,58a], S. Rettie[37], W.F. Rettie[35], J.G. Reyes Rivera[110], E. Reynolds[18a], O.L. Rezanova[40], P. Reznicek[137], H. Riani[36d], N. Ribaric[52], E. Ricci[79a,79b], R. Richter[113], S. Richter[48a,48b], E. Richter-Was[87b], M. Ridel[131], S. Ridouani[36d], P. Rieck[121], P. Riedler[37], E.M. Riefel[48a,48b], J.O. Rieger[118], M. Rijssenbeek[152], M. Rimoldi[37], L. Rinaldi[24b,24a], P. Rincke[56,168], G. Ripellino[168], I. Riu[13], J.C. Rivera Vergara[172], F. Rizatdinova[125], E. Rizvi[97], B.R. Roberts[18a], S.S. Roberts[140], D. Robinson[33], M. Robles Manzano[103], A. Robson[60], A. Rocchi[77a,77b], C. Roda[75a,75b], S. Rodriguez Bosca[37], Y. Rodriguez Garcia[23a], A.M. Rodríguez Vera[119], S. Roe[37], J.T. Roemer[37], O. Røhne[129], C.P.A. Roland[131], J. Roloff[30], A. Romaniouk[80], E. Romano[74a,74b], M. Romano[24b], A.C. Romero Hernandez[169], N. Rompotis[95], L. Roos[131], S. Rosati[76a], B.J. Rosser[41], E. Rossi[130], E. Rossi[73a,73b], L.P. Rossi[62], L. Rossini[55], R. Rosten[123], M. Rotaru[28b], B. Rottler[55], D. Rousseau[67], D. Rousso[49], S. Roy-Garand[162], A. Rozanov[105], Z.M.A. Rozario[60], Y. Rozen[157], A. Rubio Jimenez[170], V.H. Ruelas Rivera[19], T.A. Ruggeri[1], A. Ruggiero[130], A. Ruiz-Martinez[170], A. Rummler[37], Z. Rurikova[55], N.A. Rusakovich[40], H.L. Russell[172], G. Russo[76a,76b], J.P. Rutherfoord[7], S. Rutherford Colmenares[33], M. Rybar[137], P. Rybczynski[87a], E.B. Rye[129], A. Ryzhov[46], J.A. Sabater Iglesias[57], H.F-W. Sadrozinski[140], F. Safai Tehrani[76a], S. Saha[1], M. Sahinsoy[83], A. Saibel[170], B.T. Saifuddin[124], M. Saimpert[139], M. Saito[160], T. Saito[160],

2025 JINST 20 P02018

A. Sala[72a,72b], D. Salamani[37], A. Salnikov[150], J. Salt[170], A. Salvador Salas[158], D. Salvatore[45b,45a], F. Salvatore[153], A. Salzburger[37], D. Sammel[55], E. Sampson[94], D. Sampsonidis[159,e], D. Sampsonidou[127], J. Sánchez[170], V. Sanchez Sebastian[170], H. Sandaker[129], C.O. Sander[49], J.A. Sandesara[106], M. Sandhoff[178], C. Sandoval[23b], L. Sanfilippo[64a], D.P.C. Sankey[138], T. Sano[90], A. Sansoni[54], L. Santi[37], C. Santoni[42], H. Santos[134a,134b], A. Santra[176], E. Sanzani[24b,24a], K.A. Saoucha[89b], J.G. Saraiva[134a,134d], J. Sardain[7], O. Sasaki[85], K. Sato[164], C. Sauer[37], E. Sauvan[4], P. Savard[162,ah], R. Sawada[160], C. Sawyer[138], L. Sawyer[100], C. Sbarra[24b], A. Sbrizzi[24b,24a], T. Scanlon[99], J. Schaarschmidt[143], U. Schäfer[103], A.C. Schaffer[67,46], D. Schaile[112], R.D. Schamberger[152], C. Scharf[19], M.M. Schefer[20], V.A. Schegelsky[38], D. Scheirich[137], M. Schernau[141e], C. Scheulen[57], C. Schiavi[58b,58a], M. Schioppa[45b,45a], B. Schlag[150], S. Schlenker[37], J. Schmeing[178], M.A. Schmidt[178], K. Schmieden[103], C. Schmitt[103], N. Schmitt[103], S. Schmitt[49], L. Schoeffel[139], A. Schoening[64b], P.G. Scholer[35], E. Schopf[148], M. Schott[25], S. Schramm[57], T. Schroer[57], H-C. Schultz-Coulon[64a], M. Schumacher[55], B.A. Schumm[140], Ph. Schune[139], H.R. Schwartz[140], A. Schwartzman[150], T.A. Schwarz[109], Ph. Schwemling[139], R. Schwienhorst[110], F.G. Sciacca[20], A. Sciandra[30], G. Sciolla[27], F. Scuri[75a], C.D. Sebastiani[37], K. Sedlaczek[119], S.C. Seidel[116], A. Seiden[140], B.D. Seidlitz[43], C. Seitz[49], J.M. Seixas[84b], G. Sekhniaidze[73a], L. Selem[61], N. Semprini-Cesari[24b,24a], A. Semushin[180,38], D. Sengupta[57], V. Senthilkumar[170], L. Serin[67], M. Sessa[77a,77b], H. Severini[124], F. Sforza[58b,58a], A. Sfyrla[57], Q. Sha[14], E. Shabalina[56], H. Shaddix[119], A.H. Shah[33], R. Shaheen[151], J.D. Shahinian[132], D. Shaked Renous[176], M. Shamim[37], L.Y. Shan[14], M. Shapiro[18a], A. Sharma[37], A.S. Sharma[171], P. Sharma[30], P.B. Shatalov[38], K. Shaw[153], S.M. Shaw[104], Q. Shen[145a], D.J. Sheppard[149], P. Sherwood[99], L. Shi[99], X. Shi[14], S. Shimizu[85], C.O. Shimmin[179], I.P.J. Shipsey[130,*], S. Shirabe[91], M. Shiyakova[40,aa], M.J. Shochet[41], D.R. Shope[129], B. Shrestha[124], S. Shrestha[123,al], I. Shreyber[40], M.J. Shroff[172], P. Sicho[135], A.M. Sickles[169], E. Sideras Haddad[34g,167], A.C. Sidley[118], A. Sidoti[24b], F. Siegert[51], Dj. Sijacki[16], F. Sili[93], J.M. Silva[53], I. Silva Ferreira[84b], M.V. Silva Oliveira[30], S.B. Silverstein[48a], S. Simion[67], R. Simoniello[37], E.L. Simpson[104], H. Simpson[153], L.R. Simpson[109], S. Simsek[83], S. Sindhu[56], P. Sinervo[162], S.N. Singh[27], S. Singh[30], S. Sinha[49], S. Sinha[104], M. Sioli[24b,24a], K. Sioulas[9], I. Siral[37], E. Sitnikova[49], J. Sjölin[48a,48b], A. Skaf[56], E. Skorda[21], P. Skubic[124], M. Slawinska[88], I. Slazyk[17], V. Smakhtin[176], B.H. Smart[138], S.Yu. Smirnov[141b], Y. Smirnov[83], L.N. Smirnova[38,a], O. Smirnova[101], A.C. Smith[43], D.R. Smith[166], E.A. Smith[41], J.L. Smith[104], M.B. Smith[35], R. Smith[150], H. Smitmanns[103], M. Smizanska[94], K. Smolek[136], P. Smolyanskiy[136], A.A. Snesarev[40], H.L. Snoek[118], S. Snyder[30], R. Sobie[172,ac], A. Soffer[158], C.A. Solans Sanchez[37], E.Yu. Soldatov[40], U. Soldevila[170], A.A. Solodkov[34g], S. Solomon[27], A. Soloshenko[40], K. Solovieva[55], O.V. Solovyanov[42], P. Sommer[51], A. Sonay[13], W.Y. Song[163b], A. Sopczak[136], A.L. Sopio[53], F. Sopkova[29b], J.D. Sorenson[116], I.R. Sotarriva Alvarez[142], V. Sothilingam[64a], O.J. Soto Sandoval[141c,141b], S. Sottocornola[69], R. Soualah[89a], Z. Soumaimi[36e], D. South[49], N. Soybelman[176], S. Spagnolo[71a,71b], M. Spalla[113], D. Sperlich[55], B. Spisso[73a,73b], D.P. Spiteri[60], L. Splendori[105], M. Spousta[137], E.J. Staats[35], R. Stamen[64a], E. Stanecka[88], W. Stanek-Maslouska[49], M.V. Stange[51], B. Stanislaus[18a], M.M. Stanitzki[49], B. Stapf[49], E.A. Starchenko[38], G.H. Stark[140], J. Stark[92], P. Staroba[135], P. Starovoitov[89b], R. Staszewski[88], G. Stavropoulos[47], A. Stefl[37], P. Steinberg[30], B. Stelzer[149,163a], H.J. Stelzer[133],

2025 JINST 20 P02018

O. Stelzer-Chilton[163a], H. Stenzel[59], T.J. Stevenson[153], G.A. Stewart[37], J.R. Stewart[125], M.C. Stockton[37], G. Stoicea[28b], M. Stolarski[134a], S. Stonjek[113], A. Straessner[51], J. Strandberg[151], S. Strandberg[48a,48b], M. Stratmann[178], M. Strauss[124], T. Strebler[105], P. Strizenec[29b], R. Ströhmer[173], D.M. Strom[127], R. Stroynowski[46], A. Strubig[48a,48b], S.A. Stucci[30], B. Stugu[17], J. Stupak[124], N.A. Styles[49], D. Su[150], S. Su[63], W. Su[145b], X. Su[63], D. Suchy[29a], K. Sugizaki[132], V.V. Sulin[38], M.J. Sullivan[95], D.M.S. Sultan[130], L. Sultanaliyeva[38], S. Sultansoy[3b], S. Sun[177], W. Sun[14], O. Sunneborn Gudnadottir[168], N. Sur[105], M.R. Sutton[153], H. Suzuki[164], M. Svatos[135], P.N. Swallow[33], M. Swiatlowski[163a], T. Swirski[173], I. Sykora[29a], M. Sykora[137], T. Sykora[137], D. Ta[103], K. Tackmann[49,z], A. Taffard[166], R. Tafirout[163a], Y. Takubo[85], M. Talby[105], A.A. Talyshev[38], K.C. Tam[65b], N.M. Tamir[158], A. Tanaka[160], J. Tanaka[160], R. Tanaka[67], M. Tanasini[152], Z. Tao[171], S. Tapia Araya[141f], S. Tapprogge[103], A. Tarek Abouelfadl Mohamed[110], S. Tarem[157], K. Tariq[14], G. Tarna[28b], G.F. Tartarelli[72a], M.J. Tartarin[92], P. Tas[137], M. Tasevsky[135], E. Tassi[45b,45a], A.C. Tate[169], G. Tateno[160], Y. Tayalati[36e,ab], G.N. Taylor[108], W. Taylor[163b], A.S. Tegetmeier[92], P. Teixeira-Dias[98], J.J. Teoh[162], K. Terashi[160], J. Terron[102], S. Terzo[13], M. Testa[54], R.J. Teuscher[162,ac], A. Thaler[80], O. Theiner[57], T. Theveneaux-Pelzer[105], O. Thielmann[178], D.W. Thomas[98], J.P. Thomas[21], E.A. Thompson[18a], P.D. Thompson[21], E. Thomson[132], R.E. Thornberry[46], C. Tian[63], Y. Tian[57], V. Tikhomirov[83], Yu.A. Tikhonov[38], S. Timoshenko[38], D. Timoshyn[137], E.X.L. Ting[1], P. Tipton[179], A. Tishelman-Charny[30], S.H. Tlou[34g], K. Todome[142], S. Todorova-Nova[137], S. Todt[51], L. Toffolin[70a,70c], M. Togawa[85], J. Tojo[91], S. Tokár[29a], O. Toldaiev[69], G. Tolkachev[105], M. Tomoto[85,114], L. Tompkins[150,p], E. Torrence[127], H. Torres[92], E. Torró Pastor[170], M. Toscani[31], C. Tosciri[41], M. Tost[11], D.R. Tovey[146], T. Trefzger[173], P.M. Tricarico[13], A. Tricoli[30], I.M. Trigger[163a], S. Trincaz-Duvoid[131], D.A. Trischuk[27], A. Tropina[40], L. Truong[34c], M. Trzebinski[88], A. Trzupek[88], F. Tsai[152], M. Tsai[109], A. Tsiamis[159], P.V. Tsiareshka[40], S. Tsigaridas[163a], A. Tsirigotis[159,v], V. Tsiskaridze[162], E.G. Tskhadadze[156a], M. Tsopoulou[159], Y. Tsujikawa[90], I.I. Tsukerman[38], V. Tsulaia[18a], S. Tsuno[85], K. Tsuri[122], D. Tsybychev[152], Y. Tu[65b], A. Tudorache[28b], V. Tudorache[28b], S. Turchikhin[58b,58a], I. Turk Cakir[3a], R. Turra[72a], T. Turtuvshin[40], P.M. Tuts[43], S. Tzamarias[159,e], E. Tzovara[103], Y. Uematsu[85], F. Ukegawa[164], P.A. Ulloa Poblete[141c,141b], E.N. Umaka[30], G. Unal[37], A. Undrus[30], G. Unel[166], J. Urban[29b], P. Urrejola[141a], G. Usai[8], R. Ushioda[161], M. Usman[111], F. Ustuner[53], Z. Uysal[83], V. Vacek[136], B. Vachon[107], T. Vafeiadis[37], A. Vaitkus[99], C. Valderanis[112], E. Valdes Santurio[48a,48b], M. Valente[163a], S. Valentinetti[24b,24a], A. Valero[170], E. Valiente Moreno[170], A. Vallier[92], J.A. Valls Ferrer[170], D.R. Van Arneman[118], T.R. Van Daalen[143], A. Van Der Graaf[50], H.Z. Van Der Schyf[34g], P. Van Gemmeren[6], M. Van Rijnbach[37], S. Van Stroud[99], I. Van Vulpen[118], P. Vana[137], M. Vanadia[77a,77b], U.M. Vande Voorde[151], W. Vandelli[37], E.R. Vandewall[125], D. Vannicola[158], L. Vannoli[54], R. Vari[76a], E.W. Varnes[7], C. Varni[18b], D. Varouchas[67], L. Varriale[170], K.E. Varvell[154], M.E. Vasile[28b], L. Vaslin[85], A. Vasyukov[40], L.M. Vaughan[125], R. Vavricka[137], T. Vazquez Schroeder[13], J. Veatch[32], V. Vecchio[104], M.J. Veen[106], I. Veliscek[30], L.M. Veloce[162], F. Veloso[134a,134c], S. Veneziano[76a], A. Ventura[71a,71b], S. Ventura Gonzalez[139], A. Verbytskyi[113], M. Verducci[75a,75b], C. Vergis[97], M. Verissimo De Araujo[84b], W. Verkerke[118], J.C. Vermeulen[118], C. Vernieri[150], M. Vessella[166], M.C. Vetterli[149,ah], A. Vgenopoulos[103], N. Viaux Maira[141f], T. Vickey[146], O.E. Vickey Boeriu[146], G.H.A. Viehhauser[130], L. Vigani[64b], M. Vigl[113], M. Villa[24b,24a], M. Villaplana Perez[170],

2025 JINST 20 P02018

E.M. Villhauer[53], E. Vilucchi[54], M.G. Vincter[35], A. Visibile[118], C. Vittori[37], I. Vivarelli[24b,24a], E. Voevodina[113], F. Vogel[112], J.C. Voigt[51], P. Vokac[136], Yu. Volkotrub[87b], E. Von Toerne[25], B. Vormwald[37], K. Vorobev[38], M. Vos[170], K. Voss[148], M. Vozak[37], L. Vozdecky[124], N. Vranjes[16], M. Vranjes Milosavljevic[16], M. Vreeswijk[118], N.K. Vu[145b,145a], R. Vuillermet[37], O. Vujinovic[103], I. Vukotic[41], I.K. Vyas[35], J.F. Wack[33], S. Wada[164], C. Wagner[150], J.M. Wagner[18a], W. Wagner[178], S. Wahdan[178], H. Wahlberg[93], C.H. Waits[124], J. Walder[138], R. Walker[112], W. Walkowiak[148], A. Wall[132], E.J. Wallin[101], T. Wamorkar[18a], A.Z. Wang[140], C. Wang[103], C. Wang[11], H. Wang[18a], J. Wang[65c], P. Wang[104], P. Wang[99], R. Wang[62], R. Wang[6], S.M. Wang[155], S. Wang[14], T. Wang[63], T. Wang[63], W.T. Wang[81], W. Wang[14], X. Wang[169], X. Wang[145a], X. Wang[49], Y. Wang[115a], Y. Wang[63], Z. Wang[109], Z. Wang[145b,52,145a], Z. Wang[109], C. Wanotayaroj[85], A. Warburton[107], R.J. Ward[21], A.L. Warnerbring[148], N. Warrack[60], S. Waterhouse[98], A.T. Watson[21], H. Watson[53], M.F. Watson[21], E. Watton[60], G. Watts[143], B.M. Waugh[99], J.M. Webb[55], C. Weber[30], H.A. Weber[19], M.S. Weber[20], S.M. Weber[64a], C. Wei[63], Y. Wei[55], A.R. Weidberg[130], E.J. Weik[121], J. Weingarten[50], C. Weiser[55], C.J. Wells[49], T. Wenaus[30], B. Wendland[50], T. Wengler[37], N.S. Wenke[113], N. Wermes[25], M. Wessels[64a], A.M. Wharton[94], A.S. White[62], A. White[8], M.J. White[1], D. Whiteson[166], L. Wickremasinghe[128], W. Wiedenmann[177], M. Wielers[138], C. Wiglesworth[44], D.J. Wilbern[124], H.G. Wilkens[37], J.J.H. Wilkinson[33], D.M. Williams[43], H.H. Williams[132], S. Williams[33], S. Willocq[106], B.J. Wilson[104], D.J. Wilson[104], P.J. Windischhofer[41], F.I. Winkel[31], F. Winklmeier[127], B.T. Winter[55], M. Wittgen[150], M. Wobisch[100], T. Wojtkowski[61], Z. Wolffs[118], J. Wollrath[37], M.W. Wolter[88], H. Wolters[134a,134c], M.C. Wong[140], E.L. Woodward[43], S.D. Worm[49], B.K. Wosiek[88], K.W. Woźniak[88], S. Wozniewski[56], K. Wraight[60], C. Wu[21], M. Wu[115b], M. Wu[117], S.L. Wu[177], X. Wu[57], X. Wu[63], Y. Wu[63], Z. Wu[4], J. Wuerzinger[113,af], T.R. Wyatt[104], B.M. Wynne[53], S. Xella[44], L. Xia[115a], M. Xia[15], M. Xie[63], A. Xiong[127], J. Xiong[18a], D. Xu[14], H. Xu[63], L. Xu[63], R. Xu[132], T. Xu[109], Y. Xu[143], Z. Xu[53], Z. Xu[115a], B. Yabsley[154], S. Yacoob[34a], Y. Yamaguchi[85], E. Yamashita[160], H. Yamauchi[164], T. Yamazaki[18a], Y. Yamazaki[86], S. Yan[60], Z. Yan[106], H.J. Yang[145a,145b], H.T. Yang[63], S. Yang[63], T. Yang[65c], X. Yang[37], X. Yang[14], Y. Yang[160], Y. Yang[63], W-M. Yao[18a], C.L. Yardley[153], H. Ye[56], J. Ye[14], S. Ye[30], X. Ye[63], Y. Yeh[99], I. Yeletskikh[40], B. Yeo[18b], M.R. Yexley[99], T.P. Yildirim[130], P. Yin[43], K. Yorita[175], S. Younas[28b], C.J.S. Young[37], C. Young[150], N.D. Young[127], Y. Yu[63], J. Yuan[14,115c], M. Yuan[109], R. Yuan[145b,145a], L. Yue[99], M. Zaazoua[63], B. Zabinski[88], I. Zahir[36a], A. Zaio[58b,58a], Z.K. Zak[88], T. Zakareishvili[170], S. Zambito[57], J.A. Zamora Saa[141d], J. Zang[160], D. Zanzi[55], R. Zanzottera[72a,72b], O. Zaplatilek[136], C. Zeitnitz[178], H. Zeng[14], J.C. Zeng[169], D.T. Zenger Jr[27], O. Zenin[38], T. Ženiš[29a], S. Zenz[97], S. Zerradi[36a], D. Zerwas[67], M. Zhai[14,115c], D.F. Zhang[146], J. Zhang[144a], J. Zhang[6], K. Zhang[14,115c], L. Zhang[63], L. Zhang[115a], P. Zhang[14,115c], R. Zhang[177], S. Zhang[92], T. Zhang[160], X. Zhang[145a], Y. Zhang[143], Y. Zhang[99], Y. Zhang[63], Y. Zhang[115a], Z. Zhang[18a], Z. Zhang[144a], Z. Zhang[67], H. Zhao[143], T. Zhao[144a], Y. Zhao[35], Z. Zhao[63], Z. Zhao[63], A. Zhemchugov[40], J. Zheng[115a], K. Zheng[169], X. Zheng[63], Z. Zheng[150], D. Zhong[169], B. Zhou[109], H. Zhou[7], N. Zhou[145a], Y. Zhou[15], Y. Zhou[115a], Y. Zhou[7], C.G. Zhu[144a], J. Zhu[109], X. Zhu[145b], Y. Zhu[145a], Y. Zhu[63], X. Zhuang[14], K. Zhukov[69], N.I. Zimine[40], J. Zinsser[64b], M. Ziolkowski[148], L. Živković[16], A. Zoccoli[24b,24a], K. Zoch[62], T.G. Zorbas[146], O. Zormpa[47], W. Zou[43], L. Zwalinski[37]

[1] *Department of Physics, University of Adelaide, Adelaide; Australia*

2025 JINST 20 P02018

[2] Department of Physics, University of Alberta, Edmonton AB; Canada
[3] [(a)] Department of Physics, Ankara University, Ankara; [(b)] Division of Physics, TOBB University of Economics and Technology, Ankara; Türkiye
[4] LAPP, Université Savoie Mont Blanc, CNRS/IN2P3, Annecy; France
[5] APC, Université Paris Cité, CNRS/IN2P3, Paris; France
[6] High Energy Physics Division, Argonne National Laboratory, Argonne IL; United States of America
[7] Department of Physics, University of Arizona, Tucson AZ; United States of America
[8] Department of Physics, University of Texas at Arlington, Arlington TX; United States of America
[9] Physics Department, National and Kapodistrian University of Athens, Athens; Greece
[10] Physics Department, National Technical University of Athens, Zografou; Greece
[11] Department of Physics, University of Texas at Austin, Austin TX; United States of America
[12] Institute of Physics, Azerbaijan Academy of Sciences, Baku; Azerbaijan
[13] Institut de Física d'Altes Energies (IFAE), Barcelona Institute of Science and Technology, Barcelona; Spain
[14] Institute of High Energy Physics, Chinese Academy of Sciences, Beijing; China
[15] Physics Department, Tsinghua University, Beijing; China
[16] Institute of Physics, University of Belgrade, Belgrade; Serbia
[17] Department for Physics and Technology, University of Bergen, Bergen; Norway
[18] [(a)] Physics Division, Lawrence Berkeley National Laboratory, Berkeley CA; [(b)] University of California, Berkeley CA; United States of America
[19] Institut für Physik, Humboldt Universität zu Berlin, Berlin; Germany
[20] Albert Einstein Center for Fundamental Physics and Laboratory for High Energy Physics, University of Bern, Bern; Switzerland
[21] School of Physics and Astronomy, University of Birmingham, Birmingham; United Kingdom
[22] [(a)] Department of Physics, Bogazici University, Istanbul; [(b)] Department of Physics Engineering, Gaziantep University, Gaziantep; [(c)] Department of Physics, Istanbul University, Istanbul; Türkiye
[23] [(a)] Facultad de Ciencias y Centro de Investigaciónes, Universidad Antonio Nariño, Bogotá; [(b)] Departamento de Física, Universidad Nacional de Colombia, Bogotá; Colombia
[24] [(a)] Dipartimento di Fisica e Astronomia A. Righi, Università di Bologna, Bologna; [(b)] INFN Sezione di Bologna; Italy
[25] Physikalisches Institut, Universität Bonn, Bonn; Germany
[26] Department of Physics, Boston University, Boston MA; United States of America
[27] Department of Physics, Brandeis University, Waltham MA; United States of America
[28] [(a)] Transilvania University of Brasov, Brasov; [(b)] Horia Hulubei National Institute of Physics and Nuclear Engineering, Bucharest; [(c)] Department of Physics, Alexandru Ioan Cuza University of Iasi, Iasi; [(d)] National Institute for Research and Development of Isotopic and Molecular Technologies, Physics Department, Cluj-Napoca; [(e)] National University of Science and Technology Politechnica, Bucharest; [(f)] West University in Timisoara, Timisoara; [(g)] Faculty of Physics, University of Bucharest, Bucharest; Romania
[29] [(a)] Faculty of Mathematics, Physics and Informatics, Comenius University, Bratislava; [(b)] Department of Subnuclear Physics, Institute of Experimental Physics of the Slovak Academy of Sciences, Kosice; Slovak Republic
[30] Physics Department, Brookhaven National Laboratory, Upton NY; United States of America
[31] Universidad de Buenos Aires, Facultad de Ciencias Exactas y Naturales, Departamento de Física, y CONICET, Instituto de Física de Buenos Aires (IFIBA), Buenos Aires; Argentina
[32] California State University, CA; United States of America
[33] Cavendish Laboratory, University of Cambridge, Cambridge; United Kingdom
[34] [(a)] Department of Physics, University of Cape Town, Cape Town; [(b)] iThemba Labs, Western Cape; [(c)] Department of Mechanical Engineering Science, University of Johannesburg, Johannesburg; [(d)] National Institute of Physics, University of the Philippines Diliman (Philippines); [(e)] University of South Africa, Department of Physics, Pretoria; [(f)] University of Zululand, KwaDlangezwa; [(g)] School of Physics, University of the Witwatersrand, Johannesburg; South Africa
[35] Department of Physics, Carleton University, Ottawa ON; Canada
[36] [(a)] Faculté des Sciences Ain Chock, Université Hassan II de Casablanca; [(b)] Faculté des Sciences, Université Ibn-Tofail, Kénitra; [(c)] Faculté des Sciences Semlalia, Université Cadi Ayyad, LPHEA-Marrakech; [(d)] LPMR, Faculté des Sciences, Université Mohamed Premier, Oujda; [(e)] Faculté des sciences, Université Mohammed V, Rabat; [(f)] Institute of Applied Physics, Mohammed VI Polytechnic University, Ben Guerir; Morocco

2025 JINST 20 P02018

[37] CERN, Geneva; Switzerland
[38] Affiliated with an institute covered by a cooperation agreement with CERN
[39] Affiliated with an institute formerly covered by a cooperation agreement with CERN
[40] Affiliated with an international laboratory covered by a cooperation agreement with CERN
[41] Enrico Fermi Institute, University of Chicago, Chicago IL; United States of America
[42] LPC, Université Clermont Auvergne, CNRS/IN2P3, Clermont-Ferrand; France
[43] Nevis Laboratory, Columbia University, Irvington NY; United States of America
[44] Niels Bohr Institute, University of Copenhagen, Copenhagen; Denmark
[45] [(a)] Dipartimento di Fisica, Università della Calabria, Rende; [(b)] INFN Gruppo Collegato di Cosenza, Laboratori Nazionali di Frascati; Italy
[46] Physics Department, Southern Methodist University, Dallas TX; United States of America
[47] National Centre for Scientific Research "Demokritos", Agia Paraskevi; Greece
[48] [(a)] Department of Physics, Stockholm University; [(b)] Oskar Klein Centre, Stockholm; Sweden
[49] Deutsches Elektronen-Synchrotron DESY, Hamburg and Zeuthen; Germany
[50] Fakultät Physik , Technische Universität Dortmund, Dortmund; Germany
[51] Institut für Kern- und Teilchenphysik, Technische Universität Dresden, Dresden; Germany
[52] Department of Physics, Duke University, Durham NC; United States of America
[53] SUPA - School of Physics and Astronomy, University of Edinburgh, Edinburgh; United Kingdom
[54] INFN e Laboratori Nazionali di Frascati, Frascati; Italy
[55] Physikalisches Institut, Albert-Ludwigs-Universität Freiburg, Freiburg; Germany
[56] II. Physikalisches Institut, Georg-August-Universität Göttingen, Göttingen; Germany
[57] Département de Physique Nucléaire et Corpusculaire, Université de Genève, Genève; Switzerland
[58] [(a)] Dipartimento di Fisica, Università di Genova, Genova; [(b)] INFN Sezione di Genova; Italy
[59] II. Physikalisches Institut, Justus-Liebig-Universität Giessen, Giessen; Germany
[60] SUPA - School of Physics and Astronomy, University of Glasgow, Glasgow; United Kingdom
[61] LPSC, Université Grenoble Alpes, CNRS/IN2P3, Grenoble INP, Grenoble; France
[62] Laboratory for Particle Physics and Cosmology, Harvard University, Cambridge MA; United States of America
[63] Department of Modern Physics and State Key Laboratory of Particle Detection and Electronics, University of Science and Technology of China, Hefei; China
[64] [(a)] Kirchhoff-Institut für Physik, Ruprecht-Karls-Universität Heidelberg, Heidelberg; [(b)] Physikalisches Institut, Ruprecht-Karls-Universität Heidelberg, Heidelberg; Germany
[65] [(a)] Department of Physics, Chinese University of Hong Kong, Shatin, N.T., Hong Kong; [(b)] Department of Physics, University of Hong Kong, Hong Kong; [(c)] Department of Physics and Institute for Advanced Study, Hong Kong University of Science and Technology, Clear Water Bay, Kowloon, Hong Kong; China
[66] Department of Physics, National Tsing Hua University, Hsinchu; Taiwan
[67] IJCLab, Université Paris-Saclay, CNRS/IN2P3, 91405, Orsay; France
[68] Centro Nacional de Microelectrónica (IMB-CNM-CSIC), Barcelona; Spain
[69] Department of Physics, Indiana University, Bloomington IN; United States of America
[70] [(a)] INFN Gruppo Collegato di Udine, Sezione di Trieste, Udine; [(b)] ICTP, Trieste; [(c)] Dipartimento Politecnico di Ingegneria e Architettura, Università di Udine, Udine; Italy
[71] [(a)] INFN Sezione di Lecce; [(b)] Dipartimento di Matematica e Fisica, Università del Salento, Lecce; Italy
[72] [(a)] INFN Sezione di Milano; [(b)] Dipartimento di Fisica, Università di Milano, Milano; Italy
[73] [(a)] INFN Sezione di Napoli; [(b)] Dipartimento di Fisica, Università di Napoli, Napoli; Italy
[74] [(a)] INFN Sezione di Pavia; [(b)] Dipartimento di Fisica, Università di Pavia, Pavia; Italy
[75] [(a)] INFN Sezione di Pisa; [(b)] Dipartimento di Fisica E. Fermi, Università di Pisa, Pisa; Italy
[76] [(a)] INFN Sezione di Roma; [(b)] Dipartimento di Fisica, Sapienza Università di Roma, Roma; Italy
[77] [(a)] INFN Sezione di Roma Tor Vergata; [(b)] Dipartimento di Fisica, Università di Roma Tor Vergata, Roma; Italy
[78] [(a)] INFN Sezione di Roma Tre; [(b)] Dipartimento di Matematica e Fisica, Università Roma Tre, Roma; Italy
[79] [(a)] INFN-TIFPA; [(b)] Università degli Studi di Trento, Trento; Italy
[80] Universität Innsbruck, Department of Astro and Particle Physics, Innsbruck; Austria
[81] University of Iowa, Iowa City IA; United States of America
[82] Department of Physics and Astronomy, Iowa State University, Ames IA; United States of America
[83] Istinye University, Sariyer, Istanbul; Türkiye

2025 JINST 20 P02018

[84] [(a)] Departamento de Engenharia Elétrica, Universidade Federal de Juiz de Fora (UFJF), Juiz de Fora; [(b)] Universidade Federal do Rio De Janeiro COPPE/EE/IF, Rio de Janeiro; [(c)] Instituto de Física, Universidade de São Paulo, São Paulo; [(d)] Rio de Janeiro State University, Rio de Janeiro; [(e)] Federal University of Bahia, Bahia; Brazil
[85] KEK, High Energy Accelerator Research Organization, Tsukuba; Japan
[86] Graduate School of Science, Kobe University, Kobe; Japan
[87] [(a)] AGH University of Krakow, Faculty of Physics and Applied Computer Science, Krakow; [(b)] Marian Smoluchowski Institute of Physics, Jagiellonian University, Krakow; Poland
[88] Institute of Nuclear Physics Polish Academy of Sciences, Krakow; Poland
[89] [(a)] Khalifa University of Science and Technology, Abu Dhabi; [(b)] University of Sharjah, Sharjah; United Arab Emirates
[90] Faculty of Science, Kyoto University, Kyoto; Japan
[91] Research Center for Advanced Particle Physics and Department of Physics, Kyushu University, Fukuoka; Japan
[92] L2IT, Université de Toulouse, CNRS/IN2P3, UPS, Toulouse; France
[93] Instituto de Física La Plata, Universidad Nacional de La Plata and CONICET, La Plata; Argentina
[94] Physics Department, Lancaster University, Lancaster; United Kingdom
[95] Oliver Lodge Laboratory, University of Liverpool, Liverpool; United Kingdom
[96] Department of Experimental Particle Physics, Jožef Stefan Institute and Department of Physics, University of Ljubljana, Ljubljana; Slovenia
[97] School of Physics and Astronomy, Queen Mary University of London, London; United Kingdom
[98] Department of Physics, Royal Holloway University of London, Egham; United Kingdom
[99] Department of Physics and Astronomy, University College London, London; United Kingdom
[100] Louisiana Tech University, Ruston LA; United States of America
[101] Fysiska institutionen, Lunds universitet, Lund; Sweden
[102] Departamento de Física Teorica C-15 and CIAFF, Universidad Autónoma de Madrid, Madrid; Spain
[103] Institut für Physik, Universität Mainz, Mainz; Germany
[104] School of Physics and Astronomy, University of Manchester, Manchester; United Kingdom
[105] CPPM, Aix-Marseille Université, CNRS/IN2P3, Marseille; France
[106] Department of Physics, University of Massachusetts, Amherst MA; United States of America
[107] Department of Physics, McGill University, Montreal QC; Canada
[108] School of Physics, University of Melbourne, Victoria; Australia
[109] Department of Physics, University of Michigan, Ann Arbor MI; United States of America
[110] Department of Physics and Astronomy, Michigan State University, East Lansing MI; United States of America
[111] Group of Particle Physics, University of Montreal, Montreal QC; Canada
[112] Fakultät für Physik, Ludwig-Maximilians-Universität München, München; Germany
[113] Max-Planck-Institut für Physik (Werner-Heisenberg-Institut), München; Germany
[114] Graduate School of Science and Kobayashi-Maskawa Institute, Nagoya University, Nagoya; Japan
[115] [(a)] Department of Physics, Nanjing University, Nanjing; [(b)] School of Science, Shenzhen Campus of Sun Yat-sen University; [(c)] University of Chinese Academy of Science (UCAS), Beijing; China
[116] Department of Physics and Astronomy, University of New Mexico, Albuquerque NM; United States of America
[117] Institute for Mathematics, Astrophysics and Particle Physics, Radboud University/Nikhef, Nijmegen; Netherlands
[118] Nikhef National Institute for Subatomic Physics and University of Amsterdam, Amsterdam; Netherlands
[119] Department of Physics, Northern Illinois University, DeKalb IL; United States of America
[120] [(a)] New York University Abu Dhabi, Abu Dhabi; [(b)] United Arab Emirates University, Al Ain; United Arab Emirates
[121] Department of Physics, New York University, New York NY; United States of America
[122] Ochanomizu University, Otsuka, Bunkyo-ku, Tokyo; Japan
[123] Ohio State University, Columbus OH; United States of America
[124] Homer L. Dodge Department of Physics and Astronomy, University of Oklahoma, Norman OK; United States of America
[125] Department of Physics, Oklahoma State University, Stillwater OK; United States of America
[126] Palacký University, Joint Laboratory of Optics, Olomouc; Czech Republic
[127] Institute for Fundamental Science, University of Oregon, Eugene, OR; United States of America
[128] Graduate School of Science, Osaka University, Osaka; Japan
[129] Department of Physics, University of Oslo, Oslo; Norway
[130] Department of Physics, Oxford University, Oxford; United Kingdom

2025 JINST 20 P02018

[131] LPNHE, Sorbonne Université, Université Paris Cité, CNRS/IN2P3, Paris; France
[132] Department of Physics, University of Pennsylvania, Philadelphia PA; United States of America
[133] Department of Physics and Astronomy, University of Pittsburgh, Pittsburgh PA; United States of America
[134] [(a)] Laboratório de Instrumentação e Física Experimental de Partículas - LIP, Lisboa; [(b)] Departamento de Física, Faculdade de Ciências, Universidade de Lisboa, Lisboa; [(c)] Departamento de Física, Universidade de Coimbra, Coimbra; [(d)] Centro de Física Nuclear da Universidade de Lisboa, Lisboa; [(e)] Departamento de Física, Universidade do Minho, Braga; [(f)] Departamento de Física Teórica y del Cosmos, Universidad de Granada, Granada (Spain); [(g)] Departamento de Física, Instituto Superior Técnico, Universidade de Lisboa, Lisboa; Portugal
[135] Institute of Physics of the Czech Academy of Sciences, Prague; Czech Republic
[136] Czech Technical University in Prague, Prague; Czech Republic
[137] Charles University, Faculty of Mathematics and Physics, Prague; Czech Republic
[138] Particle Physics Department, Rutherford Appleton Laboratory, Didcot; United Kingdom
[139] IRFU, CEA, Université Paris-Saclay, Gif-sur-Yvette; France
[140] Santa Cruz Institute for Particle Physics, University of California Santa Cruz, Santa Cruz CA; United States of America
[141] [(a)] Departamento de Física, Pontificia Universidad Católica de Chile, Santiago; [(b)] Millennium Institute for Subatomic physics at high energy frontier (SAPHIR), Santiago; [(c)] Instituto de Investigación Multidisciplinario en Ciencia y Tecnología, y Departamento de Física, Universidad de La Serena; [(d)] Universidad Andres Bello, Department of Physics, Santiago; [(e)] Instituto de Alta Investigación, Universidad de Tarapacá, Arica; [(f)] Departamento de Física, Universidad Técnica Federico Santa María, Valparaíso; Chile
[142] Department of Physics, Institute of Science, Tokyo; Japan
[143] Department of Physics, University of Washington, Seattle WA; United States of America
[144] [(a)] Institute of Frontier and Interdisciplinary Science and Key Laboratory of Particle Physics and Particle Irradiation (MOE), Shandong University, Qingdao; [(b)] School of Physics, Zhengzhou University; China
[145] [(a)] School of Physics and Astronomy, Shanghai Jiao Tong University, Key Laboratory for Particle Astrophysics and Cosmology (MOE), SKLPPC, Shanghai; [(b)] Tsung-Dao Lee Institute, Shanghai; China
[146] Department of Physics and Astronomy, University of Sheffield, Sheffield; United Kingdom
[147] Department of Physics, Shinshu University, Nagano; Japan
[148] Department Physik, Universität Siegen, Siegen; Germany
[149] Department of Physics, Simon Fraser University, Burnaby BC; Canada
[150] SLAC National Accelerator Laboratory, Stanford CA; United States of America
[151] Department of Physics, Royal Institute of Technology, Stockholm; Sweden
[152] Departments of Physics and Astronomy, Stony Brook University, Stony Brook NY; United States of America
[153] Department of Physics and Astronomy, University of Sussex, Brighton; United Kingdom
[154] School of Physics, University of Sydney, Sydney; Australia
[155] Institute of Physics, Academia Sinica, Taipei; Taiwan
[156] [(a)] E. Andronikashvili Institute of Physics, Iv. Javakhishvili Tbilisi State University, Tbilisi; [(b)] High Energy Physics Institute, Tbilisi State University, Tbilisi; [(c)] University of Georgia, Tbilisi; Georgia
[157] Department of Physics, Technion, Israel Institute of Technology, Haifa; Israel
[158] Raymond and Beverly Sackler School of Physics and Astronomy, Tel Aviv University, Tel Aviv; Israel
[159] Department of Physics, Aristotle University of Thessaloniki, Thessaloniki; Greece
[160] International Center for Elementary Particle Physics and Department of Physics, University of Tokyo, Tokyo; Japan
[161] Graduate School of Science and Technology, Tokyo Metropolitan University, Tokyo; Japan
[162] Department of Physics, University of Toronto, Toronto ON; Canada
[163] [(a)] TRIUMF, Vancouver BC; [(b)] Department of Physics and Astronomy, York University, Toronto ON; Canada
[164] Division of Physics and Tomonaga Center for the History of the Universe, Faculty of Pure and Applied Sciences, University of Tsukuba, Tsukuba; Japan
[165] Department of Physics and Astronomy, Tufts University, Medford MA; United States of America
[166] Department of Physics and Astronomy, University of California Irvine, Irvine CA; United States of America
[167] University of West Attica, Athens; Greece
[168] Department of Physics and Astronomy, University of Uppsala, Uppsala; Sweden
[169] Department of Physics, University of Illinois, Urbana IL; United States of America
[170] Instituto de Física Corpuscular (IFIC), Centro Mixto Universidad de Valencia - CSIC, Valencia; Spain
[171] Department of Physics, University of British Columbia, Vancouver BC; Canada

2025 JINST 20 P02018

[172] Department of Physics and Astronomy, University of Victoria, Victoria BC; Canada
[173] Fakultät für Physik und Astronomie, Julius-Maximilians-Universität Würzburg, Würzburg; Germany
[174] Department of Physics, University of Warwick, Coventry; United Kingdom
[175] Waseda University, Tokyo; Japan
[176] Department of Particle Physics and Astrophysics, Weizmann Institute of Science, Rehovot; Israel
[177] Department of Physics, University of Wisconsin, Madison WI; United States of America
[178] Fakultät für Mathematik und Naturwissenschaften, Fachgruppe Physik, Bergische Universität Wuppertal, Wuppertal; Germany
[179] Department of Physics, Yale University, New Haven CT; United States of America
[180] Yerevan Physics Institute, Yerevan; Armenia

[a] Also Affiliated with an institute covered by a cooperation agreement with CERN
[b] Also at An-Najah National University, Nablus; Palestine
[c] Also at Borough of Manhattan Community College, City University of New York, New York NY; United States of America
[d] Also at Center for High Energy Physics, Peking University; China
[e] Also at Center for Interdisciplinary Research and Innovation (CIRI-AUTH), Thessaloniki; Greece
[f] Also at CERN, Geneva; Switzerland
[g] Also at CMD-AC UNEC Research Center, Azerbaijan State University of Economics (UNEC); Azerbaijan
[h] Also at Département de Physique Nucléaire et Corpusculaire, Université de Genève, Genève; Switzerland
[i] Also at Departament de Fisica de la Universitat Autonoma de Barcelona, Barcelona; Spain
[j] Also at Department of Financial and Management Engineering, University of the Aegean, Chios; Greece
[k] Also at Department of Mathematical Sciences, University of South Africa, Johannesburg; South Africa
[l] Also at Department of Modern Physics and State Key Laboratory of Particle Detection and Electronics, University of Science and Technology of China, Hefei; China
[m] Also at Department of Physics, Bolu Abant Izzet Baysal University, Bolu; Türkiye
[n] Also at Department of Physics, California State University, Sacramento; United States of America
[o] Also at Department of Physics, King's College London, London; United Kingdom
[p] Also at Department of Physics, Stanford University, Stanford CA; United States of America
[q] Also at Department of Physics, Stellenbosch University; South Africa
[r] Also at Department of Physics, University of Fribourg, Fribourg; Switzerland
[s] Also at Department of Physics, University of Thessaly; Greece
[t] Also at Department of Physics, Westmont College, Santa Barbara; United States of America
[u] Also at Faculty of Physics, Sofia University, 'St. Kliment Ohridski', Sofia; Bulgaria
[v] Also at Hellenic Open University, Patras; Greece
[w] Also at Henan University; China
[x] Also at Imam Mohammad Ibn Saud Islamic University; Saudi Arabia
[y] Also at Institucio Catalana de Recerca i Estudis Avancats, ICREA, Barcelona; Spain
[z] Also at Institut für Experimentalphysik, Universität Hamburg, Hamburg; Germany
[aa] Also at Institute for Nuclear Research and Nuclear Energy (INRNE) of the Bulgarian Academy of Sciences, Sofia; Bulgaria
[ab] Also at Institute of Applied Physics, Mohammed VI Polytechnic University, Ben Guerir; Morocco
[ac] Also at Institute of Particle Physics (IPP); Canada
[ad] Also at Institute of Physics, Azerbaijan Academy of Sciences, Baku; Azerbaijan
[ae] Also at National Institute of Physics, University of the Philippines Diliman (Philippines); Philippines
[af] Also at Technical University of Munich, Munich; Germany
[ag] Also at The Collaborative Innovation Center of Quantum Matter (CICQM), Beijing; China
[ah] Also at TRIUMF, Vancouver BC; Canada
[ai] Also at Università di Napoli Parthenope, Napoli; Italy
[aj] Also at University of Colorado Boulder, Department of Physics, Colorado; United States of America
[ak] Also at University of the Western Cape; South Africa
[al] Also at Washington College, Chestertown, MD; United States of America
[am] Also at Yeditepe University, Physics Department, Istanbul; Türkiye
[*] Deceased

2025 JINST 20 P02018